Die approbierte Originalversion dieser Diplom-/Masterarbeit ist an der Hauptbibliothek der Technischen Universität Wien aufgestellt (http://www.ub.tuwien.ac.at).

The approved original version of this diploma or master thesis is available at the main library of the Vienna University of Technology (http://www.ub.tuwien.ac.at/englweb/).

M A S T E R' S T H E S I S

MICROMECHANICAL EXPLANATION OF ANISOTROPIC BONE ELASTICITY: ROLE OF BONDED NEEDLE-TYPE MINERAL CRYSTALS, CROSSLINKED COLLAGEN MOLECULES, AS WELL AS OF LACUNAR AND VASCULAR POROSITY

D I P L O M A R B E I T

MIKROMECHANISCHE ERKLÄRUNG DER ANISOTROPEN KNOCHENELASTIZITÄT: ZUR ROLLE VERBUNDENER NADELARTIGER MINERALKRISTALLE, QUERVERNETZTER KOLLAGENMOLEKÜLE SOWIE VON LACUNAE UND VASKULÄRPOREN

ausgeführt zum Zwecke der Erlangung des akademischen
Grades eines Diplom-Ingenieurs

unter der Leitung von

Ao.Univ.Prof. Dipl.-Ing. Dr.techn. **Christian Hellmich**
Institut für Mechanik der Werkstoffe und Strukturen (E202)

eingereicht an der Technischen Universität Wien
Fakultät für Bauingenieurwesen

von

Andreas FRITSCH
Matr.-Nr.: 9925071
A. Baumgartner-Str. 44/C4, A-1230 Wien, Österreich

Wien, im September 2005

Abstract

This master's thesis comprises two scientific papers in the field of bone biomechanics, written together with Prof. Christian Hellmich (Vienna University of Technology) and Prof. Luc Dormieux (École Nationale des Ponts et Chaussées, Marne-la-Vallée, France). The first article (Chapter 2) discusses the question of the homogenization of elastic properties of porous polycrystals that are characteristic for a number of biological and man-made materials. We consider (i) uniform, (ii) axisymmetrical orientation distribution of linear elastic, isotropic needles. The latter requires derivation of the Hill tensor for arbitrarily oriented ellipsoidal inclusions with one axis tending towards infinity, embedded in a transversely isotropic matrix; this is accomplished by a new technique. For a porosity lower 0.4, the elastic properties of the polycrystal with uniformly oriented needles are quasi-identical to those of a polycrystal with solid spheres. However, as opposed to the sphere-based model, the needle-based model does not predict a percolation threshold. As regards axisymmetrical orientation distribution of needles, two effects are remarkable: Firstly, the sharper the cone of orientations the higher the anisotropy of the polycrystal. Secondly, for a given cone, the anisotropy increases with the porosity. These results confirm the very high degree of orientation randomness of crystals building up mineral foams in bone tissues.

A micromechanical multi-step homogenization model for the elasticity of bone is extended and improved in the second article (Chapter 3). This extension provides further evidence that universal design principles are valid for entire classes of biological materials. They concern the mechanical interaction between the elementary components (hydroxyapatite, collagen, water), governing the elasticity of the hierarchically organized material at all different observation scales. We here quantify these principles through continuum micromechanics laws for elasticity of extravascular and extracellular bone materials, building up osteons in cortical bone and trabecular struts or plates in spongy bones: At a scale of 5 microns, we envision the extracellular bone matrix or ultrastructure as mineral foam with collagen fibril inclusions. At a lower scale, the morphology of the mineralized collagen fibrils is carefully resolved: At a scale of 10 nm, long cylindrical collagen molecules, attached

to each other at their ends by $\sim$ 1.5 nm long crosslinks, form a contiguous matrix with intermolecular water inclusions, called wet collagen. At a length scale of several hundred nanometers, wet collagen and mineral crystal agglomerations interpenetrate each other to form the mineralized fibril. At a scale above the ultrastructure, with hundred micrometers characteristic length, lacunae are embedded in extracellular bone matrix, forming the extravascular bone material. The micromechanical model, based on tissue-independent ('universal') stiffness properties of hydroxyapatite, collagen, and water, is validated through independent experiments on stiffness and composition of a large number of different cortical and trabecular bone specimens across the vertebrate animal kingdom, both at the ultrastructural and at the extravascular observation scale. Mean relative errors between stiffness experiments and model estimates do not exceed 10%, which reflects a predictive precision never attained so far.

Kurzfassung

Die vorliegende Diplomarbeit umfasst zwei wissenschaftliche Artikel auf dem Gebiet der Biomechanik von Knochen, die zusammen mit Prof. Christian Hellmich (Technische Universität Wien) und Prof. Luc Dormieux (École Nationale des Ponts et Chaussées, Marne-la-Vallée, Frankreich) verfasst wurden. Der erste Beitrag (Kapitel 2) widmet sich der Homogenisierung der elastischen Eigenschaften von porösen Polykristallen, welche für eine Reihe von natürlichen und künstlichen Materialien charakteristisch sind. Wir betrachten (i) eine uniforme und (ii) eine axialsymmetrische (kegelförmige) Verteilung der Ausrichtung von linear elastischen, isotropen Nadeln. Letzteres erfordert die Herleitung des Hill-Tensors für beliebig orientierte ellipsoidale Einschlüsse mit einer unendlich langen Achse, eingebettet in eine transversal isotrope Matrix. Dies wird mittels einer neuen Methode bewerkstelligt. Es zeigt sich, dass für eine Porosität kleiner 0.4 die elastischen Eigenschaften des Polykristalls mit uniform orientierten Nadeln quasi-identisch mit denjenigen eines Polykristalls mit kugelförmigen Einschlüssen sind. Im Gegensatz zu dem Kugelmodell sagt das Nadelmodell keine Perkolationsgrenze voraus. Hinsichtlich der axialsymmetrischen Verteilung der Ausrichtung der Nadeln sind zwei Effekte bemerkenswert: Erstens, je spitzer der Kegel der Ausrichtungen, desto stärker die Anisotropie des Polykristalls. Zweitens, für einen gegebenen Verteilungskegel nimmt die Anisotropie mit wachsender Porosität zu. Diese Ergebnisse bestätigen den hohen Grad der Unordnung der Kristalle, welche den Mineralschaum in Knochengeweben aufbauen.

Die Erweiterung und Verbesserung eines mehrstufigen mikromechanischen Modells für die Knochenelastizität ist Gegenstand des zweiten Artikels (Kapitel 3). Ein solches Verfahren untersucht die Gültigkeit universeller Bauprinzipien für ganze Klassen von biologischen Materialien. Sie betreffen die mechanische Wechselwirkung zwischen den Elementarkomponenten (Hydroxyapatit, Kollagen, Wasser), die die Elastizität auf allen Beobachtungsskalen des hierarchisch aufgebauten Materials bestimmen. Wir quantifizieren diese Prinzipien mittels der kontinuumsmikromechanischen Gesetze für die Elastizität von extravaskulärem und extrazellulärem Knochenma-

terial, welches die Osteonen in der *Corticalis* und Trabekelbälkchen oder -platten in der *Spongiosa* aufbauen: Auf einer Skala von 5 μm sehen wir die extrazelluläre Knochenmatrix oder Ultrastruktur als Mineralschaum mit Kollagenfibrillen an. Auf einer niedrigeren Skala wird die Morphologie der mineralisierten Kollagenfibrille sorgfältig aufgelöst: Im Bereich von 10 nm bilden lange, zylindrische Kollagenmoleküle, die an ihren Enden durch $\sim$ 1.5 nm lange Querverbindungen vernetzt sind, eine zusammenhängende Matrix mit intermolekularen Wassereinschlüssen, genannt 'feuchtes Kollagen'. Auf einer Längenskala von einigen hundert Nanometern durchdringen 'feuchtes Kollagen' und Ansammlungen von Mineralkristallen einander und formen so die mineralisierte Fibrille. Auf einer Längenskala oberhalb der Ultrastruktur mit hundert Mikrometern charakteristischer Länge sind Lacunae in die extrazelluläre Matrix eingebettet und formen so das extravaskuläre Knochenmaterial. Das auf gewebeunabhängigen ('universellen') Steifigkeiten von Hydroxyapatit, Kollagen und Wasser basierende mikromechanische Modell wird durch unabhängige Experimente von Steifigkeit und Zusammensetzung zahlreicher, verschiedener (cortischer wie spongiöser) Proben über das Wirbeltierreich hinweg, sowohl auf dem Ultrastrukturniveau als auch auf dem des extravaskulären Knochenmaterials, getestet. Die mittleren relativen Fehler zwischen Steifigkeitsexperimenten und Modellvorhersagen überschreiten 10 % nicht: Dies spiegelt eine bisher unerreichte Präzision wider.

Danksagung

Zunächst möchte ich mich bei meinem Betreuer Prof. Christian Hellmich für seine Unterstützung beim Verfassen dieser Diplomarbeit bedanken. Er hat mit seiner interessanten Vorlesung über aktuelle Fragestellungen an der Kreuzung von Biologie, Chemie und Mechanik mein Interesse an der Biomechanik geweckt, welches zuerst zu einer Großen Projektarbeit und schließlich zu der vorliegenden Arbeit geführt hat. Seine ambitionierte Herangehensweise sowie sein großes Vertrauen gestatteten mir, zusammen mit ihm und Prof. Dormieux zwei wissenschaftliche Artikel zu verfassen, die zur Publikation eingereicht wurden. Prof. Hellmich ermöglichte mir darüber hinaus zwei Forschungsaufenthalte an der École Nationale des Ponts et Chaussées, Marne-la-Vallée, einer der renommiertesten Ingenieurhochschulen Frankreichs, bei denen die Grundlagen für den ersten Artikel dieser Diplomarbeit geschaffen wurden. Bei dieser Gelegenheit danke ich dem gesamten Team des Laboratoire des Matériaux et des Structures du Génie Civil, insbesondere Prof. Luc Dormieux, Samir Maghous und Jean-François Barthélémy, die mir jedes Mal einen herzlichen Empfang bereiteten. Durch die intensive Betreuung durch Prof. Dormieux konnte ich wertvolles Wissen gewinnen und viele Resultate nach Wien mitnehmen und anwenden.

Die Aufenthalte in Paris wurden nicht zuletzt nur möglich dank der Unterstützung durch den Österreichischen Akademischen Austauschdienst, der diese im Rahmen eines Mobilitätsprogrammes förderte.

Mein Dank gilt weiters Karin Hofstetter und Bernhard Pichler für etliche hilfreiche Hinweise und Erklärungen zur Mikromechanik oder zur verwendeten Software.

Nicht zuletzt möchte ich mich bei meinen Eltern für ihre Unterstützung beim Absolvieren des Studiums herzlich bedanken, weiters bei meiner Freundin Sylvia, meiner Schwester und allen Freunden für ihr Verständnis und aufmunternde Worte, die mir in manch anstrengender Phasen eine Hilfe waren.

Contents

1 Introduction **1**

2 Article *Comptes Rendus Mecanique* **3**

3 Article *Biomech. Model. Mechanobiol.* **12**

4 Summary and Perspective **34**

A Source codes for Chapter 2 **35**
A.1 SCS_sph.mws 35
A.2 eq_cyl_020.mws 38
A.3 expansion.mws 40
A.4 SCS_cyl_thetamax.mws 42

B Source codes for Chapter 3 **47**
B.1 trab.m 47
B.2 ultrasonic_BMMB2005.m 51
B.3 ashman84_human.m 57
B.4 ashman88.m 61
B.5 lees_ultra_ax.m 65
B.6 lees_ultra_rad.m 72
B.7 mccarthy90_horse.m 81
B.8 hom_wetcol_MT.m 85
B.9 hom_fib_SCS.m 86
B.10 hom_ef.m 88
B.11 hom_ultra_MT.m 89
B.12 hom_exhav.m 90
B.13 fun_kSCS.m 91
B.14 fun_muSCS.m 91
B.15 fun_Psph_1111.m 91
B.16 fun_Psph_1122.m 92
B.17 fun_Psph_1133.m 92

B.18 fun_Psph_2323.m 93
B.19 fun_Psph_3333.m 93

Chapter 1

Introduction

Bone is a material with a complex hierarchical organization showing a great variability and diversity. The explanation for the elasticity of bone from its internal structure and compositions, i.e. from the dosage of the elementary components (collagen, water, hydroxyapatite) and their interactions, has motivated substantial scientific work, documented in a series of articles by [Hellmich and Ulm, 2003, 2002a,b, Hellmich et al., 2004b,a, Hellmich, 2005]. There, it has been shown that the average mineral concentration in the non-collageneous space (the space not occupied by collagen molecules) is the same inside and outside the fibrils and that – opposing to other hypothesis – bone functions as collagen-reinforced mineral matrix.

Based on this results, a series of micromechanical models for the elasticity of bone [Hellmich and Ulm, 2003, 2002a,b, Hellmich et al., 2004b,a, Hellmich, 2005], which are able to deliver predictions that are far better than standard density-elasticity correlations, have been developed. While the precision of the aforementioned micromechanical models, rigorously tested through independent experimental sets from a huge data base, has been continuously increased, some issues were left that required deeper discussions. Two of them are discussed in this Thesis: The first concerns representation of a mineral foam in the bone ultrastructure on the basis of spherical mineral inclusions rather than mineral needles with a certain distribution function. The second concerns model overestimation of bone shear stiffness. In the ultrastructure of bones and mineralized tissues, at a length scale of several hundred microns, needle-like platelets of hydroxyapatite crystals and the water in the intercrystalline space build up a contiguous network or mineral foam. In the first article (Chapter 2) it is investigated if the distribution of needles can be appropriately considered by representing the solid phase simply by spherical inclusions, or if the use of uniformly or axisymmetrically oriented cylindrical inclusions delivers more accurate results. This work required the

derivation of a new expression for the Hill-tensor used in micromechanics, which was accomplished in cooperation with Prof. Luc Dormieux from the École Nationale des Ponts et Chaussées in Paris, France.

The four-step homogenization model, presented in [Hellmich, 2005] was characterized by an overestimation of the shear stiffness of bone (frequently relevant in fracture scenarios). It was expected that the neglect of both collagen and micropore orientation was responsible for this. However, comprehensive computations showed that features derived from detailed morphometry (expressed in measures such as Mean Intercept Length (MIL) or Oriented Volume (OV) [Whitehouse, 1974, Harrigan and Mann, 1984, Odgaard et al., 1990]) do not play a paramount role – therefore the activities shifted from the micropores to the nanolevel of bone. After testing several morphological concepts the introduction of the concept of 'wet collagen' at a new scale at the level of several nanometers turned out to improve the model and to reduce the overestimation of shear. The results are documented in the second article (Chapter 3).

After a short outlook (Chapter 4), the source codes for the calculations can be found in the Appendix.

Chapter 2

Porous polycrystals built up by uniformly and axisymmetrically oriented needles: Homogenization of elastic properties (manuscript submitted to *Comptes Rendus Mecanique*)

This article was submitted to the journal 'Comptes Rendus Mecanique' (Académie des sciences, 23, quai de Conti, 75006 Paris, France).

NOTICE: This is the author's version of a work that was accepted for publication in *Comptes Rendus Mecanique*. Changes resulting from the publishing process, such as peer review, editing, corrections, structural formatting, and other quality control mechanisms may not be reflected in this document. Changes may have been made to this work since it was submitted for publication. A definitive version was subsequently published:
A. Fritsch, L. Dormieux, and Ch. Hellmich. Porous polycrystals built up by uniformly and axisymmetrically oriented needles: Homogenization of elastic properties. *Comptes Rendus Mecanique*, 334:151 – 157, 2006. doi:10.1016/j.crme.2006.01.008, available online at www.sciencedirect.com

Porous polycrystals built up by uniformly and axisymmetrically oriented needles: Homogenization of elastic properties

Andreas Fritsch [a], Luc Dormieux [b], Christian Hellmich [a]

[a] *Institute for Mechanics of Materials and Structures, Vienna University of Technology (TU Wien), 1040 Vienna, Austria*
[b] *LMSGC, UMR 113, CNRS/ENPC/LCPC, 77455 Marne-la-Vallée, France*

Received *****; accepted after revision +++++

Presented by £££££

Abstract

Porous polycrystal-type microstructures built up of needle-like platelets or sheets are characteristic for a number of biological and man-made materials. Herein, we consider (i) uniform, (ii) axisymmetrical orientation distribution of linear elastic, isotropic needles. The latter requires derivation of the Hill tensor for arbitrarily oriented ellipsoidal inclusions with one axis tending towards infinity, embedded in a transversely isotropic matrix; this is accomplished by a new technique. For a porosity lower 0.4, the elastic properties of the polycrystal with uniformly oriented needles are quasi-identical to those of a polycrystal with solid spheres. However, as opposed to the sphere-based model, the needle-based model does not predict a percolation threshold. As regards axisymmetrical orientation distribution of needles, two effects are remarkable: Firstly, the sharper the cone of orientations the higher the anisotropy of the polycrystal. Secondly, for a given cone, the anisotropy increases with the porosity. These results confirm the very high degree of orientation randomness of crystals building up mineral foams in bone tissues.

To cite this article: A. Fritsch, L. Dormieux, Ch. Hellmich, C. R. Mecanique 333 (2005).

Résumé

Polycristaux poreux constitués d'aiguilles orientées de façon uniforme ou axisymétrique : homogénéisation des propriétés élastiques.

De nombreux matériaux biologiques ou manufacturés présentent une microstructure poreuse à morphologie polycristalline constituée de feuillets ou d'aiguilles. On s'intéresse ici à des cristaux solides élancés dont les orientations sont distribuées de façon uniforme ou axisymétrique. Dans ce dernier cas, l'approche micromécanique proposée fait appel à la connaissance du tenseur de Hill pour une inclusion ellipsoidale d'élancement infini plongée dans un milieu isotrope transverse. On présente à ce sujet une nouvelle méthode de calcul. Pour une porosité inférieure à 0.4, les propriétés élastiques du polycristal estimées à partir d'un schéma basé sur des inclusions ellipsoidales sont très proches de celles obtenues avec un schéma basé sur des inclusions sphériques. En revanche, à la différence du schéma basé sur des inclusions sphériques, le schéma basé sur des inclusions ellipsoidales ne prédit pas de seuil de percolation. En ce qui concerne la situation d'une distribution axisymétrique des orientations des cristaux solides, deux effets méritent d'être soulignés. D'une part, l'anisotropie est d'autant plus marquée que l'angle du cône des orientations diminue. D'autre part, à angle de cône donné, l'anisotropie augmente avec la porosité. Ces résultats confirment le caractère très largement désordonné de l'orientation des cristaux constituant des mousses minérales dans les tissus osseux.

Pour citer cet article : A. Fritsch, L. Dormieux, Ch. Hellmich, C. R. Mecanique 333 (2005).

Key words: porous polycrystal ; orientation distribution ; micromechanics ; biomechanics ; Hill tensor ; anisotropy
Mots-clés : polycristal poreux ; distribution des orientations ; micromécanique ; biomécanique ; tenseur de Hill ; anisotropie

1. Introduction

Porous polycrystal-type microstructures built up of needle-like platelets or sheets can be found in a number of biological and man-made materials; such as bone [1, 2] or eggs [3], or at the cement paste level of concrete [4]. We here deal with homogenization of their overall (linear) elastic properties, by means of self-consistent schemes. Thereby, the solid phase (needles) is represented by cylindrical inclusions (a cylinder being the limit case of a prolate spheroid with its long axis being very much larger than its spherical axis), and the (empty) pore inclusions (drained conditions) are spherical; extension to pressurized pores according to [5] is straightforward. Subsequently, we consider (i) uniform, (ii) axisymmetrical orientation distribution of the isotropic needles with elasticity tensor $\mathbb{C}_s$, bulk and shear moduli k_s and μ_s.

2. Uniform orientation distribution of needles

Uniformly oriented needles result in isotropic elastic properties of the polycrystal. The corresponding stiffness estimate $\mathbb{C}^{SCS}$ reads as

$$\begin{aligned}\mathbb{C}^{SCS} = (1-f)\,\mathbb{C}_s :&< [\mathbb{I} + \mathbb{P}^{SCS}_{cyl} : (\mathbb{C}_s - \mathbb{C}^{SCS})]^{-1} >: \\ &\{(1-f) < [\mathbb{I} + \mathbb{P}^{SCS}_{cyl} : (\mathbb{C}_s - \mathbb{C}^{SCS})]^{-1} > + f\,(\mathbb{I} - \mathbb{P}^{SCS}_{sph} : \mathbb{C}^{SCS})^{-1}\}^{-1}\end{aligned} \tag{1}$$

with

$$< [\mathbb{I} + \mathbb{P}^{SCS}_{cyl} : (\mathbb{C}_s - \mathbb{C}^{SCS})]^{-1} >= \int_{\varphi=0}^{2\pi}\int_{\vartheta=0}^{\pi} [\mathbb{I} + \mathbb{P}^{SCS}_{cyl}(\vartheta,\varphi)\,(\mathbb{C}_s - \mathbb{C}^{SCS})]^{-1} \frac{\sin\vartheta\,\mathrm{d}\vartheta\,\mathrm{d}\varphi}{4\pi} \tag{2}$$

where $\mathbb{I}$, $I_{ijkl} = 1/2(\delta_{ik}\delta_{jl} + \delta_{il}\delta_{kj})$, is the fourth-order unity tensor, δ_{ij} is the Kronecker delta, f denotes the porosity, $\mathbb{P}^{SCS}_{sph}$ and $\mathbb{P}^{SCS}_{cyl}$ is the fourth-order Hill tensor for spherical and cylindrical inclusions, respectively. The Hill tensor for spherical inclusions, $\mathbb{P}^{SCS}_{sph}$, is widely available in the open literature [6, 19]. The components of the Hill tensor for cylindrical inclusions embedded in an isotropic medium are given for a base frame coinciding with the long axis of the cylinder [6]. Transformation of Hill tensors related to differently oriented cylindrical inclusions, to one reference frame can be expressed by Euler angles ϑ and φ, rendering $\mathbb{P} = \mathbb{P}^{SCS}_{cyl}(\vartheta,\varphi)$ in Eqn.(2).

The numerical solution of (1), expressed in terms of couples of elastic constants, (E^{SCS}, ν^{SCS}) or (k^{SCS}, μ^{SCS}), shows that the Young's modulus E^{SCS} is practically independent of the value of Poisson's ratio ν_s.

The question arises whether uniform orientation of needles can be appropriately considered by representing the solid phase simply by spherical inclusions. The corresponding classical self-consistent estimate $\mathbb{C}^{SCS}$ reads as

$$\mathbb{C}^{SCS} = (1-f)\,\mathbb{C}_s : \{\mathbb{I} + \mathbb{P}^{SCS}_{sph} : (\mathbb{C}_s - \mathbb{C}^{SCS})\}^{-1} \tag{3}$$

In case of an incompressible solid phase ($k_s \to \infty$), (3) can be solved analytically:

$$\mu^{SCS} = \mu_s \frac{3(1-2f)}{3-f}, \quad k^{SCS} = \frac{4(1-f)}{3f}\mu^{SCS} \tag{4}$$

Email addresses: `Andreas.Fritsch@mail.imws.tuwien.ac.at` (Andreas Fritsch), `dormieux@lmsgc.enpc.fr` (Luc Dormieux), `christian.hellmich@tuwien.ac.at` (Christian Hellmich).

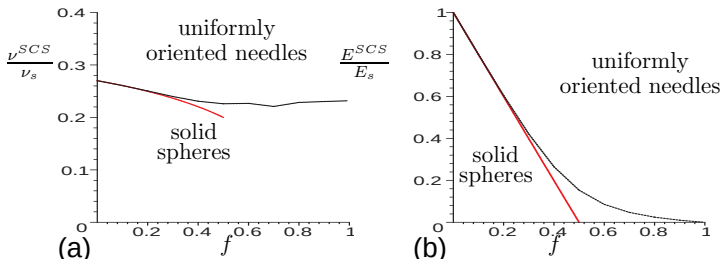

Figure 1. (a) Poisson's ratio and (b) Young's modulus of isotropic porous polycrystals, predicted by the sphere-based and needle-based models, respectively ($\nu_s = 0.2$).

This scheme shows a percolation threshold exactly equal to $f = \frac{1}{2}$, for any value of the Poisson coefficient ν_s of the solid phase. As for a compressible solid phase, the homogenized Young's modulus E^{SCS} can still be approximated by the affine expression $E_s(1-2f)$ with an error of at most 4 % relative to the exact solution, i.e. E^{SCS} is quasi-independent of Poisson's ratio.

On the interval $0 < f < 0.4$, the self-consistent stiffness estimates based on uniformly oriented solid needles are quasi-identical to those based on solid spheres [Fig. 1 (a) and (b)]. Particularly, in the vicinity of $f = 0$, the first-order expansions of the homogenized elastic constants with respect to the porosity read for both models as:

$$\frac{E^{SCS}}{E_s} = 1 - \frac{3}{2}\frac{(1-\nu_s)(5\nu_s+9)}{7-5\nu_s}f \quad ; \quad \nu_{SCS} = \nu_s + f\frac{3(1-5\nu_s)(1-\nu_s^2)}{2(7-5\nu_s)} \tag{5}$$

$$\frac{k^{SCS}}{k_s} = 1 - \frac{3}{2}\frac{1-\nu_s}{1-2\nu_s}f \quad ; \quad \frac{\mu^{SCS}}{\mu_s} = 1 - 15\frac{1-\nu_s}{7-5\nu_s}f \tag{6}$$

However, as opposed to the sphere-based model, the needle-based model does not predict any percolation threshold, i.e. E^{SCS}, k^{SCS} and $\mu^{SCS} \to 0$ only if the volume fraction of the solid phase becomes very small ($f \to 1$). This is a major difference between the two models, drawing the attention to the range of higher porosity, i.e. $f > 0.4$ (Figure 1). A first-order expansion in the vicinity of $f = 1$ of μ^{SCS} (resp. k^{SCS}) can be sought in the form $\mu^{SCS} \sim m(1-f)$ [resp. $k^{SCS} \sim k(1-f)$]. Analytical expressions for m and k can be derived and proven to be independent of ν_s :

$$m = \frac{71-2\sqrt{79}}{1575}, \; k = \frac{-8+2\sqrt{79}}{189} \tag{7}$$

Accordingly, the limit of ν^{SCS} when f tends towards 1 is independent of ν_s as well :

$$\lim_{f\to 1} \nu^{SCS} = \frac{17-\sqrt{79}}{35} \tag{8}$$

3. Axisymmetric orientation distribution of needles

Axisymmetrically oriented needles result in transversely isotropic elastic properties of the polycrystal. Let us again denote by ϑ and φ the angles defining the orientation of solid needles represented as cylindrical inclusions, with ϑ being defined with respect to the symmetry axis of the orientation distribution. We assume ϑ=const. in the cone $[0, \vartheta_{max}]$. The corresponding stiffness estimate still obeys (1), while (2) now reads as

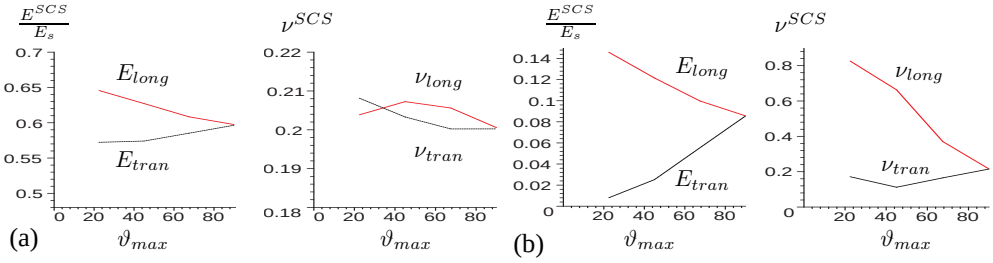

Figure 2. Effect of anisotropic distribution of crystal orientations on the longitudinal and transverse Young's moduli and Poisson ratios ($\nu_s = 0.2$, (a) $f = 0.2$, (b) $f = 0.6$).

$$< (\mathbb{I} + \mathbb{P}^{SCS}_{cyl} : \delta\,\mathbb{C})^{-1} >= \int_{\varphi=0}^{2\pi} \int_{\vartheta=0}^{\vartheta_{max}} [\mathbb{I} + \mathbb{P}^{SCS}_{cyl}(\vartheta,\varphi)\,(\mathbb{C}_s - \mathbb{C}^{SCS})]^{-1} \frac{\sin\vartheta\,\mathrm{d}\vartheta\,\mathrm{d}\varphi}{2\pi(1-\cos\vartheta_{max})} \tag{9}$$

and while the Hill tensors $\mathbb{P}^{SCS}_{cyl}$ and $\mathbb{P}^{SCS}_{sph}$ now refer to inclusions in a transversely isotropic material. Expressions for $\mathbb{P}^{SCS}_{sph}$ can be found in [1], and for determination of $\mathbb{P}^{SCS}_{cyl}$ we present a new technique in the Appendix. Two effects are remarkable (Fig. 2): Firstly, as expected, the sharper the cone of orientations the higher is the anisotropy of the polycrystal. Secondly, the higher the porosity the more pronounced is the effect of the non-uniform needle orientation distribution, on both the Young's modulus and the Poisson's ratio.

4. Discussion

The present results are also noteworthy from a biomechanical viewpoint: In the ultrastructure of bones and mineralized tissues hydroxyapatite crystals build up a contiguous network or mineral foam [2, 1]. Single crystals have typical dimensions of 50 nm average length, 25 nm average width, and 1 to 7 nm thickness [7, 8]. In a first approximation, they are often characterized as needles [8, 9, 10]. This renders the homogenization schemes developed here as appropriate for mineral foams occuring in bones. In particular, agreement between homogenized elastic properties of uniformly oriented needles with those of spheres for a porosity lower 0.4 (Fig. 1) confirms the use of self-consistent schemes with spherical inclusions for hydroxyapatite polycrystals [1], which have been validated by the experimental data of [11, 12]. At higher porosities, however, the needle-based scheme seems to be superior to the sphere-based scheme, since the former accounts for contiguity of the crystals, leading to non-zero homogenized stiffness, while the latter exhibits a percolation threshold beyond which the homogenized stiffness vanishes. Indeed, elasticity experiments [13] reveal that mineral crystals do contribute to the overall stiffness of low-mineralized turkey leg tendon, with a mineral foam porosity larger than 50%.

The present results also confirm the very high degree of orientation randomness of crystals in bone tissues, revealed already by chemical [14] or mechanical [2] means: Any remarkable orientation of needles leads to high anisotropy ratios E_{tran}/E_{long} far beyond two, and up to ten (Fig. 2). In real bone ultrastructure, however, this ratio lies always markedly below two [15, 11, 2].

Appendix A. Hill tensor for arbitrarily oriented cylindrical inclusions embedded in a transversely isotropic material

The starting point is the classical expression for the Hill tensor (see for instance [16],[17]) :

$$\mathbb{P} = \frac{\omega_2\,\omega_3}{4\pi} \int\limits_{|\xi|=1} \frac{\mathbf{\Gamma}}{(\boldsymbol{\xi}\cdot\mathbf{A}^T\cdot\mathbf{A}\cdot\boldsymbol{\xi})^{3/2}}\,\mathrm{d}S(\boldsymbol{\xi}) \tag{A.1}$$

$\boldsymbol{\xi}$ is the unit length vector pointing from the origin of the sphere to the surface element $\mathrm{d}S(\boldsymbol{\xi})$. The second-order tensor $\mathbf{A}$ describes the shape of the ellipsoid, with base vectors $\mathbf{w}_1, \mathbf{w}_2$ and $\mathbf{w}_3$ pointing in the principal directions of the ellipsoid,

$$\mathbf{A} = \mathbf{w}_1\otimes\mathbf{w}_1 + \omega_2\,\mathbf{w}_2\otimes\mathbf{w}_2 + \omega_3\,\mathbf{w}_3\otimes\mathbf{w}_3, \quad \omega_3 \gg 1 \tag{A.2}$$

The fourth-order tensor $\mathbf{\Gamma}$ is defined as

$$\mathbf{\Gamma} = \boldsymbol{\xi}\overset{s}{\otimes}\mathbf{K}^{-1}\overset{s}{\otimes}\boldsymbol{\xi}, \quad \mathbf{K} = \boldsymbol{\xi}\cdot\mathbb{C}\cdot\boldsymbol{\xi} \tag{A.3}$$

The second-order tensor $\mathbf{K}$ is the acoustic tensor, $\mathbb{C}$ is the stiffness tensor of the transversely isotropic matrix. $\overset{s}{\otimes}$ denotes the symmetrized tensor product.

The technique presented hereafter adapts the ideas presented in [18] and [19] to cylindrical inclusions. First, we consider the denominator of expression (A.1). The unit vector $\boldsymbol{\xi}$ can be expressed in spherical coordinates $\Phi \in [0, 2\pi]$ and $\Theta \in [0, \pi]$ as $\xi_1 = \sin\Theta\,\cos\Phi$, $\xi_2 = \sin\Theta\,\sin\Phi$ and $\xi_3 = \cos\Theta$, so that $\mathrm{d}S = \sin\Theta\,\mathrm{d}\Phi\,\mathrm{d}\Theta$. Since

$$\boldsymbol{\xi}\cdot\mathbf{A}^T\cdot\mathbf{A}\cdot\boldsymbol{\xi} = \omega_3^2\cos^2\Theta + \sin^2\Theta\,(\cos^2\Phi + \omega_2^2\sin^2\Phi)$$

we find with $x = \cos\Theta$ and $\gamma^2 = \frac{1}{\omega_3^2}(\cos^2\Phi + \omega_2^2\sin^2\Phi)$

$$\mathbb{P} = \frac{\omega_2}{4\pi}\int\limits_0^{2\pi}\int\limits_{-1}^{1} \frac{\gamma^2}{[x^2 + (1-x^2)\gamma^2]^{3/2}}\,\frac{\mathbf{\Gamma}(x,\Phi)}{\cos^2\Phi + \omega_2^2\sin^2\Phi}\,(-\mathrm{d}x)\,\mathrm{d}\Phi \tag{A.4}$$

Considering $\omega_3 \to \infty\,(\gamma \to 0)$, and use of the "Dirac delta function" $\delta(x)$

$$\lim_{\gamma\to 0}\frac{\gamma^2}{[x^2 + (1-x^2)\,\gamma^2]^{3/2}} = 2\,\delta(x), \quad \int \delta(x)\,f(x)\,dx = f(0) \tag{A.5}$$

yields, with $\omega_2 = 1$,

$$\mathbb{P} = \frac{1}{2\pi}\int\limits_0^{2\pi}\mathbf{\Gamma}(\Theta = \frac{\pi}{2}, \Phi)\,\mathrm{d}\Phi \tag{A.6}$$

Next, we consider the numerator of Eqn. (A.1), $\mathbf{\Gamma} = \boldsymbol{\xi}\overset{s}{\otimes}\mathbf{K}^{-1}\overset{s}{\otimes}\boldsymbol{\xi}$. Expressing $\boldsymbol{\xi}$ and $\mathbf{K}$ in terms of the base vectors $\mathbf{w}_1$ and $\mathbf{w}_2$, while adopting $z = \cot\Phi$, yields

$$\boldsymbol{\xi} = \cos\Phi\,\mathbf{w}_1 + \sin\Phi\,\mathbf{w}_2 = \sin\Phi(z\,\mathbf{w}_1 + \mathbf{w}_2) \tag{A.7}$$

$$\mathbf{K} = \boldsymbol{\xi}\cdot\mathbb{C}\cdot\boldsymbol{\xi} = \sin^2\Phi\,((z\,\mathbf{w}_1 + \mathbf{w}_2)\cdot\mathbb{C}\cdot(z\,\mathbf{w}_1 + \mathbf{w}_2))\sin^2\Phi\,\underbrace{(z^2\mathbf{Q} + z(\mathbf{R} + \mathbf{R}^T) + \mathbf{T})}_{\mathbf{K}'(z)} \tag{A.8}$$

when having introduced the second-order tensors $\mathbf{Q}, \mathbf{R}$ and $\mathbf{T}$ as

$$\mathbf{Q} = \mathbf{w}_1 \cdot \mathbb{C} \cdot \mathbf{w}_1,\ \mathbf{R} = \mathbf{w}_1 \cdot \mathbb{C} \cdot \mathbf{w}_2,\ \mathbf{T} = \mathbf{w}_2 \cdot \mathbb{C} \cdot \mathbf{w}_2 \tag{A.9}$$

$$\mathbf{K}(\Phi) = \sin^2\Phi \underbrace{(z^2\mathbf{Q} + z(\mathbf{R} + \mathbf{R}^T) + \mathbf{T})}_{\mathbf{K}'(z)} \tag{A.10}$$

$\mathbf{K}'(z)$ is a second-order polynomial. In order to obtain the inverse of $\mathbf{K}'(z)$, we use the matrix of cofactors (algebraic complements) $\mathbf{co}\,\mathbf{K}'$,

$$(\mathbf{K}(z))^{-1} = \frac{1}{\sin^2\Phi}\,(\mathbf{K}')^{-1} = \frac{1}{\sin^2\Phi}\,\frac{1}{\det\mathbf{K}'}\,(\mathbf{co}\,\mathbf{K}') \tag{A.11}$$

The determinant of $\mathbf{K}'$, $\det\mathbf{K}'$, is a sixth-order polynomial. Thus

$$\begin{aligned}\boldsymbol{\Gamma} &= \boldsymbol{\xi} \overset{s}{\otimes} \mathbf{K}^{-1} \overset{s}{\otimes} \boldsymbol{\xi} = \frac{1}{\sin^2\Phi}\,\frac{1}{\det\mathbf{K}'}\,(\boldsymbol{\xi} \overset{s}{\otimes} (\mathbf{co}\,\mathbf{K}') \overset{s}{\otimes} \boldsymbol{\xi}) = \\ &= \frac{1}{\sin^2\Phi}\,\frac{1}{\det\mathbf{K}'}\,(\sin^2\Phi\,(z\,\mathbf{w}_1 + \mathbf{w}_2) \overset{s}{\otimes} (\mathbf{co}\,\mathbf{K}') \overset{s}{\otimes} (z\,\mathbf{w}_1 + \mathbf{w}_2))\end{aligned} \tag{A.12}$$

Insertion of Eqn. (A.12) into Eqn. (A.6) and use of $\Phi = \operatorname{arccot} z$ yields

$$\mathbb{P} = \frac{1}{2\pi}\int_{\Phi=0}^{2\pi} \boldsymbol{\Gamma}\,\mathrm{d}\Phi = \frac{1}{2\pi}\,2\int_{z=-\infty}^{\infty} \boldsymbol{\Gamma}\,\frac{\mathrm{d}z}{1+z^2} \tag{A.13}$$

$$= \frac{1}{\pi}\int_{-\infty}^{\infty} \frac{(z\,\mathbf{w}_1 + \mathbf{w}_2) \overset{s}{\otimes} (\mathbf{co}\,\mathbf{K}') \overset{s}{\otimes} (z\,\mathbf{w}_1 + \mathbf{w}_2)}{(\det\mathbf{K}')\,(1+z^2)}\,\mathrm{d}z \tag{A.14}$$

The integrand in (A.14) is a rational fraction with a sixth-order polynomial in the numerator and an eighth-order polynomial in the denominator. Hence, the integration can be based on the Residue Theorem:

$$\int_{-\infty}^{\infty} f(z)\,dz = 2i\pi \sum_j \mathrm{Res}(f,\, z_j), \tag{A.15}$$

where z_j are the poles with a positive imaginary part, of the function $f(z)$

References

[1] Ch. Hellmich, J.-F. Barthélémy, and L. Dormieux. Mineral-collagen interactions in elasticity of bone ultrastructure – a continuum micromechanics approach. *European Journal of Mechanics A-Solids*, 23:783 – 810, 2004.

[2] Ch. Hellmich and F.-J. Ulm. Are mineralized tissues open crystal foams reinforced by crosslinked collagen? – some energy arguments. *Journal of Biomechanics*, 35:1199 – 1212, 2002.

[3] H. Silyn-Roberts and R.M. Sharp. Crystal growth and the role of the organic network in eggshell biomineralization. *Proceedings of the Royal Society of London, Series B*, 227(1248):303 – 324, 1986.

[4] V. Baroughel-Bouny. Caractérisation des pâtes de ciment et des bétons - méthodes, analyse, interprétation [Characterization of cement pastes and concretes - methods, analysis, interpretations]. Technical report, Laboratoire Central des Ponts et Chaussées, Paris, France, 1994. In French.

[5] X. Chateau and L. Dormieux. Micromechanics of saturated and unsaturated porous media. *International Journal for Numerical and Analytical Methods in Geomechanics*, 26:831 – 844, 2002.

[6] J.D. Eshelby. The determination of the elastic field of an ellipsoidal inclusion, and related problems. *Proceedings of the Royal Society London, Series A*, 241:376 – 396, 1957.

[7] S. Weiner and H.D. Wagner. The material bone: structure - mechanical function relations. *Annual Review of Materials Science*, 28:271 – 298, 1998.

[8] P. Fratzl, S. Schreiber, and K. Klaushofer. Bone mineralization as studied by small-angle X-ray scattering. *Connective Tissue Research*, 34(4):247 – 254, 1996.

[9] N. Sasaki. Orientation of mineral in bovine bone and the anisotropic mechanical properties of plexiform bone. *Journal of Biomechanics*, 24:57 – 61, 1991.

[10] P. Fratzl, N. Fratzl-Zelman, K. Klaushofer, G. Vogl, and K. Koller. Nucleation and growth of mineral crystals in bone studied by small-angle X-ray scattering. *Calcified Tissue International*, 48:407 – 413, 1991.

[11] S. Lees, J.M. Ahern, and M. Leonard. Parameters influencing the sonic velocity in compact calcified tissues of various species. *Journal of the Acoustical Society of America*, 74(1):28 – 33, 1983.

[12] S. Lees. Considerations regarding the structure of the mammalian mineralized osteoid from viewpoint of the generalized packing model. *Connective Tissue Research*, 16:281 – 303, 1987.

[13] S. Lees and E.A. Page. A study of some properties of mineralized turkey leg tendon. *Connective Tissue Research*, 28:263 – 287, 1992.

[14] F. Peters, K. Schwarz, and M. Epple. The structure of bone studied with synchrotron x-ray diffraction, x-ray absorption spectroscopy and thermal analysis. *Thermochimica Acta*, 361:131 – 138, 2000.

[15] S. Lees, J.D. Heeley, and P.F. Cleary. A study of some properties of a sample of bovine cortical bone using ultrasound. *Calcified Tissue International*, 29:107 – 117, 1979.

[16] N. Laws. The determination of stress and strain concentrations at an ellipsoidal inclusion in an anisotropic material. *Journal of Elasticity*, 7(1):91 – 97, 1977.

[17] N. Laws. A note on penny-shaped cracks in transversely isotropic materials. *Mechanics of Materials*, 4:209 – 212, 1985.

[18] C. Gruescu, V. Monchiet, and D. Kondo. Eshelby tensor for a crack in an orthotropic elastic medium. *Comptes Rendus Mécanique*, 2005. in press.

[19] A. Suvorov and G.J. Dvorak. Rate forms of the eshelby and hill tensors. *Int. J. Solids Structures*, 39:5659 – 5678, 2002.

Chapter 3

Quantifying universal design principles governing anisotropic elasticity of cortical and trabecular, extracellular and extravascular bone materials, across various mammalian species (manuscript submitted to *Biomechanics and Modeling in Mechanobiology*)

This article was submitted to the journal 'Biomechanics and Modeling in Mechanobiology'.

NOTICE: This is the author's version of a work that was accepted for publication in *Journal of Theoretical Biology.* Changes resulting from the publishing process, such as peer review, editing, corrections, structural formatting, and other quality control mechanisms may not be reflected in this document. Changes may have been made to this work since it was submitted for publication. A definitive version was subsequently published:
A. Fritsch and Ch. Hellmich. 'Universal' microstructural patterns in cortical and trabecular, extracellular and extravascular bone materials: Micromechanics-based prediction of anisotropic elasticity. *Journal of Theoretical Biology*, 244(4):597 – 620, 2007. doi:10.1016/j.jtbi.2006.09.013, available online at www.sciencedirect.com

Biomechanics and Modeling in Mechanobiology manuscript No.
(will be inserted by the editor)

Quantifying universal design principles governing anisotropic elasticity of cortical and trabecular, extracellular and extravascular bone materials, across various mammalian species

Andreas Fritsch, Christian Hellmich

Institute for Mechanics of Materials and Structures, Vienna University of Technology (TU Wien), 1040 Vienna, Austria
e-mail: christian.hellmich@tuwien.ac.at
Tel.: +43-1-58801-20220
Fax: +43-1-58801-20299

Received: August 2005 / Revised version: date

Abstract Biological materials are characterized by an astonishing variability and diversity. Still, once a (hierarchical) composite material has been adopted within a living organism, its fundamental building principles remain largely unchanged during biological evolution. Hence, entire classes of biological materials exhibit common (universal) principles of (micro)mechanical design. Design principles concern the mechanical interaction between the elementary components, governing the elasticity of the material at all different observation scales. We here quantify these principles through continuum micromechanics laws for elasticity of extravascular and extracellular bone materials, building up osteons in cortical bone and trabecular struts or plates in spongy bones: At a scale of 5 microns, we envision the extracellular bone matrix or ultrastructure as mineral foam with collagen fibril inclusions. At a lower scale, the morphology of the mineralized collagen fibrils is carefully resolved: At a scale of 10 nm, long cylindrical collagen molecules, attached to each other at their ends by ~ 1.5 nm long crosslinks, form a contiguous matrix with intermolecular water inclusions, called wet collagen. At a length scale of several hundred nanometers, wet collagen and mineral crystal agglomerations interpenetrate each other to form the mineralized fibril. At a scale above the ultrastructure, with hundred micrometers characteristic length, lacunae are embedded in extracellular bone matrix, forming the extravascular bone material. The micromechnical model, based on tissue-independent ('univeral') stiffness properties of hydroxyapatite, collagen, and water, is validated through independent experiments on stiffness and composition of a large number of different cortical and trabecular bone specimens, both at the ultrastructural and at the extravascular observation scale. Mean relative errors between stiffness experiments and model estimates do not exceed 10%, which reflects a predictive precision never attained so far.

Correspondence to: Christian Hellmich

1 Introduction

Biological materials are characterized by an astonishing variability and diversity. Their hierarchical organizations are often well suited and seemingly optimized to fulfill specific mechanical functions. This has motivated research in the fields of bionics and biomimetics. The aforementioned optimization is primarily driven by selection during the biological evolution process. However, it is of great importance to notice that selection is realized at the level of the individual plant or animal (and not at the material level). Therefore, material optimization in the strictest sense of the word does not take place. Rather, once a (hierarchical) composite material has been adopted within a living organism, its fundamental building principles (morphologies or universal patterns of architectural organization [Gould and Lewontin, 1979]) remain largely unchanged during evolution. Hence, entire classes of biological materials exhibit common (universal) principles of (micro)mechanical design.

This design firstly concerns observation scales at which typical morphological features can be discerned, across the entire material class. As regards bone, Katz et al. [1984] were the first to point out the importance of its hierarchical organization for its mechanical properties [Katz, 1980], distinguishing five levels of hierarchical organization, which have been quite generally accepted in the scientific community:

– The macrostructure at an observation scale of several mm to cm, where cortical (or compact) bone

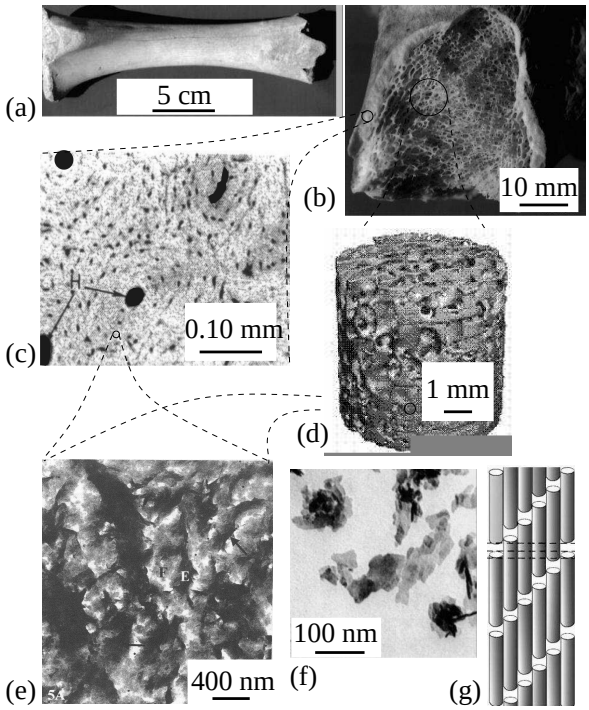

Fig. 1 Hierarchical organization of bone: (a) whole long bone (macrostructure)(+); (b) section through long bone (macrostructure)(+); (c) osteonal cortical bone (microstructure)(o); (d) trabecular spaceframe (microstructure)(□); (e) ultrastructure(×); (f) hydroxyapatite crystals (elementary components)(+); (g) collagen molecules (elementary components)(+); (+)... from [Weiner and Wagner, 1998], permission requested from Annual Reviews, www.AnnualReviews.org; (o)... from [Lees et al., 1979a], permission for reproduction requested from the Acoustical Society of America; (□)... from [Ding and Hvid, 2000], permission for reproduction requested from Elsevier Science; (×) ... from [Prostak and Lees, 1996], permission for reproduction requested from Springer Verlag, p.478, Fig. 5a

and trabecular (or spongy) bone can be distinguished [Fig. 1(a) and (b)];

- The microstructure at an observation scale of several 100 μm to several mm, where cylindrical units called osteons build up cortical bone, and where the single trabecular struts or plates can be distinguished [Fig.1(c) and (d)];
- The ultrastructure (or extracellular solid bone matrix) at an observation scale of 1 to 10 μm, comprising the material building up both trabecular struts and osteons [Fig.1(e)].
- Within the ultrastructure, collagen-rich domains [light areas in Fig.1(e)] and collagen-free domains [dark areas in Fig.1(e)] can be distinguished at an observation scale of several hundred nanometers. Commonly, these domains are referred to as fibrils and extrafibrillar space.
- Finally, at an observation scale of several ten nanometers, the so-called elementary components of mineralized tissues can be distinguished. These are
  - Plate or needle-shaped mineral crystals consisting of impure hydroxyapatite (HA; $Ca_{10}[PO_4]_6[OH]_2$) with typical 1 to 5 nm thickness, and 25 to 50 nm length [Weiner and Wagner, 1998] [Fig.1(f)];
  - Long cylindrically shaped collagen molecules with a diameter of about 1.2 nm and a length of about 300 nm [Lees, 1987], which are self-assembled in staggered organizational schemes (fibrils) with characteristic diameters of 50 to 500 nm [Cusack and Miller, 1979, Miller, 1984, Lees et al., 1990, 1994b, Weiner et al., 1997, Weiner and Wagner, 1998, Rho et al., 1998, Prostak and Lees, 1996], [Fig.1(g)]; several covalently bonded fibrils are sometimes referred to as fibers;

- Different non-collagenous organic molecules, predominantly lipids and proteins [Urist et al., 1983, Hunter et al., 1996]; and
- Water.

Secondly, the aforementioned design principles concern the mechanical interaction between the elementary components, governing the elasticity of the material at all different observation scales. A long debate concerns the question on whether bone anisotropy is predominantly caused by the mineral (as proposed by Currey [1969] and followed by many researchers [Katz, 1980, 1981, Sasaki, 1991, Mammone and Hudson, 1993, Pidaparti et al., 1996, Ascenzi, 1999, Jäger and Fratzl, 2000]) or by the collagen (as proposed by Lees et al. [1979b] and Cusack and Miller [1979]).

The first proposition refers to envisioning the bone ultrastructure as 'mineral-reinforced collagen matrix', while the second is consistent with the concept of a 'collagen-reinforced mineral matrix'. The latter concept has been corroborated in recent years, independently by computational homogenization techniques [Crolet et al., 1993, Aoubiza et al., 1996, Arnoux et al., 2002], by materials science [Benezra Rosen et al., 2002], and by basic mechanical energy considerations close to those of cellular solids [Hellmich and Ulm, 2002a].

The arguments put forward in [Benezra Rosen et al., 2002] and [Hellmich and Ulm, 2002a] have even motivated Currey to withdraw his 1969 proposition, in favor of describing mineral and collagen as (quote from [Currey, 2003]) 'continuous phases that are nevertheless intimately spatially entangled'.

Accordingly, the micromechanical concept of 'collagen inclusions embedded in a mineral foam', having shown remarkable predictive capabilities when validated through independent experiments on stiffness and composition of a large number of different cortical and trabecular bones [Hellmich and Ulm, 2002b, Hellmich et al., 2004b], was further refined, by introducing an interpenetrating network of collagen and minerals, representing the mineralized collagen fibril, being, at a larger scale, embedded into the extrafibrillar mineral foam. Corresponding micromechanical formulations showed improved predictive capabilities, both at the ultrastructural scale [Hellmich et al., 2004a], and at that of the microstructure [Hellmich, 2005].

These micromechanical formulations provide some quantitative evidence on the aforementioned universal design principles. Remarkably, they allow for translation [Torabia and Hellmich, 2004, Torabia, 2004] of chemical information accessible *in-vivo* into mechanical properties necessary for reliable structural analyses of bone [Kober et al., 2005], with great potential for patient-specific failure risk assessment. Still, the aforementioned micromechanical models tend to overestimate the anisotropic shear stiffness of bone [Hellmich, 2005], which motivates further refinement of the micromechanical representation of bone's hierarchical organization. Thereby, (i) further resolution of the inner structure of the mineralized fibril, and (ii) consideration of the lacunar porosity hosting osteocytes, not explicitly introduced in Katz' hierarchical organization levels [Katz et al., 1984], turn out to be mandatory, as described in Section 3 of this paper; before, a short summary on linear elastic continuum micromechanics is given in Section 2. Validation of the micromechanics model (Section 4) is followed by a thorough discussion of the strengths and limitations of the proposed approach, and an outlook to future activities (Section 5).

2 Fundamentals of continuum micromechanics – linear elasticity

In continuum micromechanics [Suquet, 1997, Zaoui, 2002], a material is understood as a micro-heterogeneous body filling a representative volume element (RVE) with characteristic length ℓ, $\ell \gg d$, d standing for the characteristic length of inhomogeneities within the RVE (see Fig. 2), and $\ell \ll \mathcal{L}$, $\mathcal{L}$ standing for the characteristic lengths of geometry or loading of a structure built up by the material defined on the RVE. The 'homogenized' mechanical behavior of the material, i.e. the relation between homogeneous deformations acting on the boundary of the RVE and resulting (average) stresses, can then be estimated from the mechanical behavior of different homogeneous phases (representing the inhomogeneities within the RVE), their dosages within the RVE, their characteristic shapes, and their interactions. Based on matrix-inclusion problems [Eshelby, 1957, Laws, 1977], an estimate for the 'homogenized' stiffness of a material reads as [Zaoui, 2002]

$$\mathbb{C}^{est} = \sum_r f_r \mathbb{c}_r : \left[\mathbb{I} + \mathbb{P}_r^0 : (\mathbb{c}_r - \mathbb{C}^0)\right]^{-1} : \left\{\sum_s f_s \left[\mathbb{I} + \mathbb{P}_s^0 : (\mathbb{c}_s - \mathbb{C}^0)\right]^{-1}\right\}^{-1} \quad (1)$$

where $\mathbb{c}_r$ and f_r denote the elastic stiffness and the volume fraction of phase r, respectively, and $\mathbb{I}$ is the fourth-order unity tensor. The two sums are taken over all phases of the heterogeneous material in the RVE. The fourth-order Hill tensor $\mathbb{P}_r^0$ accounts for the characteristic shape of phase r in a matrix with stiffness $\mathbb{C}^0$. Choice of this stiffness describes the interactions between the phases: For $\mathbb{C}^0$ coinciding with one of the phase stiffnesses (Mori-Tanaka scheme [Mori and Tanaka, 1973, Wakashima and Tsukamoto, 1991]), a composite material is represented (contiguous matrix with inclusions); for $\mathbb{C}^0 = \mathbb{C}^{est}$ (self-consistent scheme [Hershey, 1954, Hill, 1963]), a dispersed arrangement of the phases is considered (typical for polycrystals). If a single phase exhibits a heterogeneous microstructure itself, its mechanical behavior can be estimated by introduction of

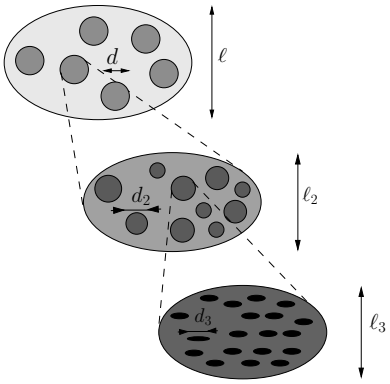

Fig. 2 Multistep homogenization

an RVE within this phase, with dimensions $\ell_2 \leq d$, comprising again smaller phases with characteristic length $d_2 \ll \ell_2$, and so on (see Fig. 2).

This leads to a multistep homogenization scheme. Such a procedure will be applied to mammalian cortical and trabecular bone materials in the sequel.

3 Micromechanical representation of hierarchical organisation of bone materials

The three-step homogenization scheme introduced in [Hellmich et al., 2004a] for bone ultrastructure is extended here by two additional homogenization steps (Fig. 3): The first of them refers to an observation scale of several nanometers, concerning collagen molecules and intermolecular, water-filled spaces. We call the homogenized material 'wet collagen' [Section 3.1 and Fig. 3(a)]. At the fibrillar observation scale, wet collagen and mineral crystal agglomerations build up the mineralized fibril [Section 3.2 and Fig. 3(b)]. At the ultrastructural scale, the extrafibrillar mineral foam {Section 3.3 and Fig. 3(c), [Hellmich and Ulm, 2002a, Hellmich et al., 2004a]} and mineralized fibrils form the extracellular bone matrix or ultrastructure [Section 3.4 and Fig. 3(d)]. The second new homogenization step refers to extravascular bone material at an observation scale of $\ell \approx 100$ μm [compare bar in Fig. 1(c)], consisting of lacunar pores in an ultrastructural matrix [Section 3.5 and Fig. 3(e)]. At an even higher observation scale, that of the microstructure with $\ell \approx 500$ μm, this extravascular matrix would be perforated by Haversian canals (in cortical bone) or by intertrabecular porosity (in trabecular bone). Material mechanics at that scale is beyond the scope of the present manuscript.

3.1 Wet collagen

Within an RVE $\mathring{V}_{wetcol}$ of wet collagen with $\ell_{wetcol} \approx$ 10 nm characteristic length [Fig. 3(a)], we homogenize over the staggered organization of cylindrical collagen molecules {Fig. 1(g), [Hodge and Petruska, 1963, Miller, 1984]}, which are attached to each other at their ends by ∼1.5 nm long crosslinks {[Lees et al., 1984b, Bailey et al., 1998], see also Section 4.3, Eq.(35)ff.}. Thereby, the intermolecular space is represented by cylindrical inclusions hosting water containing mechanically insignificant amounts of non-collageneous organic matter. These inclusions are embedded into a contiguous matrix built up by molecular collagen [Fig. 3(a)]. The volume fractions occupied by the two phases 'molecular collagen' and 'intermolecular space' are $\mathring{f}_{col}$ and $\mathring{f}_{im}$, $\mathring{f}_{col} + \mathring{f}_{im} = 1$. Using a Mori-Tanaka scheme for the estimation of the stiffness of the composite material 'wet collagen', $\mathbb{C}^{MT}_{wetcol}$, we specify (1) for one (cylindrical) inclusion phase (intermolecular water) and a matrix of molecular collagen, i.e. for $r \in [col, im]$, for $\mathbb{c}_{im} = 3\, k_{H_2O}\, \mathbb{J}$, with $J_{ijkl} = 1/3\, \delta_{ij}\, \delta_{kl}$ as the volumetric part of the fourth order unity tensor $\mathbb{I}$, and $\mathbb{C}^0 = \mathbb{c}_{col}$ according to Table 1, as well as for $\mathbb{P}^0_{im} = \mathbb{P}^{col}_{cyl}$; resulting in

$$\mathbb{C}^{MT}_{wetcol} = \left\{(1-\mathring{f}_{im})\mathbb{c}_{col} + \mathring{f}_{im}\mathbb{c}_{im} : \left[\mathbb{I} + \mathbb{P}^{col}_{cyl} : (\mathbb{c}_{im} - \mathbb{c}_{col})\right]^{-1}\right\} : \left\{(1-\mathring{f}_{im})\mathbb{I} + \mathring{f}_{im}\left[\mathbb{I} + \mathbb{P}^{col}_{cyl} : (\mathbb{c}_{im} - \mathbb{c}_{col})\right]^{-1}\right\}^{-1} \quad (2)$$

$\mathbb{P}^{col}_{cyl}$ refers to a cylindrical inclusion in a transversely isotropic matrix with stiffness $\mathbb{c}_{col}$, where the plane of isotropy is oriented perpendicular to the long axis of the cylinder. The non-zero components of the symmetric tensor $\mathbb{P}^{col}_{cyl}$ read as follows [Hellmich et al., 2004a]:

$$P^{col}_{cyl,1111} = P^{col}_{cyl,2222} = = 1/8\,(5\, c_{col,1111} - 3\, c_{col,1122})/c_{col,1111}/\mathcal{D}_2\,, \quad (3)$$

$$P^{col}_{cyl,1122} = P^{col}_{cyl,2211} = = -1/8\,(c_{col,1111} + c_{col,1122})/c_{col,1111}/\mathcal{D}_2\,, \quad (4)$$

$$P^{col}_{cyl,2323} = P^{col}_{cyl,1313} = 1/(8\, c_{col,2323})\,, \quad (5)$$

$$P^{col}_{cyl,1212} = 1/8\,(3\, c_{col,1111} - c_{col,1122})/c_{col,1111}/\mathcal{D}_2 \quad (6)$$

whereby

$$\mathcal{D}_2 = c_{col,1111} - c_{col,1122} \quad (7)$$

3.2 Mineralized collagen fibril

Within an RVE $\check{V}_{fib}$ of fibrillar material [Fig. 3(b)] with characteristic length of ℓ_{fib}=100-500 nm [Cusack and Miller, 1979, Miller, 1984, Prostak and Lees, 1996], the phases 'hydroxyapatite (HA)' and 'wet collagen' occupy volume fractions $\check{f}_{HA}$ and $\check{f}_{wetcol}$, $\check{f}_{HA} + \check{f}_{wetcol} = 1$. The crystals form agglomerations of typical size $d_{HA} \approx$

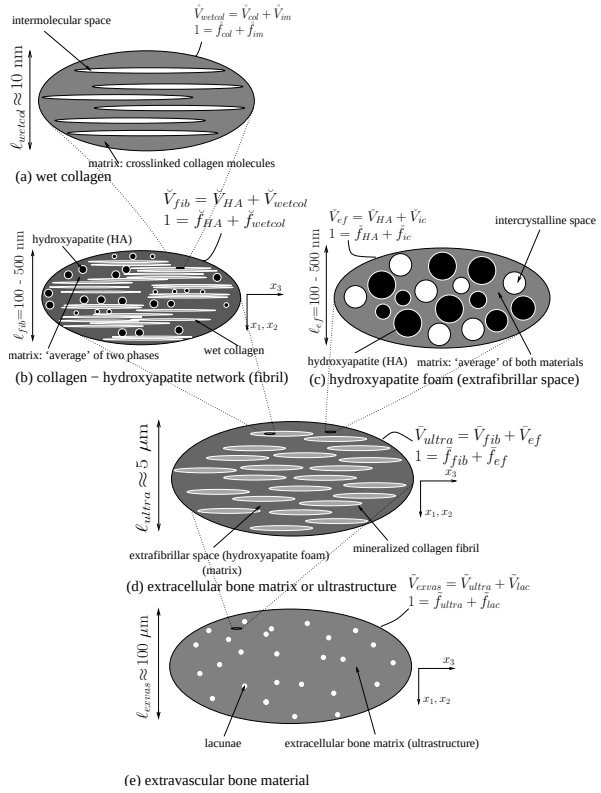

Fig. 3 Micromechanical representation of bone material by means of a five-step homogenization procedure

10 nm [Landis et al., 1996], filling (during the mineralization process) the gap zones in the collagen fibrils, before spreading through the fibrils. Both phases interpenetrate each other, which motivates the use of a self-consistent scheme, with spherical inclusions for the mineral phase, and with cylindrical inclusions for the wet collagen phase. Accordingly, in order to estimate the stiffness of the mineralized collagen fibril, $\mathbb{C}^{SCS}_{fib}$, (1) is specified for one spherical inclusion phase (mineral) and one cylindrical inclusion phase (wet collagen), i.e. for $r \in [HA, wetcol]$, for $\mathbb{c}_{HA} = 3\,k_{HA}\,\mathbb{J} + 2\,\mu_{HA}\,\mathbb{K}$ ($\mathbb{K} = \mathbb{I} - \mathbb{J}$ is the deviatoric part of the fourth-order unity tensor $\mathbb{I}$), according to Table 1, and for $\mathbb{c}_{wetcol} = \mathbb{C}^{MT}_{wetcol}$ from (2), for $\mathbb{C}^0 = \mathbb{C}^{SCS}_{fib}$, as well as for $\mathbb{P}^0_{HA} = \mathbb{P}^{fib}_{sph}$ and $\mathbb{P}^0_{wetcol} = \mathbb{P}^{fib}_{cyl}$; resulting in

$$\begin{aligned}
&\mathbb{C}^{SCS}_{fib} = \\
&\Big\{\breve{f}_{wetcol}\,\mathbb{C}^{MT}_{wetcol} : \Big[\mathbb{I} + \mathbb{P}^{fib}_{cyl} : \Big(\mathbb{C}^{MT}_{wetcol} - \mathbb{C}^{SCS}_{fib}\Big)\Big]^{-1} \\
&+\breve{f}_{HA}\,\mathbb{c}_{HA} : \Big[\mathbb{I} + \mathbb{P}^{fib}_{sph} : \Big(\mathbb{c}_{HA} - \mathbb{C}^{SCS}_{fib}\Big)\Big]^{-1}\Big\} : \\
&\Big\{\breve{f}_{wetcol}\,\Big[\mathbb{I} + \mathbb{P}^{fib}_{cyl} : \Big(\mathbb{C}^{MT}_{wetcol} - \mathbb{C}^{SCS}_{fib}\Big)\Big]^{-1} \\
&+\breve{f}_{HA}\,\Big[\mathbb{I} + \mathbb{P}^{fib}_{sph} : \Big(\mathbb{c}_{HA} - \mathbb{C}^{SCS}_{fib}\Big)\Big]^{-1}\Big\}^{-1}
\end{aligned} \tag{8}$$

The non-zero components of $\mathbb{P}^{fib}_{cyl}$ follow from substitution of '$c_{col,ijkl}$' by '$C^{SCS}_{fib,ijkl}$' in (3)-(7). The non-zero components of $\mathbb{P}^{fib}_{sph}$ follow from substitution of 'C^0_{ijkl}' by '$C^{SCS}_{fib,ijkl}$' in Eq.(57) to Eq.(63), see Appendix. For implicit solution of (8), we refer to [Hellmich et al., 2004a].

3.3 Extrafibrillar space: Hydroxyapatite foam

Within an RVE $\check{V}_{ef}$ of hydroxyapatite foam with ℓ_{ef} =100-500 nm characteristic length [see Fig. 3(c)], the phases 'hydroxyapatite (HA)' with d_{HA}=1-10 nm [Fratzl et al., 1991, Lees et al., 1994b, Eppell et al., 2001] and 'intercrystalline space (ic)' occupy volume fractions $\check{f}_{HA}$ and $\check{f}_{ic}$, $\check{f}_{HA} + \check{f}_{ic} = 1$. The considerable disorder of the hydroxyapatite crystals in the foam, shown by Lees et al. [1994b], Fratzl et al. [1996], Peters et al. [2000], Benezra Rosen et al. [2002], Hellmich and Ulm [2002a], motivates the use of a self-consistent scheme with inclusions of spherical shape [Hellmich and Ulm, 2002b, Hellmich et al., 2004a]. Accordingly, in order to estimate the stiffness of the extrafibrillar mineral foam, $\mathbb{C}_{ef}^{SCSII}$, (1) is specified for two (spherical) inclusion phases, i.e. for $r \in [HA, ic]$, for $\mathbb{c}_{HA} = 3\,k_{HA}\,\mathbb{J} + 2\,\mu_{HA}\,\mathbb{K}$ and $\mathbb{c}_{ic} = 3\,k_{H_2O}\,\mathbb{J}$, according to Table 1, for $\mathbb{C}^0 = \mathbb{C}_{ef}^{SCSII}$, and for $\mathbb{P}_{HA}^0 = \mathbb{P}_{ic}^0 = \mathbb{P}_{sph}^{ef}$; resulting in

$$\mathbb{C}_{ef}^{SCSII} = \left\{ \sum_r \check{f}_r\,\mathbb{c}_r : \left[\mathbb{I} + \mathbb{P}_{sph}^{ef} : (\mathbb{c}_r - \mathbb{C}_{ef}^{SCSII})\right]^{-1} \right\} : \left\{ \sum_s \check{f}_s \left[\mathbb{I} + \mathbb{P}_{sph}^{ef} : (\mathbb{c}_s - \mathbb{C}_{ef}^{SCSII})\right]^{-1} \right\}^{-1}, \quad r, s \in [HA, ic] \quad (9)$$

$\mathbb{P}_{sph}^{ef}$, the Hill tensor for a spherical inclusion in an isotropic matrix of stiffness $\mathbb{C}_{ef}^{SCSII}$, is of the form [Eshelby, 1957, Zaoui, 1997]

$$\mathbb{P}_{sph}^{ef} = \mathbb{S}_{sph}^{Esh,ef} : \mathbb{C}_{ef}^{SCSII,-1}, \quad (10)$$

$$\mathbb{S}_{sph}^{Esh,ef} = \alpha_{ef}^{SCSII}\,\mathbb{J} + \beta_{ef}^{SCSII}\,\mathbb{K} \quad (11)$$

with

$$\alpha_{ef}^{SCSII} = \frac{3\,k_{ef}^{SCSII}}{3\,k_{ef}^{SCSII} + 4\,\mu_{ef}^{SCSII}}$$
$$\beta_{ef}^{SCSII} = \frac{6\,(k_{ef}^{SCSII} + 2\,\mu_{ef}^{SCSII})}{5\,(3\,k_{ef}^{SCSII} + 4\,\mu_{ef}^{SCSII})} \quad (12)$$

For implicit solution of (9), together with (10)-(12), with respect to $\mathbb{C}_{ef}^{SCSII}$, we refer to [Hellmich and Ulm, 2002b, Hellmich et al., 2004a].

3.4 Extracellular bone matrix or ultrastructure

Within an RVE $\bar{V}_{ultra}$ of bone ultrastructure with $\ell_{ultra} \approx$ 5 μm characteristic length [see Fig. 3(d)], cylindrical fibrillar inclusions are embedded in a contiguous matrix built up by the mineral foam material of homogenization step III (9). The volume fractions occupied by the two phases 'mineralized collagen fibril' and 'extrafibrillar space' are $\bar{f}_{fib}$ and $\bar{f}_{ef}$, $\bar{f}_{fib} + \bar{f}_{ef} = 1$. Using a Mori-Tanaka scheme for the estimation of the stiffness of the composite material 'extracellular bone matrix or ultrastructure', $\mathbb{C}_{ultra}^{MTII}$, we specify (1) for one (cylindrical) inclusion phase (mineralized collagen fibrils), and one extrafibrillar matrix, i.e. for $r \in [fib, ef]$, for $\mathbb{c}_{fib} = \mathbb{C}_{fib}^{SCS}$ from (8), for $\mathbb{C}^0 = \mathbb{c}_{ef} = \mathbb{C}_{ef}^{SCSII}$ from (9), and for $\mathbb{P}_{fib}^0 = \mathbb{P}_{cyl}^{ef}$; resulting in

$$\mathbb{C}_{ultra}^{MTII} = \left\{ (1 - \bar{f}_{fib})\mathbb{C}_{ef}^{SCSII} + \bar{f}_{fib}\mathbb{C}_{fib}^{SCS} : \left[\mathbb{I} + \mathbb{P}_{cyl}^{ef} : (\mathbb{C}_{fib}^{SCS} - \mathbb{C}_{ef}^{SCSII})\right]^{-1} \right\} : \left\{ (1 - \bar{f}_{fib})\mathbb{I} + \bar{f}_{fib} \left[\mathbb{I} + \mathbb{P}_{cyl}^{ef} : (\mathbb{C}_{fib}^{SCS} - \mathbb{C}_{ef}^{SCSII})\right]^{-1} \right\}^{-1} \quad (13)$$

The non-zero components of $\mathbb{P}_{cyl}^{ef}$ follow from substitution of '$c_{col,ijkl}$' by '$C_{ef,ijkl}^{SCS}$' in (3)-(7).

3.5 Extravascular bone material

Within an RVE V_{exvas} of extravascular bone material with $\ell_{exvas} \approx 100\ \mu$m characteristic length [see Fig. 3(e)], osteocyte-filled cavities called lacunae with characteristic length d_{lac}=5-15 μm, Fig. 2.12 and 2.14 of [Martin et al., 1998], are embedded in a contiguous matrix built up by the extracellular bone material of homogenization step IV (13). The volume fractions occupied by the two phases 'extracellular bone matrix (ultrastructure)' and 'lacunae' are $\tilde{f}_{ultra}$ and $\tilde{f}_{lac}$, $\tilde{f}_{ultra} + \tilde{f}_{lac} = 1$. Using again the Mori-Tanaka scheme for the estimation of the stiffness of the composite 'extravascular bone material', $\mathbb{C}_{exvas}^{MTIII}$, we specify (1) for one spherical inclusion phase (lacunae), and one extracellular bone matrix, i.e. for $r \in [ultra, lac]$, for $\mathbb{c}_{lac} = 3\,k_{H_2O}\,\mathbb{J}$ (Table 1), for $\mathbb{C}^0 = \mathbb{c}_{ultra} = \mathbb{C}_{ultra}^{MTII}$ from (13), and for $\mathbb{P}_{lac}^0 = \mathbb{P}_{sph}^{ultra}$; resulting in

$$\mathbb{C}_{exvas}^{MTIII} = \left\{ \tilde{f}_{ultra}\mathbb{C}_{ultra}^{MTII} + \tilde{f}_{lac}\,\mathbb{c}_{lac} : \left[\mathbb{I} + \mathbb{P}_{sph}^{ultra} : (\mathbb{c}_{lac} - \mathbb{C}_{ultra}^{MTII})\right]^{-1} \right\} : \left\{ \tilde{f}_{ultra}\,\mathbb{I} + \tilde{f}_{lac} \left[\mathbb{I} + \mathbb{P}_{sph}^{ultra} : (\mathbb{c}_{lac} - \mathbb{C}_{ultra}^{MTII})\right]^{-1} \right\}^{-1} \quad (14)$$

The non-zero components of $\mathbb{P}_{sph}^{ultra}$ follow from substitution of 'C_{ijkl}^0' by '$C_{ultra,ijkl}^{MTII}$' in Eq.(57) to Eq.(63), see Appendix.

4 Validation of micromechanical model

4.1 Strategy

In the line of Popper, who stated that a theory – as long as it has not been falsified – will be 'the more satisfactory the greater the severity of independent tests it survives', cited from [Mayr, 1997], p.49, the verification of the micromechanical representation of cortical and trabecular bone materials at the ultrastructural

(extracellular) and the extravascular level will rest on two independent experimental sets: The stiffness values $\mathbb{C}^{MTII}_{ultra}$ and $\mathbb{C}^{MTIII}_{exvas}$ predicted by the micromechanical model on the basis of tissue-independent phase stiffness properties $\mathbb{c}_{HA} = 3\,k_{HA}\,\mathbb{J} + 2\,\mu_{HA}\,\mathbb{K}$, $\mathbb{c}_{col}$, k_{H_2O} (experimental set I, Table 1) for tissue-specific composition data $\tilde{f}_{lac}$, $\bar{f}_{fib}$, $\check{f}_{HA}$, $\breve{f}_{HA}$, and $\mathring{f}_{col}$ (experimental set IIa, Subsection 4.3) are compared to corresponding experimentally determined tissue-specific stiffness values $\mathbb{C}^{exp}$ (experimental set IIb, Subsection 4.4).

4.2 'Universal' phase stiffness values – Experimental set I

Concerning the tissue-independent ('universal') phase properties, being the same for all tissues discussed herein, we consider the following experiments: Tests with an ultrasonic inferometer coupled with a solid media pressure apparatus [Katz and Ukraincik, 1971, Gilmore and Katz, 1982] reveal the isotropic elastic properties of hydroxyapatite powder, which, in view of the largely disordered arrangement of minerals [Lees et al., 1994b, Fratzl et al., 1996, Peters et al., 2000, Hellmich and Ulm, 2002a], are sufficient for the characterization of the mineral phase [Hellmich and Ulm, 2002b, Hellmich et al., 2004b]. Given the absence of direct measurements of (molecular) collagen, the elastic properties of (molecular) collagen are approximated by those of dry rat tail tendon, a tissue consisting almost exclusively of collagen. By means of Brillouin light scattering, Cusack and Miller [1979] have determined the respective five independent elastic constants of a transvesely isotropic material (Table 1). We assign the standard bulk modulus of water (Table 1) to phases comprising water with mechanically insignificant non-collageneous organic matter or osteocytes. In case of dry tissues, we adopt $k_{H_2O} = 0$.

4.3 Determination of tissue-specific volume fractions – Experimental set IIa

Experimental validation of the five-step homogenization procedure [Eq.(2) to (14)] requires determination of the volume fractions within the five considered RVEs (Fig. 3).

As concerns the extravascular scale [Fig. 3(e)], the corresponding volume fractions were dervied from measurements at a scale of one to several mm (microstructure of bone). This scale is accessible by polarized light microscopy [Fig.1(c)], which visualizes, in cortical bone, Haversian canals and lacunae. Hence, polarized light microscopic images can be used for determination of the (microstructural) volume fractions of vascular and lacunar porosity, f_{vas} and f_{lac}, through

$$f_{vas} = \frac{\text{area of Haversian canals in field of view}}{\text{total area of field of view}} \quad (15)$$

$$f_{lac} = \frac{\text{area of lacunae in field of view}}{\text{total area of field of view}} \quad (16)$$

At the extravascular scale [Fig. 3(e)] the lacunar volume fraction follows to be

$$\tilde{f}_{lac} = \frac{f_{lac}}{1 - f_{vas}} \quad (17)$$

f_{vas} is related to the activity of osteoblasts and osteoclasts, biological cells being temporarily active in Haversian canals and intertrabecular space, see standard textbook such as [Martin et al., 1998]. f_{vas} increases under osteoclastic activity (osteoclasts resorb extracellular bone material), and f_{vas} decreases under osteoblastic activity (osteoblasts lay down osteoid, i.e. yet unmineralized bone ultrastructure, at the surfaces of Haversian canals or of trabecular plates or struts). Reflecting a certain equilibrium between osteoclastic and osteoblastic activity, f_{vas} ranges from 50 % to more than 95 % in trabecular bone, e.g. [Turner et al., 1990], f_{vas}=2...5 % in healthy cortical bone under normal physiological conditions, and reaches up to 50 % in cortical bone under abnormal physiological conditions, such as overtraining, drug treatment, or extreme age [McCarthy et al., 1990, Lees et al., 1994a, Sietsema, 1995]. In contrast to f_{vas}, $\tilde{f}_{lac}$ depends only on the way osteoblasts work: When laying down osteoid, a typical fraction of osteoblasts become buried in this newly formed ultrastructure, leading to the formation of lacunae. Hence, $\tilde{f}_{lac}$, as opposed to f_{vas}, always lies within a quite narrow range of values.

Evaluation of the image shown in Fig.1 of Lees et al. [1979a] [see Fig. 1(c)] through Eq.(15) renders f_{vas} = 3%, typical for mammalian cortical bone under normal physilogical conditions [Sietsema, 1995], considered in the upper half of Table 2 and in Table 4. From the same picture, Eq.(16) and (17) render f_{lac}=2 % and $\tilde{f}_{lac}$=2.1 %, the latter being typical for any kind of mammalian bone [Frost, 1962, Baylink and Wergedal, 1971, Morris et al., 1982, Zhang et al., 1998, Cowin, 1999]. As regards the drug–treated rabbits investigated by Lees et al. [1994b], we determined f_{vas} as the volume fraction of Haversian canals from micrographs of diaphyseal cross sections of femoral specimens (Fig. 9 and 10 of [Lees et al., 1994a], see column 6 of Table 2).

One may sum up f_{vas} and f_{lac} to get the total porosity discernable in a light microscope, which one may term microporosity $f_{\mu por}$,

$$f_{\mu por} = f_{vas} + f_{lac} \quad (18)$$

McCarthy et al. [1990] determined this microporosity from microradiographs of overtrained race horses, viewed under a low power microscope. Respective data are given in Table 6, showing also the microstructural mass density of the specimens with empty Haversian

phase	bulk modulus k [GPa]	shear modulus μ [GPa]	experimental source
hydroxyapatite	$k_{HA} = 82.6$	$\mu_{HA} = 44.9$	[Katz and Ukraincik, 1971]
water containing non-collageneous organics or osteocytes	$k_{H_2O} = 2.3$	$\mu_{H_2O} = 0$	
	c_{ijkl} [GPa]	c_{ijkl} [GPa]	
collagen	$c_{col,3333} = 17.9$ $c_{col,1111} = 11.7$	$c_{col,1133} = 7.1$ $c_{col,1122} = 5.1$ $c_{col,1313} = 3.3$	[Cusack and Miller, 1979]

Table 1 'Universal' (tissue and location-independent) isotropic (or transversely isotropic) phase stiffness values

canals, $\rho_{\mu,empty}$. $\tilde{f}_{lac}$=2.1 % [Eq.(17) and discussion below] allows for determination of the (microstructural) volume fraction of the Haversian canals through

$$f_{vas} = \frac{f_{\mu por} - \tilde{f}_{lac}}{1 - \tilde{f}_{lac}} \tag{19}$$

see Table 6.

Determination of the ultrastructural volume fractions of mineral and collagen, $\bar{f}_{HA}$ and $\bar{f}_{col}$, rests on volume measurements and weighing experiments on wet, dehydrated and demineralized cortical bone specimens, performed by Lees et al. [1979b, 1983], Lees [1987]. These experiments give access to the microstructural weight fractions of water, of organic matter, and of mineral, $WF^{\mu}_{H_2O}$, WF^{μ}_{org} and WF^{μ}_{HA}; and to the microstructural mass densities of wet tissues, $\rho_{\mu,wet}$ (with wet ultrastructure and water-filled lacunae and Haversian canals), and of dry tissues, $\rho_{\mu,dry}$ (Tables 2 and 4). Combination of the latter values with microporosity $f_{\mu por}$ [Eq.(18)] and the mass density of water, $\rho_{H_2O} = 1$ g/ml, yields the mass density of (wet or dry) ultrastructure, see e.g. [Hellmich et al., 2004b],

$$\rho_{ultra,wet} = \frac{\rho_{\mu,wet} - \rho_{H_2O}\, f_{\mu por}}{1 - f_{\mu por}} \tag{20}$$

and

$$\rho_{ultra,dry} = \frac{\rho_{\mu,dry}}{1 - f_{\mu por}} \tag{21}$$

as well as the weight fraction of water-filled micropores in (wet) bone specimens, see e.g. [Torabia, 2004],

$$WF^{\mu}_{\mu por} = \frac{\rho_{H_2O} \times f_{\mu por}}{\rho_{\mu,wet}} \tag{22}$$

$WF_{\mu por}$ allows for scale transition of the weight fractions from the microstructural to the ultrastructural scale, see e.g. [Torabia, 2004],

$$WF^{ultra}_{HA} = \frac{WF^{\mu}_{HA}}{1 - WF^{\mu}_{\mu por}} \tag{23}$$

$$WF^{ultra}_{org} = \frac{WF^{\mu}_{org}}{1 - WF^{\mu}_{\mu por}} \tag{24}$$

This completes the set of quantities necessary for computation of $\bar{f}_{HA}$ and $\bar{f}_{col}$ in wet tissues, through

$$\bar{f}_{HA,wet} = \frac{\rho_{ultra,wet}}{\rho_{HA}} \times WF^{ultra}_{HA} \tag{25}$$

$$\bar{f}_{col,wet} = \frac{\rho_{ultra,wet}}{\rho_{col}} \times 0.9 \times WF^{ultra}_{org} \tag{26}$$

where $\rho_{HA} = 3.00$ g/cm^3 [Lees, 1987, Hellmich, 2005] is the mass density of hydroxyapatite, and $\rho_{col} \approx \rho_{org} = 1.41$ g/cm^3 is the mass density of collagen. Eq.(26) accounts for the fact that, in mineralized tissues, about 90% per mass of the organic matter is collagen [Urist et al., 1983, Lees, 1987, Weiner and Wagner, 1998]. For dry tissues, $\bar{f}_{HA}$ and $\bar{f}_{col}$ read as

$$\bar{f}_{HA,dry} = \frac{WF^{ultra}_{HA}}{WF^{ultra}_{HA} + WF^{ultra}_{org}} \times \frac{\rho_{ultra,dry}}{\rho_{HA}} \tag{27}$$

$$\bar{f}_{col,dry} = \frac{0.9WF^{ultra}_{org}}{WF^{ultra}_{HA} + WF^{ultra}_{org}} \times \frac{\rho_{ultra,dry}}{\rho_{col}} \tag{28}$$

see Tables 2 and 3 for a compilation of values determined from experiments of Lees et al. [1979b, 1983], Lees [1987], Lees et al. [1994a].

It is interesting to note that the dehydration–demineralization tests of Lees et al. [1979b], Lees [1987], Lees et al. [1995] reveal seemingly universal composition laws, valid throughout the entire vertebrate animal kingdom. In fact, the ultrastructural mineral volume fraction $\bar{f}_{HA}$ is linearly dependent on the ultrastructural mass density $\rho_{ultra,wet}$, which can be expressed by a regression function of the form [Hellmich and Ulm, 2002a, Hellmich, 2005]

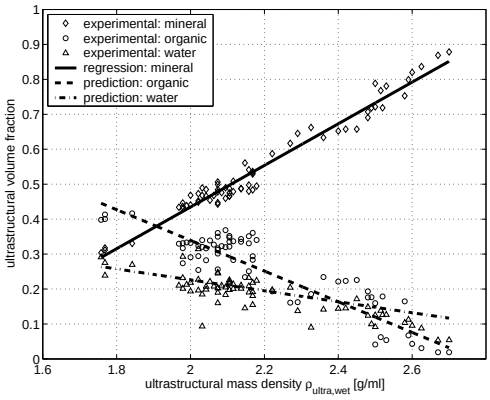

Fig. 4 Composition of bone ultrastructure; linear relationship between ultrastructural mineral volume fraction and tissue mass density (see diamond-marked experimental data of Lees et al. [1979b], Lees [1987], Lees et al. [1995], and solid-line regression function Eqn.(29)): Predictions of ultrastructural organic and water volume fraction (dashed and dash-dotted lines representing Eqn.(31) and (32)) agree well with circle-marked and triangle-marked experimental data of Lees et al. [1979b], Lees [1987], Lees et al. [1995]; see also [Torabia, 2004, Hellmich, 2005]

$$\mathcal{F}_{\bar{f}_{HA,wet}} = \mathcal{A} \times \rho_{ultra,wet} + \mathcal{B} \tag{29}$$

with $\mathcal{A} = 0.59$ ml/g and $\mathcal{B} = -0.75$. Thereby, we considered a microporosity $f_{\mu por}$ =5 % according to Fig. 1(c) for the long bone tissues of Lees et al. [1979b], Lees [1987] and $f_{\mu por}$=0 % for the hyperpycnotic tissues of Lees [1987], Lees et al. [1995], see Fig. 4. The statistical relevance of this relationship $\mathcal{F}_{\bar{f}_{HA,wet}}(\rho_{ultra,wet})$ is underlined by a correlation coefficient of $r^2 = 97$ %. Combination of (29) with

$$\rho_{ultra,wet} = \bar{f}_{H_2O,wet}\,\rho_{H_2O} + \bar{f}_{org,wet}\,\rho_{org} + \bar{f}_{HA,wet}\,\rho_{HA} \tag{30}$$

with $1 = \bar{f}_{org} + \bar{f}_{H_2O} + \bar{f}_{HA}$, and with $\bar{f}_{col} = 0.9 \times \bar{f}_{org}$ [compare (26)] yields a function for the collagen content in wet tissues [Torabia, 2004, Hellmich, 2005]

$$\mathcal{F}_{\bar{f}_{col,wet}}(\rho_{ultra,wet}) = 0.9 \times \mathcal{F}_{\bar{f}_{org,wet}}(\rho_{ultra,wet})$$

whereby

$$\mathcal{F}_{\bar{f}_{org,wet}}(\rho_{ultra,wet}) = \frac{1}{\rho_{H_2O} - \rho_{org}} \times \left\{\mathcal{F}_{\bar{f}_{HA,wet}}(\rho_{ultra,wet}) \times [\rho_{HA} - \rho_{H_2O}] - \rho_{ultra,wet} + \rho_{H_2O}\right\} \tag{31}$$

This prediction $\mathcal{F}_{\bar{f}_{org,wet}}(\rho_{ultra,wet})$ (dashed line in Fig. 4) compares well with the experimental data of Lees et al. [1979b], Lees [1987], Lees et al. [1995], indicated by circles in Fig. 4. The same is true for the ultrastructural water volume fraction,

$$\mathcal{F}_{\bar{f}_{H_2O,wet}}(\rho_{ultra,wet}) = 1 - \mathcal{F}_{\bar{f}_{org,wet}}(\rho_{ultra,wet}) - \mathcal{F}_{\bar{f}_{HA,wet}}(\rho_{ultra,wet}) \tag{32}$$

see dash-dotted line and triangle markers in Fig. 4. The relationships shown in Fig. 4 provoke the seemingly reasonable concept of a constant ratio between mineral increase and water/collagen decrease during biomineralization. Although the experiments of Lees et al. [1979b], Lees [1987], Lees et al. [1995] were all performed on cortical bone, the strong similarity of the ultrastructure in cortical bone and of that in trabecular bone [Gong et al., 1964] renders the relationships of Fig. 4 very probable to be valid also for trabecular bone.

The 'stoichiometric' functions (29), (31), and (32) are useful to estimate the ultrastructural composition of the bone specimens documented by McCarthy et al. [1990], see Table 6. In detail, $\rho_{\mu,empty}$ and $f_{\mu por}$ give access, via $\tilde{f}_{lac} = 2.1$ % and f_{vas} according to (19), to the mass density of the extravascular bone material (with water-filled lacunae),

$$\rho_{exvas} = \frac{\rho_{\mu,empty}}{1 - f_{vas}} \tag{33}$$

and to the density of the extracellular bone matrix or ultrastructure, reading as

$$\rho_{ultra,wet} = \frac{\rho_{exvas} - \rho_{H_2O}\,\tilde{f}_{lac}}{1 - \tilde{f}_{lac}} \tag{34}$$

Use of $\rho_{ultra,wet}$ in (29) and (31) yields the ultrastructural composition values $\bar{f}_{HA}$ and $\bar{f}_{col}$ (Table 6, columns 8 and 9).

The ultrastructural volume fraction of the fibrils and the extrafibrillar space, $\bar{f}_{fib}$ and $\bar{f}_{ef}$, [Fig. 3(d)] can be quantified on the basis of the generalized packing model of Lees et al. [1984b], Lees [1987], through

$$\bar{f}_{fib} = \bar{f}_{col} \times \frac{v_{fib}}{v_{col}}, \quad v_{fib} = b\,d_s\,5D \tag{35}$$

where $\bar{f}_{col}$ (wet or dry) is determined according to Eq.(26), (28), or (31), respectively. $v_{col} = 335.6\ nm^3$ is the volume of a single collagen molecule [Lees, 1987]. v_{fib} is the volume of one rhomboidal fibrillar unit with length $5D$, width b, and height d_s. b=1.47 nm is an average (rigid) collagen crosslink length valid for all mineralized tissues [Lees et al., 1984b], $D \approx 64$ nm is the axial macroperiod of staggered assemblies of type I collagen, and d_s is the tissue-specific neutron diffraction spacing between collagen molecules, which depends on the mineralization and the hydration state of the tissue [Lees et al., 1984a, Bonar et al., 1985, Lees et al., 1994b]. For wet tissues, d_s can be given in a dimensionless form [Hellmich and Ulm,

2003], as a function of $\rho_{ultra,wet}$ only. For the rather narrow range of tissue mass densities considered here, this function can be linearly approximated through

$$d_s = \mathcal{C} \times \rho_{ultra} + \mathcal{D} \tag{36}$$

where $\mathcal{C} = -0.2000, \mathcal{D} = 1.6580$ for wet tissues; and $\mathcal{C} = 0.1923, \mathcal{D} = 0.7465$ for dry tissues [Lees et al., 1984a, Lees, 1987]. Values for d_s and f_{fib}, derived from experiments of Lees et al. [1979b, 1983], Lees [1987], Lees et al. [1994a], McCarthy et al. [1990], Ashman and Rho [1988], are compiled in Tables 3, 5, 7 and 8.

The volume fractions for scales below the ultrastructure can be derived directly from $\bar{f}_{fib}$ and $\bar{f}_{col}$, on the basis of the finding of Hellmich and Ulm [2001, 2003] that the average hydroxyapatite concentration in the extracollageneous space of the ultrastructure of wet mineralized tissues is the same inside and outside the fibrils. Accordingly, the relative amount of hydroxyapatite in the extrafibrillar space reads as [Hellmich and Ulm, 2001, 2003]

$$\phi_{HA,ef} = \frac{1 - \bar{f}_{fib,wet}}{1 - \bar{f}_{col,wet}} \tag{37}$$

With this value at hand, the mineral volume fractions in the fibrillar [Fig. 3(b)] and the extrafibrillar space [Fig. 3(c)] are, for both wet and dry tissues,

$$\breve{f}_{HA} = \frac{\bar{f}_{HA}(1 - \phi_{HA,ef})}{\bar{f}_{fib}} \tag{38}$$

$$\breve{f}_{HA} = \frac{\phi_{HA,ef}\bar{f}_{HA}}{\bar{f}_{ef}} \tag{39}$$

see Tables 3 and 5 for the mammalian bones tested by Lees et al. [1979b, 1983], Lees [1987], Lees et al. [1994a], Table 7 for the equine bones tested by McCarthy et al. [1990], and Table 8 for the human and bovine bones tested by Ashman and Rho [1988].

Within the fibril, comprising the phases hydroxyapatite and wet collagen, the volume fraction of the latter reads as

$$\breve{f}_{wetcol} = 1 - \breve{f}_{HA} \tag{40}$$

Finally, the volume fraction of (molecular) collagen at the wet collagen level [Fig. 3(a)] can be calculated from $\bar{f}_{col}$ (wet or dry), through

$$\mathring{f}_{col} = \frac{\bar{f}_{col}}{\breve{f}_{wetcol}} \tag{41}$$

see Tables 3 and 5 for the mammalian bones tested by Lees et al. [1979b, 1983], Lees [1987], Lees et al. [1994a], Table 7 for the equine bones tested by McCarthy et al. [1990], and Table 8 for the human and bovine bones tested by Ashman and Rho [1988].

4.4 Elasticity experiments on bone – Experimental set IIb

Ultrasonic experiments are based on the measurements of velocities of plane waves. If the waves travel along the principal material directions of an orthotropic material, through a 3D medium, the wave propagation velocities allow for determination of the material stiffness constants, according to the theory of elastic waves [Fedorov, 1968]

$$C_{1111} = \rho v_1^2, \tag{42}$$

$$C_{2222} = \rho v_2^2, \tag{43}$$

$$C_{3333} = \rho v_3^2, \tag{44}$$

$$C_{2323} = G_{23} = \rho v_{23}^2 \tag{45}$$

$$C_{1313} = G_{13} = \rho v_{13}^2 \tag{46}$$

$$C_{1212} = G_{12} = \rho v_{12}^2 \tag{47}$$

$$C_{1122} = -\rho v_{12}^2 + \Big\{(\rho v_1^2 + \rho v_{12}^2 - 2\rho \times v_{12/12}^2)\times \times(\rho v_2^2 + \rho v_{12}^2 - 2\rho \times v_{12/12}^2)\Big\}^{1/2} \tag{48}$$

$$C_{1133} = -\rho v_{13}^2 + \Big\{(\rho v_1^2 + \rho v_{13}^2 - 2\rho \times v_{13/13}^2)\times \times(\rho v_3^2 + \rho v_{13}^2 - 2\rho \times v_{13/13}^2)\Big\}^{1/2} \tag{49}$$

$$C_{2233} = -\rho v_{23}^2 + \Big\{(\rho v_2^2 + \rho v_{23}^2 - 2\rho \times v_{23/23}^2)\times \times(\rho v_3^2 + \rho v_{23}^2 - 2\rho \times v_{23/23}^2)\Big\}^{1/2} \tag{50}$$

Hereby, ρ refers to the mass density of the material (at the ultrastructural or extravascular scale, depending on the wave length), v_i refers to a longitudinal wave travelling in the i-direction, and v_{ij} denotes the velocity of transverse waves traveling in the i-direction with particle motion in the j-direction. $v_{ij/ij}$ denotes the velocity of a (quasi-)longitudinal or a (quasi-)transverse wave traveling in the $(i+j)/\sqrt{2}$-direction with particle motion in the $i-j$ plane. Indices 1 and 2 refer to the radial (transverse) direction, and 3 refers to the axial (longitudinal) direction.

A typical device for the transmission of an elastic wave through a bone sample can be sketched as follows: A transmitter excites a specimen surface by a short impulse (signal) [Yoon and Katz, 1976] or by a continuous wave [Ashman and Rho, 1988], with an excitation frequency f. After the transition time t, a receiver records the arrival of the signal at the opposite surface of the specimen. Specimen length l and transition time t allow for computation of propagation velocity $v = l/t$. Excitation frequency f and propagation velocity v govern the wave length λ, through:

$$\lambda = \frac{v}{f} \tag{51}$$

In terms of micromechanics (see Section 2), the wavelength λ (a measure for $\mathcal{L}$) is significantly larger than

tissue	state	$\rho_{\mu,wet}$ or $\rho_{\mu,dry}$ [g/cm^3] given	WF^{μ}_{HA} [-] given	WF^{μ}_{org} [-] given	f_{vas} [-] given	v_1 [km/s] given	$C^{exp}_{ultra,1111}$ [GPa] Eqs.(17)^e, (18),(20), (21),(42)	f_{col} [-] Eqs.(17)^e,(18), (20)-(22),(24), (26),(28)	f_{HA} [-] Eqs.(17)^e,(18), (20)-(22),(23), (25),(27)	d_s [nm] Eqs.(17)^e (18),(20), (21),(36)
cow tibia	wet	2.02^a	0.68^a	0.22^a	0.03^f	3.18^a	21.0	0.30	0.48	1.24
cow tibia	wet	1.99^a	0.66^a	0.22^a	0.03^f	3.18^a	20.7	0.29	0.46	1.25
cow tibia	wet	1.95^a	0.64^a	0.23^a	0.03^f	3.18^a	20.2	0.30	0.44	1.26
cow tibia	wet	2.01^a	0.66^a	0.22^a	0.03^f	3.16^a	20.6	0.29	0.46	1.25
cow tibia	wet	2.04^a	0.64^a	0.24^a	0.03^f	3.27^a	22.4	0.33	0.46	1.24
cow tibia	wet	2.05^a	0.67^a	0.21^a	0.03^f	3.26^a	22.4	0.29	0.48	1.24
cow tibia	wet	2.07^b	0.66^c	0.22^c	0.03^f	3.32^b	23.4	0.30	0.48	1.23
elephant radius	wet	1.94^b	0.63^c	0.23^c	0.03^f	3.05^b	18.5	0.30	0.43	1.26
human femur	wet	1.93^b	0.70^c	0.23^c	0.03^f	3.13^b	19.4	0.30	0.47	1.26
deer antler	wet	1.78^b	0.51^c	0.31^c	0.03^f	2.38^b	10.3	0.37	0.32	1.29
deer antler	wet	1.74^b	0.52^c	0.32^c	0.03^f	2.40^b	10.2	0.37	0.32	1.30
cow tibia	dry	2.09^b	0.75^c	0.25^c	0.03^f	3.49^b	26.8	0.35	0.55	1.17
elephant radius	dry	1.97^b	0.73^c	0.27^c	0.03^f	3.35^b	23.3	0.35	0.51	1.15
human femur	dry	1.92^b	0.75^c	0.25^c	0.03^f	3.33^b	22.4	0.32	0.51	1.14
deer antler	dry	1.76^b	0.62^c	0.38^c	0.03^f	2.81^b	14.6	0.45	0.38	1.10
deer antler	dry	1.82^b	0.62^c	0.38^c	0.03^f	2.91^b	16.2	0.47	0.40	1.11
rabbit femur										
BAPN-treated	wet	2.05^d	0.66^d	0.20^d	0.10^g	3.33^d	24.3	0.29	0.49	1.22
BAPN-treated	wet	2.04^d	0.66^d	0.21^d	0.09^g	3.27^d	23.2	0.30	0.49	1.22
BAPN-treated	wet	2.04^d	0.66^d	0.21^d	0.03^g	3.26^d	22.3	0.29	0.47	1.24
BAPN-treated	wet	2.05^d	0.65^d	0.21^d	0.06^g	3.24^d	22.5	0.29	0.48	1.23
BAPN-treated	wet	1.98^d	0.63^d	0.21^d	0.06^g	3.11^d	20.0	0.28	0.44	1.25
BAPN-treated	wet	1.96^d	0.62^d	0.21^d	0.22^g	3.03^d	20.7	0.31	0.48	1.21
fluor-treated	wet	2.00^d	0.70^d	0.17^d	0.03^h	3.20^d	21.0	0.23	0.49	1.25
fluor-treated	wet	2.04^d	0.71^d	0.16^d	0.08^h	3.22^d	22.3	0.23	0.52	1.23
fluor-treated	wet	1.86^d	0.65^d	0.17^d	0.10^h	2.74^d	14.8	0.22	0.44	1.26
fluor-treated	wet	1.65^d	0.56^d	0.16^d	0.35^h	2.57^d	13.3	0.21	0.39	1.25

^{a} experimental data: Lees et al. [1979b]

^{b} experimental data: Lees et al. [1983]

^{c} experimental data: Lees [1987]

^{d} experimental data: Lees et al. [1994a]

^{e} computed with $\bar{f}_{lac}$ =2.1 %, according to Eq.(17) with f_{vas} =3 % and f_{lac} =2 %, determined from micrograph of Fig.1 in [Lees et al., 1979a], see also Fig. 1(c), on the basis of Eq.(15) and (16)

^{f} determined from micrograph of Fig.1 in [Lees et al., 1979a], see also Fig. 1(c), on the basis of Eq.(15)

^{g} determined from micrographs of Fig.9 in [Lees et al., 1994a]

^{h} determined from micrographs of Fig.10 in [Lees et al., 1994a]

Table 2 Compilation of experimental data for the microstructural wet and dry tissue mass densities, $\rho_{\mu,wet}$ and $\rho_{\mu,dry}$, for the weight fractions of hydroxyapatite and organic matter, WF^{μ}_{HA} and WF^{μ}_{org}, for the volume fraction of Haversian canals, f_{vas}, and for the longitudinal sonic velocity in radial direction, v_1, of various mammalian bone specimens; evaluation of experimental data for determination of the ultrastructural normal stiffness component in radial direction, $C^{exp}_{ultra,1111}$, of ultrastructural volume fractions of hydroxyapatite and collagen, $\bar{f}_{HA}$ and $\bar{f}_{col}$, as well as of the neutron diffraction spacing d_s

the characteristic length of a representative volume element (RVE) of the experimentally characterized material. This allows for interpretation of different ultrasonic tests:

- In the ultrasonic tests of Lees et al. [1979b, 1983, 1994a], excitation frequencies of 10 MHz were used. Given a typical wave propagation velocity of ~ 3 km/s in bone specimens, the characteristic corresponding wave lengths $\lambda = \mathcal{L}$ were of the order of 300 μm. The characteristic length of the experimentally characterized material must obey $\ell \ll 300$ μm, which is the case for the ultrastructure with $\ell \approx 5$ μm [Figures 1(e) and 3(d)]. Hence, the wave velocities measured in the *10 MHz - frequency regime* refer to the *elastic stiffness of bone ultrastructure*.
- In the ultrasonic tests performed by Ashman et al. [1984], Ashman and Rho [1988], McCarthy et al. [1990], excitation frequencies of 2.25 MHz were used. Given a typical velocity of ~ 3 km/s in these bone specimens, corresponding wavelengths were, according to Eq.(51), of the order of 1.3 mm. The characteristic length ℓ of experimentally characterized material must be significantly smaller than 1.3 mm. This is the case for the extravascular bone material with $\ell \approx 100$ μm , see Figure 3(e). Hence, the wave velocities measured in the *2.25 MHz - frequency regime* refer to the *stiffness of extravascular bone material*.

4.4.1 Ultrasonic tests with 10 MHz frequency – characterization of ultrastructure Lees et al. [1979b, 1983, 1994a] reported velocities v_1 and v_3 of longitudinal waves traveling in the radial and in the axial direction of cortical bone specimens; along with microstructural mass densities of wet specimens, $\rho_{\mu,wet}$, and vascular porosity f_{vas} (Tables 2 and 4, columns 3, 6 and 7). The latter give access to ultrastructural mass densities $\rho_{ultra,wet}$ and $\rho_{ultra,dry}$ via Eq.(17) with $\tilde{f}_{lac}$ =2.1 %, Eq.(18), (20), and (21). Insertion of these values for v_1, v_3, and $\rho = \rho_{ultra,wet}$ or $\rho = \rho_{ultra,dry}$, into Eq.(42) and Eq.(44) yields specimen-specific experimental stiffness values $C^{exp}_{ultra,1111}$

tissue	state	$\bar{f}_{col}$ [-] Table 2	$\bar{f}_{HA}$ [-] Table 2	d_s [nm] Table 2	$\bar{f}_{fib}$ [-] Eq.(35)	$\check{f}_{HA}$ [-] Eqs.(37), (39)	$\check{f}_{HA}$ [-] Eqs.(37), (38)	$\hat{f}_{col}$ [-] Eqs.(40), (41)
cow tibia	wet	0.30	0.48	1.24	0.52	0.68	0.29	0.42
cow tibia	wet	0.29	0.46	1.25	0.51	0.65	0.28	0.41
cow tibia	wet	0.30	0.44	1.26	0.53	0.62	0.27	0.41
cow tibia	wet	0.29	0.46	1.25	0.51	0.66	0.28	0.41
cow tibia	wet	0.33	0.46	1.24	0.58	0.68	0.29	0.47
cow tibia	wet	0.29	0.48	1.24	0.50	0.68	0.29	0.41
cow tibia	wet	0.30	0.48	1.23	0.53	0.69	0.29	0.43
elephant radius	wet	0.30	0.43	1.26	0.53	0.61	0.27	0.41
human femur	wet	0.30	0.47	1.26	0.53	0.68	0.29	0.42
deer antler	wet	0.37	0.32	1.29	0.67	0.51	0.23	0.48
deer antler	wet	0.37	0.32	1.30	0.68	0.51	0.23	0.49
cow tibia	dry	0.35	0.55	1.17	0.57	0.85	0.33	0.52
elephant radius	dry	0.35	0.51	1.15	0.57	0.78	0.30	0.50
human femur	dry	0.32	0.51	1.14	0.51	0.74	0.28	0.44
deer antler	dry	0.45	0.38	1.10	0.69	0.69	0.25	0.59
deer antler	dry	0.47	0.40	1.11	0.73	0.74	0.27	0.64
rabbit femur								
BAPN-treated	wet	0.29	0.49	1.22	0.49	0.69	0.29	0.40
BAPN-treated	wet	0.30	0.49	1.22	0.51	0.70	0.29	0.42
BAPN-treated	wet	0.29	0.47	1.24	0.50	0.66	0.28	0.40
BAPN-treated	wet	0.29	0.48	1.23	0.51	0.67	0.28	0.41
BAPN-treated	wet	0.28	0.44	1.25	0.50	0.62	0.27	0.39
BAPN-treated	wet	0.31	0.48	1.21	0.53	0.69	0.28	0.43
fluor-treated	wet	0.23	0.49	1.25	0.40	0.64	0.27	0.31
fluor-treated	wet	0.23	0.52	1.23	0.39	0.67	0.28	0.31
fluor-treated	wet	0.22	0.44	1.26	0.39	0.56	0.25	0.29
fluor-treated	wet	0.21	0.39	1.25	0.37	0.49	0.21	0.27

Table 3 Compilation of experimental data for ultrastructural volume fractions of hydroxyapatite and collagen, $\bar{f}_{HA}$ and $\bar{f}_{col}$, and for the neutron diffraction spacing d_s, of various mammalian bone specimens, taken from Table 2; evaluation of experimental data for determination of ultrastructural volume fractions of fibrils, $\bar{f}_{fib}$, of extrafibrillar and fibrillar volume fraction of mineral, $\check{f}_{HA}$ and $\check{\check{f}}_{HA}$, and of (molecular) collagen volume fraction within the wet collagen matrix, $\hat{\hat{f}}_{col}$

tissue	state	$\rho_{\mu,wet}$ or $\rho_{\mu,dry}$ [g/cm^3] given	WF^{μ}_{HA} [-] given	WF^{μ}_{org} [-] given	f_{vas} [-] given	v_3 [km/s] given	$C^{exp}_{ultra,3333}$ [GPa] Eqs.(17)^e, (18),(20), (21),(44)	$\bar{f}_{col}$ [-] Eqs.(17)^e,(18), (20)-(22),(24), (26),(28)	$\bar{f}_{HA}$ [-] Eqs.(17)^e,(18), (20)-(22),(23), (25),(27)	d_s [nm] Eqs.(17)^e (18),(20), (21),(36)
cow tibia	wet	2.06^a	0.66^a	0.22^a	0.03^f	3.92^a	32.5	0.30	0.48	1.23
cow tibia	wet	2.05^a	0.66^a	0.22^a	0.03^f	3.92^a	32.4	0.30	0.47	1.24
cow tibia	wet	2.02^a	0.62^a	0.24^a	0.03^f	3.81^a	30.1	0.32	0.44	1.24
cow tibia	wet	2.02^a	0.63^a	0.23^a	0.03^f	3.86^a	30.9	0.31	0.44	1.24
cow tibia	wet	2.00^a	0.64^a	0.23^a	0.03^f	3.90^a	31.2	0.31	0.45	1.25
cow tibia	wet	2.05^a	0.64^a	0.23^a	0.03^f	3.88^a	31.7	0.32	0.46	1.24
cow tibia	wet	2.10^a	0.67^a	0.21^a	0.03^f	3.88^a	32.5	0.30	0.49	1.23
cow tibia	wet	2.08^a	0.66^a	0.22^a	0.03^f	3.92^a	32.8	0.30	0.48	1.23
cow tibia	wet	2.06^b	0.66^c	0.22^c	0.03^f	4.18^b	37.0	0.30	0.48	1.23
elephant radius	wet	1.93^b	0.63^c	0.23^c	0.03^f	3.89^b	29.9	0.30	0.43	1.26
human femur	wet	1.96^b	0.70^c	0.23^c	0.03^f	3.76^b	28.4	0.30	0.48	1.26
deer antler	wet	1.74^b	0.51^c	0.31^c	0.03^f	3.08^b	16.9	0.36	0.31	1.30
deer antler	wet	1.73^b	0.52^c	0.32^c	0.03^f	3.15^b	17.5	0.37	0.32	1.30
cow tibia	dry	2.10^b	0.75^c	0.25^c	0.03^f	4.47^b	44.2	0.35	0.55	1.17
elephant radius	dry	1.97^b	0.73^c	0.27^c	0.03^f	4.22^b	36.9	0.35	0.51	1.15
human femur	dry	1.96^b	0.75^c	0.25^c	0.03^f	3.97^b	32.5	0.33	0.52	1.14
deer antler	dry	1.75^b	0.62^c	0.38^c	0.03^f	3.72^b	25.5	0.44	0.38	1.10
deer antler	dry	1.83^b	0.62^c	0.38^c	0.03^f	3.93^b	29.8	0.47	0.40	1.12

^{a} experimental data: [Lees et al., 1979b]

^{b} experimental data: [Lees et al., 1983]

^{c} experimental data: [Lees, 1987]

^{d} experimental data: [Lees et al., 1979a]

^{e} computed with $\bar{f}_{lac}$ =2.1 %, according to Eq.(17) with f_{vas} =3 % and f_{lac} =2 %, determined from micrograph of Fig.1 in [Lees et al., 1979a], see also Fig. 1(c), on the basis of Eq.(15) and (16)

^{f} determined from micrograph of Fig.1 in [Lees et al., 1979a], see also Fig. 1(c), on the basis of Eq.(15)

Table 4 Compilation of experimental data for the microstructural wet and dry tissue mass densities, $\rho_{\mu,wet}$ and $\rho_{\mu,dry}$, for the weight fractions of hydroxyapatite and organic matter, WF^{μ}_{HA} and WF^{μ}_{org}, for the volume fraction of Haversian canals, f_{vas}, and for the longitudinal sonic velocity in axial direction, v_3, of various mammalian bone specimens; evaluation of experimental data for determination of the ultrastructural normal stiffness component in axial direction, $C^{exp}_{ultra,3333}$, of ultrastructural volume fractions of hydroxyapatite and collagen, $\bar{f}_{HA}$ and $\bar{f}_{col}$, as well as of the neutron diffraction spacing d_s

tissue	state	f_{col} [-] Table 4	f_{HA} [-] Table 4	d_s [nm] Table 4	f_{fib} [-] Eq.(35)	f_{HA} [-] Eqs.(37), (39)	f_{HA} [-] Eqs.(37), (38)	f_{col} [-] Eqs.(40), (41)
cow tibia	wet	0.30	0.48	1.23	0.52	0.68	0.29	0.43
cow tibia	wet	0.30	0.47	1.24	0.52	0.68	0.29	0.42
cow tibia	wet	0.32	0.44	1.24	0.57	0.65	0.28	0.45
cow tibia	wet	0.31	0.44	1.24	0.55	0.65	0.28	0.44
cow tibia	wet	0.31	0.45	1.25	0.53	0.65	0.28	0.42
cow tibia	wet	0.32	0.46	1.24	0.55	0.68	0.29	0.44
cow tibia	wet	0.30	0.49	1.23	0.51	0.70	0.29	0.42
cow tibia	wet	0.30	0.48	1.23	0.52	0.69	0.29	0.43
cow tibia	wet	0.30	0.48	1.23	0.52	0.68	0.29	0.43
elephant radius	wet	0.30	0.43	1.26	0.53	0.61	0.26	0.41
human femur	wet	0.30	0.48	1.26	0.53	0.69	0.30	0.43
deer antler	wet	0.36	0.31	1.30	0.66	0.49	0.22	0.47
deer antler	wet	0.37	0.32	1.30	0.68	0.50	0.23	0.48
cow tibia	dry	0.35	0.55	1.17	0.58	0.85	0.33	0.53
elephant radius	dry	0.35	0.51	1.15	0.57	0.78	0.30	0.50
human femur	dry	0.33	0.52	1.14	0.52	0.77	0.29	0.46
deer antler	dry	0.44	0.38	1.10	0.69	0.69	0.24	0.59
deer antler	dry	0.47	0.40	1.12	0.73	0.75	0.27	0.64

Table 5 Compilation of experimental data for ultrastructural volume fractions of hydroxyapatite and collagen, $\bar{f}_{HA}$ and $\bar{f}_{col}$, and for the neutron diffraction spacing d_s, of various mammalian bone specimens, taken from Table 4; evaluation of experimental data for determination of ultrastructural volume fractions of fibrils, $\bar{f}_{fib}$, of extrafibrillar and fibrillar volume fraction of mineral, $\check{f}_{HA}$ and $\check{\check{f}}_{HA}$, and of (molecular) collagen volume fraction within the wet collagen matrix, $\hat{\hat{f}}_{col}$

and $C^{exp}_{ultra,3333}$, see Tables 2 and 4, column 8, as well as Fig. 5 (x-axis).

4.4.2 Ultrasonic tests with 2.25 MHz frequency – characterization of extravascular bone material McCarthy et al. [1990] reported velocities of longitudinal waves traveling in the radial (transverse) direction of specimens from the dorsal cortex of equine third metacarpus, $v_1 \approx v_2$, and velocities of longitudinal waves traveling in the axial (longitudinal) direction of the aforementioned equine bone specimens, v_3; along with microstructural (=apparent=macroscopic) mass densities of specimens with empty Haversian canals, $\rho_{\mu,empty}$, and microporosity $f_{\mu por}$ (Table 6, columns 1 to 4). The latter give access to extravascular mass densities ρ_{exvas} via Eq.(19) with $\tilde{f}_{lac}$ =2.1 % and Eq.(33). Insertion of these values for v_1, v_3, and $\rho = \rho_{exvas}$ into Eq.(42) and Eq.(44) yields specimen-specific experimental stiffness values $C^{exp}_{exvas,1111}$ and $C^{exp}_{exvas,3333}$, see Table 6, columns 5 and 6, as well as Fig. 6 (x-axis).

Ashman and Rho [1988] reported velocities of longitudinal waves traveling in the axial (longitudinal) direction of bovine and human trabecular bone specimens, v_3; along with extravascular mass densities ρ_{exvas} (Table 8, columns 3 and 4). Insertion of these values for v_3 and $\rho = \rho_{exvas}$ into Eqn.(44) yields specimen-specific experimental stiffness values $C^{exp}_{exvas,3333}$, see Table 8, column 5, and Figure 6 (x-axis).

Also Ashman et al. [1984] used wave lengths refering to the extravascular bone material, but based computation of stiffness values according to Eq.(42) to Eq.(50) on a microstructural mass density $\rho_{\mu,wet}$ =1.90 g/ml, averaged over 60 human femoral specimens. Hence, these stiffness values have to be corrected by the factor

$$\frac{\rho_{exvas}}{\rho_{\mu,wet}} = \frac{\rho_{\mu,wet} - \rho_{H_2O}\, f_{vas}}{(1 - f_{vas})\, \rho_{\mu,wet}} \tag{52}$$

with f_{vas} =3 % (Table 4, row 11, column 6), yielding the following experimental stiffness tensor

$$\mathbb{C}^{exp}_{exvas} = \begin{pmatrix} C_{1111} & C_{1122} & C_{1133} & 0 & 0 & 0 \\ C_{1122} & C_{2222} & C_{2233} & 0 & 0 & 0 \\ C_{1133} & C_{2233} & C_{3333} & 0 & 0 & 0 \\ 0 & 0 & 0 & 2C_{2323} & 0 & 0 \\ 0 & 0 & 0 & 0 & 2C_{1313} & 0 \\ 0 & 0 & 0 & 0 & 0 & 2C_{1212} \end{pmatrix} = \begin{pmatrix} 18.5 & 10.3 & 10.4 & 0 & 0 & 0 \\ 10.3 & 20.8 & 11.0 & 0 & 0 & 0 \\ 10.4 & 11.0 & 28.4 & 0 & 0 & 0 \\ 0 & 0 & 0 & 12.9 & 0 & 0 \\ 0 & 0 & 0 & 0 & 11.5 & 0 \\ 0 & 0 & 0 & 0 & 0 & 9.3 \end{pmatrix} \tag{53}$$

4.5 Comparison between stiffness predictions and experiments

The stiffness values at the extracellular (ultrastructural) and extravascular scale predicted by the five-step homogenization scheme [Fig. 3] for tissue-specific volume fractions (Subsection 4.3, experimental set IIa) on the basis of tissue-independent 'universal' phase stiffness properties (experimental set I, Table 1) are compared to corresponding experimentally determined tissue-specific stiffness values from experimental set IIb (Subsection 4.4). To quantify the model's predictive capabilities, we consider the mean and the standard deviation of the relative error between stiffness predictions and experiments,

$$\bar{e} = \frac{1}{n}\sum e_i = \frac{1}{n}\sum \frac{C^{pred}_{ijkl} - C^{exp}_{ijkl}}{C^{exp}_{ijkl}} \tag{54}$$

$$e_S = \left[\frac{1}{n-1}\sum (e_i - \bar{e})^2\right]^{\frac{1}{2}} \tag{55}$$

$\rho_{\mu,empty}$ g/cm^3 given	$f_{\mu por}$ [-] given	v_3 [km/s] given	v_1 [km/s] given	$C^{exp}_{exhav,3333}$ [GPa] Eqs.(19)^a, Eq.(33),(44)	$C^{exp}_{exhav,1111}$ [GPa] Eqs.(19)^a, Eq.(33),(42)	f_{vas} [-] Eq.(19)^a	$\bar{f}_{col}$ [-] Eqs.(33),(34), (29),(31)	$\bar{f}_{HA}$ [-] Eqs.(33), (34),(29)	d_s [nm] Eqs.(33), (34),(36)
2.03	0.10	4.30	3.60	40.6	28.4	0.08	0.21	0.56	1.21
2.02	0.08	4.20	3.55	37.7	27.0	0.06	0.23	0.53	1.23
2.01	0.11	4.10	3.45	36.7	26.0	0.09	0.21	0.56	1.22
2.01	0.07	4.40	3.65	40.8	28.1	0.05	0.25	0.51	1.23
2.00	0.09	4.20	3.55	37.7	27.0	0.07	0.23	0.53	1.23
2.00	0.07	4.20	3.40	37.0	24.2	0.05	0.25	0.50	1.23
2.00	0.06	4.30	3.58	38.4	26.5	0.04	0.26	0.49	1.24
1.98	0.12	4.10	3.42	36.7	25.6	0.10	0.21	0.56	1.22
1.98	0.12	4.15	3.35	37.6	24.5	0.10	0.21	0.56	1.22
1.98	0.10	4.15	3.50	36.9	26.2	0.08	0.23	0.53	1.23
1.98	0.10	4.30	3.60	39.6	27.7	0.08	0.23	0.53	1.23
1.97	0.10	4.03	3.50	34.5	26.1	0.08	0.24	0.52	1.23
1.97	0.12	4.20	3.35	38.4	24.4	0.10	0.22	0.55	1.22
1.96	0.11	4.03	3.50	34.7	26.2	0.09	0.23	0.53	1.23
1.96	0.10	4.20	3.60	37.4	27.5	0.08	0.24	0.52	1.23
1.95	0.14	3.95	3.52	34.3	27.3	0.12	0.21	0.56	1.21
1.95	0.09	4.03	3.40	33.8	24.1	0.07	0.26	0.50	1.24
1.95	0.12	4.10	3.35	36.2	24.2	0.10	0.23	0.54	1.22
1.95	0.18	4.10	3.42	38.6	27.0	0.16	0.17	0.63	1.19
1.95	0.11	4.15	3.45	36.5	25.2	0.09	0.24	0.52	1.23
1.95	0.14	4.15	3.55	37.9	27.7	0.12	0.21	0.56	1.21
1.93	0.12	4.03	3.35	34.5	23.9	0.10	0.24	0.52	1.23
1.93	0.09	4.10	3.30	34.7	22.5	0.07	0.26	0.48	1.24
1.93	0.13	4.25	3.48	38.9	26.0	0.11	0.23	0.54	1.22
1.92	0.12	4.00	3.35	33.9	23.8	0.10	0.24	0.52	1.23
1.92	0.10	4.03	3.40	33.6	24.0	0.08	0.26	0.49	1.24
1.92	0.12	4.20	3.35	37.4	23.8	0.10	0.24	0.52	1.23
1.92	0.11	4.20	3.40	37.0	24.2	0.09	0.25	0.50	1.23
1.91	0.12	4.13	3.35	35.9	23.7	0.10	0.25	0.51	1.23
1.91	0.22	4.17	3.48	41.1	28.5	0.20	0.14	0.66	1.18
1.91	0.18	4.35	3.45	42.6	26.8	0.16	0.19	0.60	1.20
1.90	0.25	3.95	3.13	38.0	23.8	0.23	0.11	0.71	1.17
1.90	0.12	4.00	3.40	33.6	24.2	0.10	0.25	0.50	1.23
1.82	0.09	4.00	3.30	31.1	21.2	0.07	0.31	0.41	1.26
1.76	0.30	3.85	3.20	35.6	24.6	0.28	0.13	0.69	1.17

^{a} computed with $\bar{f}_{lac}$ =2.1 %, according to Eq.(17), with f_{lac} = 2% and f_{vas} = 3%, determined from micrograph of Fig. 1(c) on the basis of Eqs.(15) and (16)

Table 6 Compilation of experimental data for the microstructural mass density of tissues with empty micropores, $\rho_{\mu,empty}$, for the microporosity $f_{\mu por}$, and for the longitudinal sonic velocity in axial and in transveral direction, v_3 and v_1, of equine cortical bone [McCarthy et al., 1990]; evaluation of experimental data for determination of the normal stiffness component in axial and in transversal direction, C^{exp}_{3333} and C^{exp}_{1111}, of ultrastructural volume fractions of hydroxyapatite and collagen, $\bar{f}_{HA}$ and $\bar{f}_{col}$, as well as of the neutron diffraction spacing d_s.

$\bar{f}_{col}$ [—] Table 6	$\bar{f}_{HA}$ [-] Table 6	d_s [nm] Table 6	$\bar{f}_{fib}$ [-] Eq.(35)	$\check{f}_{HA}$ [-] Eqs.(37), (39)	$\check{f}_{HA}$ [-] Eqs.(37), (38)	$\mathring{f}_{col}$ [-] Eqs.(40), (41)
0.21	0.56	1.21	0.36	0.71	0.29	0.30
0.23	0.53	1.23	0.40	0.69	0.29	0.33
0.21	0.56	1.22	0.37	0.71	0.29	0.30
0.25	0.51	1.23	0.43	0.68	0.28	0.34
0.23	0.53	1.23	0.40	0.69	0.29	0.33
0.25	0.50	1.23	0.43	0.67	0.28	0.35
0.26	0.49	1.24	0.45	0.66	0.28	0.36
0.21	0.56	1.22	0.36	0.71	0.29	0.30
0.21	0.56	1.22	0.36	0.71	0.29	0.30
0.23	0.53	1.23	0.40	0.69	0.29	0.33
0.23	0.53	1.23	0.40	0.69	0.29	0.33
0.24	0.52	1.23	0.41	0.69	0.29	0.33
0.22	0.55	1.22	0.37	0.70	0.29	0.31
0.23	0.53	1.23	0.40	0.69	0.29	0.33
0.24	0.52	1.23	0.42	0.68	0.29	0.34
0.21	0.56	1.21	0.35	0.71	0.29	0.30
0.26	0.50	1.24	0.44	0.67	0.28	0.36
0.23	0.54	1.22	0.39	0.69	0.29	0.32
0.17	0.63	1.19	0.28	0.75	0.30	0.24
0.24	0.52	1.23	0.42	0.68	0.29	0.34
0.21	0.56	1.21	0.35	0.71	0.29	0.30
0.24	0.52	1.23	0.41	0.69	0.29	0.33
0.26	0.48	1.24	0.46	0.66	0.28	0.37
0.23	0.54	1.22	0.39	0.70	0.29	0.32
0.24	0.52	1.23	0.42	0.68	0.29	0.34
0.26	0.49	1.24	0.45	0.66	0.28	0.36
0.24	0.52	1.23	0.42	0.68	0.29	0.34
0.25	0.50	1.23	0.43	0.67	0.28	0.35
0.25	0.51	1.23	0.42	0.68	0.28	0.34
0.14	0.66	1.18	0.24	0.77	0.31	0.21
0.19	0.60	1.20	0.31	0.73	0.30	0.27
0.11	0.71	1.17	0.18	0.80	0.31	0.16
0.25	0.50	1.23	0.43	0.67	0.28	0.35
0.31	0.41	1.26	0.55	0.60	0.26	0.42
0.13	0.69	1.17	0.21	0.79	0.31	0.18

Table 7 Compilation of experimental data of ultrastructural volume fractions of hydroxyapatite and collagen, $\bar{f}_{HA}$ and $\bar{f}_{col}$, as well as of neutron diffraction spacing d_s, taken from Table 6; evaluation of experimental data for determination of ultrastructural volume fractions of fibrils, $\bar{f}_{fib}$, of extrafibrillar and fibrillar volume fraction of mineral, $\check{f}_{HA}$ and $\check{\check{f}}_{HA}$, and of (molecular) collagen volume fraction within the wet collagen matrix, $\mathring{f}_{col}$

tissue	state	ρ_{exvas} [g/cm^3] given	v_3 [km/s] given	$C^{exp}_{exvas,3333}$ [GPa] Eq.(44)	$\bar{f}_{col}$ [-] Eqs.(34)^a, (29),(31)	$\bar{f}_{HA}$ [-] Eqs.(34)^a, (29)	d_s [-] Eqs.(34)^a, (36)	$\bar{f}_{fib}$ [nm] Eq.(35)	$\check{f}_{HA}$ Eqs.(37), (39)	$\check{f}_{HA}$ Eqs.(37), (38)	$\mathring{f}_{col}$ Eqs.(40), (41)
human femur	wet	1.80	2.64	12.6	0.37	0.33	1.29	0.67	0.52	0.23	0.48
human femur	wet	1.78	2.72	13.2	0.38	0.31	1.30	0.70	0.50	0.23	0.49
human femur	wet	1.73	2.75	13.1	0.40	0.28	1.31	0.74	0.47	0.21	0.51
bovine femur	wet	1.74	2.50	10.9	0.40	0.29	1.31	0.73	0.48	0.22	0.51

^{a} computed with $\tilde{f}_{lac}$ =2.1 %, according to Eq.(17), with f_{lac} = 2% and f_{vas} = 3%, determined from micrograph of Fig. 1(c) on the basis of Eqs.(15) and (16)

Table 8 Compilation of experimental data for the extravascular mass density of tissues with empty micropores, ρ_{exvas}, and for the longitudinal sonic velocity in axial direction, v_3, of human and bovine trabecular bone [Ashman and Rho, 1988]; evaluation of experimental data for determination of the normal stiffness component in axial direction, $C^{exp}_{exvas,3333}$, of ultrastructural volume fractions of hydroxyapatite and collagen, $\bar{f}_{HA}$ and $\bar{f}_{col}$, of the neutron diffraction spacing d_s, of ultrastructural volume fraction of fibrils, $\bar{f}_{fib}$, of extrafibrillar and fibrillar volume fraction of mineral, $\check{f}_{HA}$ and $\check{f}_{HA}$, as well as of (molecular) collagen volume fraction within the wet collagen matrix, $\mathring{f}_{col}$

with summation over n values C^{exp}_{ijkl} per experimental protocol.

4.5.1 Ultrastructural level Evaluation of data for various mammals (columns 3 to 6 of Tables 2 and 4) through Eq.(17) with $\tilde{f}_{lac}$ =2.1 %, Eq.(18), Eq.(20) – Eq.(28), Eq.(35)– Eq.(41) delivers composition values $\bar{f}_{fib}$, $\check{f}_{HA}$, $\check{f}_{HA}$, and $\mathring{f}_{col}$, see Tables 3 and 5, corresponding to the experimental stiffness values in Figure 5 (x-axis), see also column 8 in Tables 2 and 4. Insertion of these composition values $\bar{f}_{fib}$, $\check{f}_{HA}$, $\check{f}_{HA}$, and $\mathring{f}_{col}$ into Eq.(2) to Eq.(13) delivers tissue-specific stiffness estimates $\mathbb{C}^{MTII}_{ultra}$. Stiffness predictions $C^{pred}_{1111} = C^{MTII}_{ultra,1111}$ and $C^{pred}_{3333} = C^{MTII}_{ultra,3333}$ are compared to corresponding experimental stiffness values (Figure 5). The satisfactory agreement between model predictions and experiments is quantified by prediction errors of -3±14 % [mean value ± standard deviation according to Eq.(54) and (55)] for the axial (longitudinal) normal stiffness, and of -10±9 % for the radial (transverse) normal stiffness.

4.5.2 Extravascular level Evaluation of data for equine cortical bone (columns 1 and 2 of Table 6) through Eq.(19) with $\tilde{f}_{lac}$ =2.1 %, (33), (34), (29), (31), (35) – (41) delivers composition values $\bar{f}_{fib}$, $\check{f}_{HA}$, $\check{f}_{HA}$, $\mathring{f}_{col}$ (see Table 7), corresponding to the experimental stiffness values labelled M90 in Fig. 6 (x-axis), see also columns 5 and 6 of Table 6. Insertion of these composition values $\tilde{f}_{lac}$, $\bar{f}_{fib}$, $\check{f}_{HA}$, $\check{f}_{HA}$, and $\mathring{f}_{col}$ into Eq.(2) to Eq.(14) delivers tissue-specific stiffness estimates $\mathbb{C}^{MTIII}_{exvas}$. Stiffness predictions $C^{pred}_{1111} = C^{MTIII}_{exvas,1111}$ and $C^{pred}_{3333} = C^{MTIII}_{exvas,3333}$ are compared to corresponding experimental stiffness values labelled M90 in Figure 6. The satisfactory agreement between model predictions and experiments is quantified by prediction errors of +1±22 % [mean value ± standard deviation according to Eq.(54) and (55)] for the axial (longitudinal) normal stiffness and of +2±30 % for the radial (transverse) normal stiffness.

Evaluation of data for human and bovine trabecular bone material (column 3 of Table 8) through Eq.(34) with $\tilde{f}_{lac}$ =2.1 %, Eq.(29), (31), (35) – (41), delivers composition values $\bar{f}_{fib}$, $\check{f}_{HA}$, $\check{f}_{HA}$, $\mathring{f}_{col}$ (see Table 8), corresponding to the experimental stiffness values labelled

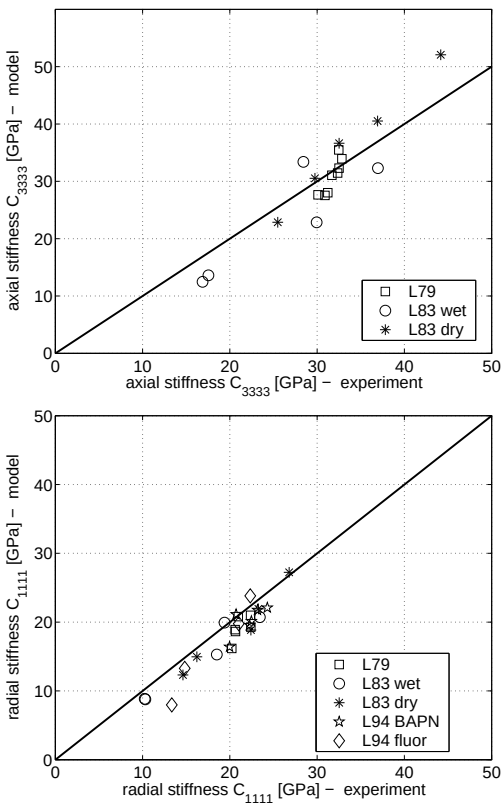

Fig. 5 Comparison between model predictions and experiments at the extracellular or ultrastructural scale [Fig. 3(d)]: (a) axial normal stiffness values, (b) radial normal stiffness values; (10 MHz ultrasonic experiments: L 79. . . [Lees et al., 1979b], L83 . . . [Lees et al., 1983], L94 . . . [Lees et al., 1994a])

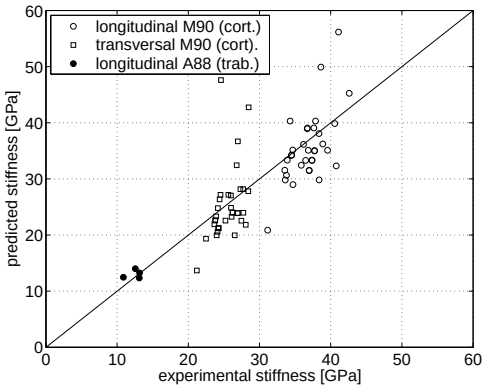

Fig. 6 Comparison between model predictions and experiments at the extravascular scale (2.25 MHz ultrasonic experiments of A88 . . . [Ashman and Rho, 1988], M90 . . . McCarthy et al. [1990])

A88 in Fig. 6 (x-axis), see also column 5 of Table 8. Insertion of these composition values $\tilde{f}_{lac}$, $\bar{f}_{fib}$, $\check{f}_{HA}$, $\check{f}_{HA}$, and $\mathring{f}_{col}$ into Eq.(2) to Eq.(14) delivers tissue-specific stiffness estimates $\mathbb{C}^{MTIII}_{exvas}$. Stiffness predictions $C^{pred}_{3333} = C^{MTIII}_{exvas,3333}$ are compared to corresponding experimental stiffness values labelled A88 in Fig. 6. The satisfactory agreement between model predictions and experiments is quantified by prediction errors of +5±10 % [mean value ± standard deviation according to Eqn.(54) and (55)].

Evaluation of data for a typical human femur tissue (Table 4, row 11, columns 3 to 6) through Eq.(17) with $\tilde{f}_{lac}$ =2.1 %, Eq.(18), (20), (22) – (24) delivers ultrastructural weight fractions of $WF^{ultra}_{HA} = 0.72$ and $WF^{ultra}_{org} = 0.24$, typical also for the average human femoral specimen tested by Ashman et al. [1984], characterized by $\rho_{\mu,wet} = 1.90$ g/ml (see Fig.9 of [Ashman et al., 1984]) and f_{vas} =3 % (Table 4). WF^{ultra}_{HA},WF^{ultra}_{org}, $\rho_{\mu,wet}$ and f_{vas} deliver, via Eq.(17) with $\tilde{f}_{lac}$ =2.1 %, (18), (20), (25), (26), (35) – (41), typical composition values of $\bar{f}_{fib} = 0.52$, $\check{f}_{HA} = 0.66$, $\check{f}_{HA} = 0.29$, and $\mathring{f}_{col} = 0.41$. Insertion of these composition values $\tilde{f}_{lac}$, $\bar{f}_{fib}$, $\check{f}_{HA}$, $\check{f}_{HA}$, and $\mathring{f}_{col}$ into Eq.(2) to Eq.(14) delivers a stiffness estimate (model prediction) of

$$\mathbb{C}^{MTIII}_{micro} = \begin{pmatrix} 18.3 & 8.1 & 8.1 & 0 & 0 & 0 \\ 8.1 & 18.3 & 8.1 & 0 & 0 & 0 \\ 8.1 & 8.1 & 28.4 & 0 & 0 & 0 \\ 0 & 0 & 0 & 12.5 & 0 & 0 \\ 0 & 0 & 0 & 0 & 12.5 & 0 \\ 0 & 0 & 0 & 0 & 0 & 10.1 \end{pmatrix} \tag{56}$$

We observe a good agreement of this prediction with experimental values of Eq.(53), being quantified by relative prediction errors of ±0% for C_{3333}, -7% for C_{1111}, 3% for C_{1313} and 9% for C_{1212}.

5 Discussion

This contribution continues a series of scientific efforts [Hellmich and Ulm, 2002b, Hellmich et al., 2004b,a, Hellmich, 2005] to predict cortical and trabecular bone elasticity from its internal structure and composition, in the framework of continuum micromechanics. In this context, a central aspect of the present manuscript is the micromechanical representation of the mineralized collagen fibril, refining an earlier proposal [Hellmich et al., 2004a]. There, minerals and collagen molecules of the same order of magnitude interact directly at a length scale of several nanometers. We here adhere to a more realistic consideration of characteristic distances involved in bonds between collagen and mineral: We consider mechanical interaction of collagen molecules at distances of around 1 nm (fibrillar organisation according to Hodge and Petruska [1963], Lees et al. [1984b], Bonar et al. [1985]) in the form of crosslinks, leading, within a material volume called 'wet collagen', to a contiguous molecular collagen phase with intermolecular water inclusions. Contrary to collagen molecules, intrafibrillar mineral crystals form agglomerations measuring tens of nanometers [Landis et al., 1996], filling progressively, during the mineralization process, the gap zones of the collagen fibrils, before spreading through the fibrils. Finally, at the level of some hundred nanometers characteristic length, mineral agglomerations and wet collagen interpenetrate each other, forming the mineralized collagen fibril. This model refinement caused a reduction of prediction errors in anisotropic shear stiffness of cortical bone material from 59% [Hellmich, 2005] down to 9%, given in Section 4.

Given the experimental scattering of data available for model validation, mean prediction errors of less than 10% for a variety of cortical and trabecular bone specimens may well support the statement that the present manuscript presents a satisfactory explanation of the elasticity of extracellular and extravascular, cortical and trabecular bone material, from its internal structure and composition, as desired at least since the late 1960s, see e.g. in [Martin et al., 1998], p.177, but never attained so far.

The aforementioned small prediction errors can also be seen as additional manifestation of the universal design principles recalled in the Introduction. In fact, we have provided qualitative assessement of the validity of the 'design plan' depicted in Fig. 3, across a diversity of cortical and trabecular bone tissues. The question might arise how precise this plan must be followed as to guarantee the here reported small prediction errors. In fact, virtually any change of the sequence of steps or of the chosen schemes (such as neglecting the lacunar porosity)

leads to exceeding the error threshold of 10%; e.g., use of a self-consistent scheme for the homogenization step I (wet collagen) results in typical errors around 20%.

Herein, we limit our presentation to observation scales of at most 100 μm, i.e. to analysis of cortical and trabecular bone material including lacunar porosity. Homogenization of the vascular porosity (Haversian and Volkmann canals in cortical bone, intertrabecular space in trabecular bone) within an additional RVE of one to several milimeters characteristic length is an open challenge, if the aformentioned prediction errors of at most 10 % shall not be exceeded. This is particularly true for trabecular bone: If we represent intertrabecular porosity simply through cylindrical pores (as proposed by [Hellmich et al., 2004b]), we face prediction errors of typically 15% to 20%, both for normal and shear stiffness properties. Remarkably, this is still more than one order of magnitude more precise than pertinent trabecular homogenization strategies [Hollister et al., 1991, 1994]; and, as regards shear stiffness, prediction errors related to our earlier model propositions [Hellmich, 2005], amounting up to 64%, are clearly undercut. Nevertheless, we plan to further reduce the aforementioned prediction errors of 15-20 %, by refining the micromechanical representation of trabecular microarchitecture, beyond the one of cylindrical pores in an extravascular bone matrix.

Alternatively, it might be worthwhile to combine the herein presented, reasonably precise anisotropic and inhomogeneous stiffness estimates for extravascular bone material [Fig. 3(a)–(e)] with detailled microstructural modeling of the trabecular microarchitecture in the framework of Micro Finite Element Modeling (μFEM), pioneered by [Rietbergen et al., 1995] and widely available nowadays. Such a combination has great potential to overcome both the aforementioned limitations of simple continuum micromechanics representations for bone microstructure and those of comtemporary μ-FE-analysis, characterized by isotropic properties of (extravascular) solid bone material.

It is important to recall that micromechanical formulations such as the one presented here give direct access to fluid pressures in pore spaces and to poroelastic properties in general [Hellmich and Ulm, 2005a,b], crucial for cell nutrition [Knothe Tate, 2003] and bone adaptation [Cowin, 1999]. This will be one focus of future activities, the other being devoted to homogenization of strength properties of bone. Recently, corresponding theoretical formulations proposed by Kreher [1990], Kreher and Molinari [1993], Dormieux et al. [2002], Barthélémy and Dormieux [2003] have been successfully applied to another class of biological materials, wood [Hofstetter et al., 2005a,b].

A Hill tensor $\mathbb{P}$ for spherical inclusions in a transversely isotropic matrix

The components of the Hill tensor $\mathbb{P}$ for spherical inclusions in a transversely isotropic matrix are given in [Hellmich et al., 2004a] and read as:

$$\begin{aligned}
P^0_{sph,1111} = \frac{1}{16}\int_{-1}^{1} & -(-5C^0_{1111}x^4C^0_{3333} - 3C^0_{1122}x^2C^0_{3333} \\
& -3C^0_{1122}x^4C^0_{2323} + 3C^0_{1122}x^4C^0_{3333} + 5C^0_{1111}x^4C^0_{2323} \\
& -10C^0_{1111}C^0_{2323}x^2 + 2x^4C^{0,2}_{1133} + 8C^0_{2323}x^4C^0_{3333} \\
& -6C^{0,2}_{2323}x^4 + 4C^0_{2323}x^4C^0_{1133} + 6C^0_{1122}C^0_{2323}x^2 + 5C^0_{1111}C^0_{2323} \\
& +5C^0_{1111}x^2C^0_{3333} - 4C^0_{2323}x^2C^0_{1133} + 6C^{0,2}_{2323}x^2 - 2x^2C^{0,2}_{1133} \\
& -3C^0_{1122}C^0_{2323})(-1+x^2)/\mathcal{D}_1 dx
\end{aligned} \tag{57}$$

$$\begin{aligned}
P^0_{sph,1122} = P^0_{sph,2211} = \frac{1}{16}\int_{-1}^{1} & (C^0_{1111}C^0_{2323} - 2C^0_{1111}C^0_{2323}x^2 \\
& +C^0_{1111}x^2C^0_{3333} + C^0_{1122}C^0_{2323} - 2C^0_{1122}C^0_{2323}x^2 \\
& +C^0_{1122}x^2C^0_{3333} + C^0_{1111}x^4C^0_{2323} - C^0_{1111}x^4C^0_{3333} \\
& +C^0_{1122}x^4C^0_{2323} - C^0_{1122}x^4C^0_{3333} - 2C^{0,2}_{2323}x^2 + 2C^{0,2}_{2323}x^4 \\
& -4C^0_{2323}x^2C^0_{1133} + 4C^0_{2323}x^4C^0_{1133} - 2x^2C^{0,2}_{1133} + 2x^4C^{0,2}_{1133}) \\
& (-1+x^2)/\mathcal{D}_1 dx
\end{aligned} \tag{58}$$

$$P^0_{sph,1133} = P^0_{sph,3311} = \frac{1}{4}\int_{-1}^{1}(-1+x^2)x^2(C^0_{2323}+C^0_{1133})/\mathcal{D}_2 dx \tag{59}$$

$$\begin{aligned}
P^0_{sph,2323} = \frac{1}{16}\int_{-1}^{1} & (4C^0_{1111}C^0_{2323}x^2 - 8C^0_{2323}x^4C^0_{1133} - 2x^4C^{0,2}_{1133} \\
& -C^0_{1122}x^4C^0_{3333} - 8C^0_{1111}x^4C^0_{2323} + 3C^0_{1111}x^4C^0_{3333} \\
& +4C^0_{1111}x^4C^0_{1133} - 4C^0_{1122}x^4C^0_{1133} + 2C^0_{1122}x^6C^0_{1133} \\
& -2C^0_{1111}x^6C^0_{1133} + C^0_{1122}x^6C^0_{1111} - 3C^0_{1122}x^4C^0_{1111} \\
& +3C^0_{1122}C^0_{1111}x^2 - 2C^0_{1111}x^2C^0_{1133} + 2C^0_{1122}x^2C^0_{1133} \\
& +8x^6C^0_{2323}C^0_{1133} - 3x^6C^0_{1111}C^0_{3333} + 4x^6C^0_{2323}C^0_{3333} \\
& +4C^0_{1111}x^6C^0_{2323} + C^0_{1122}x^6C^0_{3333} + 3C^{0,2}_{1111}x^4 \\
& -C^{0,2}_{1111}x^6 + 2C^{0,2}_{1133}x^6 - 3C^{0,2}_{1111}x^2 \\
& +C^{0,2}_{1111} - C^0_{1122}C^0_{1111})/\mathcal{D}_1 dx
\end{aligned} \tag{60}$$

$$P^0_{sph,3333} = \frac{1}{2}\int_{-1}^{1} x^2(x^2C^0_{2323} - C^0_{1111}x^2 + C^0_{1111})/\mathcal{D}_2 dx \tag{61}$$

whereby

$$
\begin{aligned}
\mathcal{D}_1 = & -2C^{0,2}_{1111}x^4C^0_{3333} + 2C^{0,2}_{2323}x^6C^0_{3333} - 4C^0_{1111}C^{0,2}_{2323}x^4 - \\
& 3C^{0,2}_{1111}C^0_{2323}x^2 + C^{0,2}_{1111}x^2C^0_{3333} + 2C^0_{1111}C^{0,2}_{2323}x^2 \\
& -2C^0_{2323}x^4C^{0,2}_{1133} - C^0_{1111}C^{0,2}_{1133}x^6 + 2C^0_{1111}C^{0,2}_{1133}x^4 \\
& +4C^{0,2}_{2323}x^6C^0_{1133} - 2C^0_{1122}C^{0,2}_{1133}x^4 + 2C^0_{2323}x^6C^{0,2}_{1133} \\
& +3C^{0,2}_{1111}x^4C^0_{2323} + C^0_{1122}C^{0,2}_{1133}x^6 - C^{0,2}_{1111}x^6C^0_{2323} \\
& +2C^0_{1111}x^6C^{0,2}_{2323} + C^{0,2}_{1111}x^6C^0_{3333} - C^0_{1111}C^{0,2}_{1133}x^2 \\
& -4C^{0,2}_{2323}x^4C^0_{1133} + C^0_{1122}C^{0,2}_{1133}x^2 + C^{0,2}_{1111}C^0_{2323} \\
& -C^0_{1122}C^0_{1111}C^0_{2323} - C^0_{1122}x^6C^0_{1111}C^0_{3333} \\
& +4C^0_{1111}x^4C^0_{2323}C^0_{1133} - 2C^0_{1111}x^2C^0_{2323}C^0_{1133} \\
& -4C^0_{1122}x^4C^0_{2323}C^0_{1133} + 2C^0_{1122}x^2C^0_{2323}C^0_{1133} \\
& +2C^0_{1122}x^6C^0_{2323}C^0_{1133} - 2C^0_{1111}x^6C^0_{2323}C^0_{1133} \\
& -3C^0_{1111}x^6C^0_{2323}C^0_{3333} + 2C^0_{1122}C^0_{1111}x^4C^0_{3333} \\
& -C^0_{1122}C^0_{2323}x^4C^0_{3333} - 3C^0_{1122}C^0_{1111}x^4C^0_{2323} \\
& -C^0_{1122}C^0_{1111}x^2C^0_{3333} + 3C^0_{1122}C^0_{1111}C^0_{2323}x^2 \\
& +3C^0_{1111}C^0_{2323}x^4C^0_{3333} + C^0_{1122}x^6C^0_{1111}C^0_{2323} \\
& +C^0_{1122}x^6C^0_{2323}C^0_{3333}
\end{aligned} \tag{62}
$$

and

$$
\begin{aligned}
\mathcal{D}_2 = & \; 2C^0_{2323}x^4C^0_{1133} + C^0_{2323}x^4C^0_{3333} + C^0_{1111}x^4C^0_{2323} \\
& -2C^0_{2323}x^2C^0_{1133} - 2C^0_{1111}C^0_{2323}x^2 + C^0_{1111}C^0_{2323} \\
& +x^4C^{0,2}_{1133} - C^0_{1111}x^4C^0_{3333} - x^2C^{0,2}_{1133} + C^0_{1111}x^2C^0_{3333}
\end{aligned} \tag{63}
$$

These integral expressions are evaluated numerically, based on an adaptive Simpson quadrature, which is standardly available in MATLAB [Hunt et al., 2001].

References

B. Aoubiza, J.M. Crolet, and A. Meunier. On the mechanical characterization of compact bone structure using homogenization theory. *Journal of Biomechanics*, 29(6):1539 – 1547, 1996.

P.J. Arnoux, J. Bonnoit, P. Chabrand, M. Jean, and M. Pithioux. Numerical damage models using a structural approach: application to bones and ligaments. *The European Physical Journal Applied Physics*, 17: 65 – 73, 2002.

M.-G. Ascenzi. A first estimation of prestress in so-called circularly fibered osteonic lamellae. *Journal of Biomechanics*, 32:935 – 942, 1999.

R.B. Ashman and J.Y. Rho. Elastic modulus of trabecular bone material. *Journal of Biomechanics*, 21(3): 177 – 181, 1988.

R.B. Ashman, S.C. Cowin, W.C. van Buskirk, and J.C. Rice. A continuous wave technique for the measurement of the elastic properties of cortical bone. *Journal of Biomechanics*, 17(5):349 – 361, 1984.

A.J. Bailey, R.G. Paul, and L. Knott. Mechanisms of maturation and ageing of collagen. *Mechanisms of Aging and Development*, 106:1 – 56, 1998.

J.-F. Barthélémy and L. Dormieux. Determination of the macroscopic strength criterion of a porous medium by nonlinear homogenization. *Comptes Rendus Mecanique*, 331:271 – 276, 2003.

D. Baylink and J. Wergedal. *Bone formation and resorption by osteocytes*, pages 257–289. Academic Press, New York, USA, 1971.

V. Benezra Rosen, L.W. Hobbs, and M. Spector. The ultrastructure of anorganic bovine bone and selected synthetic hydroxyapatites used as bone graft substitute material. *Biomaterials*, 23:921 – 928, 2002.

L.C. Bonar, S. Lees, and H.A. Mook. Neutron diffraction studies of collagen in fully mineralized bone. *Journal of Molecular Biology*, 181:265 – 270, 1985.

S.C. Cowin. Bone poroelasticity. *Journal of Biomechanics*, 32:217 – 238, 1999.

J.M. Crolet, B. Aoubiza, and A. Meunier. Compact bone: numerical simulation of mechanical characteristics. *Journal of Biomechanics*, 26(6):677 – 687, 1993.

J.D. Currey. Role of collagen and other organics in the mechanical properties of bone. *Osteoporosis International*, 14(5):S29 – S36, 2003.

J.D. Currey. The relationship between the stiffness and the mineral content of bone. *Journal of Biomechanics*, 2:477 – 480, 1969.

S. Cusack and A. Miller. Determination of the elastic constants of collagen by Brillouin light scattering. *Journal of Molecular Biology*, 135:39 – 51, 1979.

M. Ding and I. Hvid. Quantification of age-related changes in the structure model type and trabecular thickness of human tibial cancellous bone. *Bone*, 26: 291 – 295, 2000.

L. Dormieux and F.-J. Ulm, editors. *CISM Courses and lectures, Volume 480. Applied Micromechanics of Porous Media*. Springer, Wien - New York, 2005.

L. Dormieux, A. Molinari, and D. Kondo. Micromechanical approach to the behavior of poroelastic materials. *Journal of the Mechanics and Physics of Solids*, 50: 2203 – 2231, 2002.

S.J. Eppell, W. Tong, J.L. Katz, L. Kuhn, and M.J. Glimcher. Shape and size of isolated bone mineralites measured using atomic force microscopy. *Journal of Orthopaedic Research*, 19:1027 – 1034, 2001.

J.D. Eshelby. The determination of the elastic field of an ellipsoidal inclusion, and related problems. *Proceedings of the Royal Society London, Series A*, 241: 376 – 396, 1957.

F.I. Fedorov. *Theory of elastic waves in crystals*. Plenum Press, New York, 1968.

P. Fratzl, N. Fratzl-Zelman, K. Klaushofer, G. Vogl, and K. Koller. Nucleation and growth of mineral crystals in bone studied by small-angle X-ray scattering. *Calcified Tissue International*, 48:407 – 413, 1991.

P. Fratzl, S. Schreiber, and K. Klaushofer. Bone mineralization as studied by small-angle X-ray scattering. *Connective Tissue Research*, 34(4):247 – 254, 1996.

H.M. Frost. Measurement of osteocytes per unit volume and volume components of osteocytes and canaliculae (sic) in man. *Henry Ford Hospital Medical Bulletin*, 8:208 – 211, 1962.

R.S. Gilmore and J.L. Katz. Elastic properties of apatites. *Journal of Materials Science*, 17:1131 – 1141, 1982.

J.K. Gong, J.S. Arnold, and H. Cohn, S. Composition of trabecular and cortical bone. *The Anatomical Record*, 149:325 – 332, 1964.

S.J. Gould and R.C. Lewontin. The spandrels of San Marco and the Panglossian paradigm: a critique of the adaptionist program. *Proceedings of the Royal Society of London, Series B*, 205(1161):581 – 598, 1979.

Ch. Hellmich. *Microelasticity of Bone*, pages 289 – 332. In , Dormieux and Ulm [2005], 2005.

Ch. Hellmich and F.-J. Ulm. Average hydroxyapatite concentration is uniform in extracollageneous ultrastructure of mineralized tissue. *Biomechanics and Modeling in Mechanobiology*, 2:21 – 36, 2003.

Ch. Hellmich and F.-J. Ulm. Are mineralized tissues open crystal foams reinforced by crosslinked collagen? – some energy arguments. *Journal of Biomechanics*, 35:1199 – 1212, 2002a.

Ch. Hellmich and F.-J. Ulm. A micromechanical model for the ultrastructural stiffness of mineralized tissues. *Journal of Engineering Mechanics (ASCE)*, 128(8): 898 – 908, 2002b.

Ch. Hellmich and F.-J. Ulm. Hydroxyapatite is uniformly concentrated in the extracollagenous ultrastructure of mineralized tissue. In J. Middleton, N.G. Shrive, and M.L. Jones, editors, *Proceedings of the Fifth International Symposium on Computer Methods in Biomechanics and Biomedical Engineering*, Rome, Italy, 2001.

Ch. Hellmich and F.-J. Ulm. Drained and undrained poroelastic properties of healthy and pathological bone: a poro-micromechanical investigation. *Transport in Porous Media*, 58:243 – 268, 2005a.

Ch. Hellmich and F.-J. Ulm. Micro-porodynamics of bones: prediction of the 'Frenkel-Biot' slow compressional wave. *Journal of Engineering Mechanics (ASCE)*, 131(9):918 – 927, 2005b.

Ch. Hellmich, J.-F. Barthélémy, and L. Dormieux. Mineral-collagen interactions in elasticity of bone ultrastructure – a continuum micromechanics approach. *European Journal of Mechanics A-Solids*, 23:783 – 810, 2004a.

Ch. Hellmich, F.-J. Ulm, and L. Dormieux. Can the diverse elastic properties of trabecular and cortical bone be attributed to only a few tissue-independent phase properties and their interactions? – arguments from a multiscale approach. *Biomechanics and Modeling in Mechanobiology*, 2:219 – 238, 2004b.

A.V. Hershey. The elasticity of an isotropic aggregate of anisotropic cubic crystals. *Journal of Applied Mechanics (ASME)*, 21:236 – 240, 1954.

R. Hill. Elastic properties of reinforced solids: some theoretical principles. *Journal of the Mechanics and Physics of Solids*, 11:357 – 362, 1963.

A.J. Hodge and J.A. Petruska. Recent studies with the electron microscope on ordered aggregates of the tropocollagen molecule. In G.N. Ramachandran, editor, *Aspects of Protein Structure – Proceedings of a Symposium held in Madras 14 - 18 January 1963 and organized by the University of Madras, India*, pages 289 – 300. Academic Press, London and New York, 1963.

K. Hofstetter, Ch. Hellmich, and J. Eberhardsteiner. Development and experimental validation of a continuum micromechanics model for the elasticity of wood. *European Journal of Mechanics A - Solids*, 2005a. In print.

K. Hofstetter, Ch. Hellmich, and J. Eberhardsteiner. Predicting wood strength from composition and microstructure: development and experimental verification of a continuum micromechanics model. In L. Dormieux, editor, *Proceedings of 'Colloque Microstructure et Propriétés des Matériaux'*. Presses de L'École Nationale des Ponts et Chaussées, Marne-la-Vallée, France, 2005b. In print.

S.J. Hollister, D.P. Fyhrie, K.J. Jepsen, and S.A. Goldstein. Application of homogenization theory to the study of trabecular bone mechanics. *Journal of Biomechanics*, 24:825 – 839, 1991.

S.J. Hollister, J.M. Brennan, and N. Kikuchi. A homogenization sampling procedure for calculating trabecular bone effective stiffness and tissue level stress. *Journal of Biomechanics*, 27(4):433 – 444, 1994.

B.R. Hunt, R.L. Eipsman, and J.M. Rosenberg. *A Guide to MATLAB for Beginners and Experienced Users*. Cambridge University Press, Cambridge, United Kingdom, 1 edition, 2001.

G.K. Hunter, P.V. Hauschka, A.R. Poole, L.C. Rosenberg, and H.A. Goldberg. Nucleation and inhibition of hydroxyapatite formation by mineralized tissue proteins. *Biochemical Journal*, 317:59 – 64, 1996.

I. Jäger and P. Fratzl. Mineralized collagen fibrils: a mechanical model with a staggered arrangement of mineral particles. *Biophysical Journal*, 79:1737 – 1746, 2000.

J.K. Katz and K. Ukraincik. On the anisotropic elastic properties of hydroxyapatite. *Journal of Biomechanics*, 4:221 – 227, 1971.

J.L. Katz. Anisotropy of Young's modulus of bone. *Nature*, 283:106 – 107, 1980.

J.L. Katz. *Composite material models for cortical bone*, pages 171 – 184. American Society of Mechanical Engineers, New York, NY, USA, 1981.

J.L. Katz, H.S. Yoon, S. Lipson, R Maharidge, A. Meunier, and P. Christel. The effects of remodelling on the elastic properties of bone. *Calcified Tissue International*, 36:S31 – S36, 1984.

M.L. Knothe Tate. Whither flows the fluid in bone? – an osteocyte's perspective. *Journal of Biomechanics*, 36:1409 – 1424, 2003.

C. Kober, B. Erdmann, Ch. Hellmich, R. Sader, and H.-F. Zeilhofer. Consideration of anisotropic elasticity minimizes volumetric rather than shear deformation in human mandible. *Computer Methods in Biomechanics and Biomedical Engineering*, 2005. submitted for publication.

W. Kreher. Residual stresses and stored elastic energy of composites and polycrystals. *Journal of the Mechanics and Physics of Solids*, 38(1):115 – 128, 1990.

W. Kreher and A. Molinari. Residual stresses in polycrystals as influenced by grain shape and texture. *Journal of the Mechanics and Physics of Solids*, 41 (12):1955 – 1977, 1993.

W.J. Landis, K.J. Hodgens, M.J. Song, J. Arena, S. Kiyonaga, M. Marko, C. Owen, and B.F. McEwen. Mineralization of collagen may occur on fibril surfaces: Evidence from conventional and high-voltage electron microscopy and three-dimensional imaging. *Journal of Structural Biology*, 117:24 – 35, 1996.

N. Laws. The determination of stress and strain concentrations at an ellipsoidal inclusion in an anisotropic material. *Journal of Elasticity*, 7(1):91 – 97, 1977.

S. Lees. Considerations regarding the structure of the mammalian mineralized osteoid from viewpoint of the generalized packing model. *Connective Tissue Research*, 16:281 – 303, 1987.

S. Lees, P. Cleary, J.D. Heeley, and E.L. Gariepy. Distribution of sonic plesio-velocity in a compact bone sample. *Journal of Acoustic Society of America*, 66 (3):641– 646, 1979a.

S. Lees, J.D. Heeley, and P.F. Cleary. A study of some properties of a sample of bovine cortical bone using ultrasound. *Calcified Tissue International*, 29:107 – 117, 1979b.

S. Lees, J.M. Ahern, and M. Leonard. Parameters influencing the sonic velocity in compact calcified tissues of various species. *Journal of the Acoustical Society of America*, 74(1):28 – 33, 1983.

S. Lees, L.C. Bonar, and H.A. Mook. A study of dense mineralized tissue by neutron diffraction. *International Journal of Biological Macromolecules*, 6:321 – 326, 1984a.

S. Lees, M. Pineri, and M. Escoubes. A generalized packing model for type I collagen. *International Journal of Biological Macromolecules*, 6:133 – 136, 1984b.

S. Lees, N.-J. Tao, and M. Lindsay. Studies of compact hard tissues and collagen by means of Brillouin light scattering. *Connective Tissue Research*, 24:187 – 205, 1990.

S. Lees, D. Hanson, E.A. Page, and H.A. Mook. Comparison of dosage-dependent effects of beta-aminopropionitrile, sodium fluoride, and hydrocortisone on selected physical properties of cortical bone. *Journal of Bone and Mineral Research*, 9(9):1377 – 1389, 1994a.

S. Lees, K.S. Prostak, V.K. Ingle, and K. Kjoller. The loci of mineral in turkey leg tendon as seen by atomic force microscope and electron microscopy. *Calcified Tissue International*, 55:180 – 189, 1994b.

S. Lees, D. Hanson, and E.A. Page. Some acoustical properties of the otic bones of a fin whale. *Journal of the Acoustical Society of America*, 99(4):2421 – 2427, 1995.

J.F. Mammone and S.M. Hudson. Micromechanics of bone strength and failure. *Journal of Biomechanics*, 26:439 – 446, 1993.

R.B. Martin, D.B. Burr, and N.A. Sharkey. *Skeletal Tissue Mechanics*. Springer, New York, 1998.

E. Mayr. *This is biology – the science of the living world*. Harvard University Press, Cambridge, MA, USA, 1 edition, 1997.

R.N. McCarthy, L.B. Jeffcott, and R.N. McCartney. Ultrasound speed in equine cortical bone: effects of orientation, density, porosity and temperature. *Journal of Biomechanics*, 23(11):1139 – 1143, 1990.

A. Miller. Collagen: the organic matrix of bone. *Philosophical Transactions of the Royal Society in London Series B*, 304:455 – 477, 1984.

T. Mori and K. Tanaka. Average stress in matrix and average elastic energy of materials with misfitting inclusions. *Acta Metallurgica*, 21(5):571 – 574, 1973.

M.A. Morris, J.A. Lopez-Curato, S.P.F. Hughes, K.N. An, and P.J. Bassingthwaighte, J.B. adn Kelly. Fluid spaces in canine bone and marrow. *Microvascular Research*, 23:188 – 200, 1982.

F. Peters, K. Schwarz, and M. Epple. The structure of bone studied with synchrotron x-ray diffraction, x-ray absorption spectroscopy and thermal analysis. *Thermochimica Acta*, 361:131 – 138, 2000.

R.M.V. Pidaparti, A. Chandran, Y. Takano, and C.H. Turner. Bone mineral lies mainly outside the collagen fibrils: Predictions of a composite model for osteonal bone. *Journal of Biomechanics*, 29(7):909 – 916, 1996.

K.S. Prostak and S. Lees. Visualization of crystal-matrix structure. In situ demineralization of mineralized turkey leg tendon and bone. *Calcified Tissue International*, 59:474 – 479, 1996.

J.-Y. Rho, L. Kuhn-Spearing, and P. Zioupos. Mechanical properties and the hierarchical structure of bone. *Medical Engineering & Physics*, 20:92 – 102, 1998.

B. van Rietbergen, H. Weinans, R. Huiskes, and A. Odgaard. A new method to determine trabecular bone elastic properties and loading using micromechanical finite-element models. *Journal of Biomechanics*, 28:69 – 81, 1995.

N. Sasaki. Orientation of mineral in bovine bone and the anisotropic mechanical properties of plexiform bone. *Journal of Biomechanics*, 24:57 – 61, 1991.

W.K. Sietsema. Animal models of cortical porosity. *Bone*, 17(4):297S – 305S, 1995.

P. Suquet, editor. *Continuum micromechanics*. Springer, Wien – New York, 1997.

S. Torabia. Identification of a relationship between the chemical constituents of mineralized tissues: bridging computed tomography and micromechanical modeling, for noninvasive determination of elastic properties of bone. Master's thesis, Vienna University of Technology, 2004.

S. Torabia and Ch. Hellmich. In-vivo determination of elastic properties of bone, based on (p)QCT and micromechanical modeling. In P. Laugier and D. Hans, editors, *Proceedings of the 16th International Bone Densitometry Workshop, Annecy, France*, 2004.

C.H. Turner, S.C. Cowin, J.Y. Rho, R.B. Ashman, and J.C. Rice. The fabric dependence of the orthotropic elastic constants of cancellous bone. *Journal of Biomechanics*, 23(6):549 – 561, 1990.

M.R. Urist, R.J. DeLange, and G.A.M. Finerman. Bone cell differentiation and growth factors. *Science*, 220: 680 – 686, 1983.

K. Wakashima and H. Tsukamoto. Mean-field micromechanics model and its application to the analysis of thermomechanical behaviour of composite materials. *Materials Science and Engineering A*, 146(1-2):291 – 316, 1991.

S. Weiner and H.D. Wagner. The material bone: structure - mechanical function relations. *Annual Review of Materials Science*, 28:271 – 298, 1998.

S. Weiner, T. Arad, I. Sabanay, and W. Traub. Rotated plywood structure of primary lamellar bone in the rat: Orientation of the collagen fibril arrays. *Bone*, 20:509 – 514, 1997.

H.S. Yoon and J.L. Katz. Ultrasonic wave propagation in human cortical bone–II. measurements of elastic properties and microhardness. *Journal of Biomechanics*, 9: 459 – 464, 1976.

A. Zaoui. Continuum micromechanics: Survey. *Journal of Engineering Mechanics (ASCE)*, 128(8):808 – 816, 2002.

A. Zaoui. *Structural morphology and constitutive behavior of microheterogeneous materials*, pages 291 – 347. In , Suquet [1997], 1997.

D. Zhang, S. Weinbaum, and S.C. Cowin. Estimates of the peak pressures in pore water. *Journal of Biomechanical Engineering*, 120(December 1998):697 – 703, 1998.

Chapter 4

Summary and Perspective

This master's thesis contributes to the scientific effort of predicting cortical and trabecular bone elasticity from its internal structure and composition, by means of continuum micromechanics. Firstly, an existing concept for the homogenization of porous polycrystals was verified, and secondly, an earlier multi-step homogenization scheme was refined at the scale of several nanometers leading to a satisfactory agreement between stiffness experiments and corresponding model predictions .

Based on the fact that continuum micromechanics can corroborate the physical relevance of the poromechanical theory of Biot [Biot, 1955] the developments given here will lead the way to the ultrastructural and macroscopic poroelastic properties of bone tissues, such as the Biot coefficients and moduli as well as the Skempton coefficients [Hellmich and Ulm, 2005a,b]. Chemical information accessible with computed tomography (CT) will be converted into poroelastic properties [Torabia, 2004, Torabia and Hellmich, 2004], thus delivering a data base for a structural analysis of organs.

Another focus of future activities will be the upscaling of strength properties which needs the treatment of irreversible material behaviour. At the macroscopic scale it can be explained by several micromechanisms at the ultrastructural scale. Progressive damage by microcrack propagation [Dormieux and Kondo, 2004] will be investigated as well as the possibility of ductile failure of both mineral and collagen [Suquet, 1997] as stated in [Hellmich and Ulm, 2005a].

Combination of such a micromechanical law with non–invasively accessed patient–specific chemical bone composition as input, in the framework of Finite Element analysis of whole organs, will finally allow for an in vivo patient–specific biomechanics–based monitoring of fracture risk, induced by bone diseases (e.g. osteoporosis) or reduced by chemical or genetical therapy tissue. This would be a significant improvement over the current clinical practice, where the specific information characterizing the single patient is reduced to a minimum of one or only a few risk factors, related to entire statistical populations of patients.

Appendix A

Source codes for computation on porous polycrystals (Chapter 2)

The calculations were performed with MAPLE, Version 8, at the École Nationale des Ponts et Chaussées. The package 'tens3d' can be obtained from `http://jgarrigues.perso.egim-mrs.fr/tens3d.html`. The package 'eshelby' is not available for public use.

A.1 SCS_sph.mws

This MAPLE file concerns the homogenization of a porous polycrystal with a self-consistent scheme. The solid phase and the pores are represented by spheres.

```
> # SCS for spherical, isotropic inclusions
> # Comparison of percolation threshold with prolate inclusions
> # ENPC, Mai 2005
> # ****************************************
> restart;
> with(tens3d):with(eshelby):
> #
> # Definition of stiffness tensors
> # -------------------------------
> Cac:=rigi_iso(kac,muac):print(mat(Cac));
> Cs:=rigi_iso(ks,mus):
> #
> # P-tensor for spherical inclusions in isotropic media
> # ----------------------------------------------------
> P:=P_iso_sph(kac,muac):
> #
> # Contribution of solid phase
> # ---------------------------
> q1:=Iso(1) &++ (P &t2 (Cs &-- Cac)):
> q2:=inv4(q1):
> loc:=q2:
> locmoy:=(1-f) &** loc:
> Cslocmoy:= (1-f) &** (Cs &t2 loc):
> #
```

```
> # Contribution of pores
> # ---------------------
> q3:=Iso(1) &-- (P &t2 Cac):
> q4:=inv4(q3):
> locpormoy:=f &** q4:
> #
> # SCS homogenization
> # ------------------
> Chom:=Cslocmoy &t2 inv4(locmoy &++ locpormoy):
> #
> # Determination of kac and muac
> # -----------------------------
> eq1:=comp4(Cac,1,1,1,1)-simplify(comp4(Chom,1,1,1,1));
eq2:=comp4(Cac,2,3,2,3)-simplify(comp4(Chom,2,3,2,3));

> sol:=solve({eq1,eq2},{kac,muac});

> sol1:=subs(RootOf(8*_Z^2+(20*f*mus-3*f*ks-8*mus+9*ks)*_Z+18*f*ks*mus-9*ks*mus)=RR,sol);
>
> # Limit case: incompressible material
> # -----------------------------------
> musc:=limit(RootOf(8*_Z^2+(20*f*mus-3*f*ks-8*mus+9*ks)*_Z+18*f*ks*mus-9*ks*mus),
ks=infinity);
ksc:=simplify(subs(RR=musc,-4/3*RR*(2*RR+5*f*mus-2*mus)/(3*RR+5*f*mus-3*mus)))/musc;

> # Evaluate muac for a certain value of f and nu=nus
> # -------------------------------------------------
> evalf(subs(f=0.2,subs(nu=1/3,subs(ks=1/3/(1-2*nu),mus=1/2/(1+nu),RootOf(8*_Z^2+
(20*f*mus-3*f*ks-8*mus+9*ks)*_Z+18*f*ks*mus-9*ks*mus)))));

> # Plot muac as function of f for a certain value of nu=nus
> # --------------------------------------------------------
> plot(subs(nu=0.20,subs(ks=1/3/(1-2*nu),mus=1/2/(1+nu),RootOf(8*_Z^2+
(20*f*mus-3*f*ks-8*mus+9*ks)*_Z+18*f*ks*mus-9*ks*mus))),
 f=0..0.5,labels=[f,muac],title='SCS_with_spherical_inclusions');

> # Plot kac as function of f for a certain value of nu=nus
> # -------------------------------------------------------
> plot(subs(nu=0.20,subs(ks=1/3/(1-2*nu),mus=1/2/(1+nu),rhs(sol[2]))),
> f=0..0.5,labels=[f,kac],title='SCS_with_spherical_inclusions');

> # Determination of Eac, nuac
> # --------------------------
> eq11:=subs({kac=Eac/3/(1-2*nuac),muac=Eac/2/(1+nuac)},eq1):
> eq22:=subs({kac=Eac/3/(1-2*nuac),muac=Eac/2/(1+nuac)},eq2):
> sol_nu:=solve({eq11,eq22},{Eac,nuac});
> sol_nu1:=subs(RootOf((81*f^3*ks^2+90*ks*f^3*mus-156*ks*f^2*mus-216*ks^2*f^2-
40*f^2*mus-54*ks*f^2+126*f*ks+64*f*mus+144*f*ks^2+48*f*mus*ks-72*ks-
24*mus)*_Z^2+(-162*f^3*ks^2-60*ks*f^2*mus+324*ks^2*f^2-80*f^2*mus
+24*f*mus*ks+36*f*ks-144*f*ks^2+128*f*mus-48*mus-36*ks)*_Z+81*f^3*ks^2-
90*ks*f^3*mus-108*ks^2*f^2-40*f^2*mus+54*ks*f^2+96*ks*f^2*mus+36*f*ks^2-
24*f*mus*ks-90*f*ks+64*f*mus-24*mus+36*ks)=QQ,sol_nu[2]);

> # Plot nuac as function of f for a certain value of nu=nus
> # --------------------------------------------------------
> plot(subs(nu=0.2,subs(ks=1/3/(1-2*nu),mus=1/2/(1+nu),RootOf((81*f^3*ks^2+
90*ks*f^3*mus-156*ks*f^2*mus-216*ks^2*f^2-40*f^2*mus-54*ks*f^2+126*f*ks+
64*f*mus+144*f*ks^2+48*f*mus*ks-72*ks-24*mus)*_Z^2+(-162*f^3*ks^2-
60*ks*f^2*mus+324*ks^2*f^2-80*f^2*mus+24*f*mus*ks+36*f*ks-144*f*ks^2+
128*f*mus-48*mus-36*ks)*_Z+81*f^3*ks^2-90*ks*f^3*mus-108*ks^2*f^2-
40*f^2*mus+54*ks*f^2+96*ks*f^2*mus+36*f*ks^2-24*f*mus*ks-90*f*ks+64*f*mus
-24*mus+36*ks))), f=0..0.5,labels=[f,nuac],title='SCS_with_spherical_inclusions');

> # Plot Eac as function of f for a certain value of nu=nus
> # -------------------------------------------------------
> Eac1:=subs(QQ=
> RootOf((81*f^3*ks^2+90*ks*f^3*mus-156*ks*f^2*mus-216*ks^2*f^2-40*f^2*mus-
54*ks*f^2+126*f*ks+64*f*mus+144*f*ks^2+48*f*mus*ks-72*ks-24*mus)*_Z^2+
```

```
(-162*f^3*ks^2-60*ks*f^2*mus+324*ks^2*f^2-80*f^2*mus+24*f*mus*ks+36*f*ks
-144*f*ks^2+128*f*mus-48*mus-36*ks)*_Z+81*f^3*ks^2-90*ks*f^3*mus-108*ks^2*f^2-
40*f^2*mus+54*ks*f^2+96*ks*f^2*mus+36*f*ks^2-24*f*mus*ks-90*f*ks+64*f*mus-
24*mus+36*ks),rhs(sol_nu1[1])):
>
> plot(subs(nu=0.2,subs(ks=1/3/(1-2*nu),mus=1/2/(1+nu),Eac1)),f=0..0.5);
> q2:=plot(subs(nu=0.25,subs(ks=1/3/(1-2*nu),mus=1/2/(1+nu),Eac1)),f=0..0.5,view=[0..1,0..1]):
>

> # Approximation with 1st order expansion
> eq111:=numer(simplify(subs(ks=1/3/(1-2*nus),mus=1/2/(1+nus),eq11)));
> eq222:=numer(simplify(subs(ks=1/3/(1-2*nus),mus=1/2/(1+nus),eq22)));


> E1dv:=(convert(series(subs(Eac=1*(1-a*f),nuac=nus-b*f,eq111),f=0,3),polynom));
> E2dv:=simplify(convert(series(subs(Eac=1*(1-a*f),nuac=nus-b*f,eq222),f=0,4),polynom));

> sol1:=solve({E1dv,E2dv},{a,b}):
> sol1[1];
```

A.2 eq_cyl_020.mws

This MAPLE file concerns the homogenization of a porous polycrystal with a self-consistent scheme. The solid phase is represented by uniformly oriented needles (cylinders), the pores by spheres.

```
> # SCS for cylindrical inclusions (solid phase)
> # Equations for determination of (kac, muac) / (Eac, nuac)
> # Plot Eac, nuac as function of f for nus=0.20
> # ENPC, Mai 2005
> restart:

> eq11 :=
> (4*ks*mus*muac*f-4*muac*ks*mus+12*ks*f*muac^2-12*muac^2*ks+24*ks*f*kac
> *muac-12*kac*muac*ks+9*ks*kac^2*f+4*kac*muac*mus+3*mus*kac^2*f+12*kac*
> muac^2-3*kac^2*f*muac+12*muac*kac^2)/(12*ks*muac*f+9*ks*f*kac+4*muac*m
> us+3*mus*f*kac+12*muac^2-3*f*kac*muac+12*kac*muac);


> eq2 :=
> (-81*ks*mus^3*kac^2-168*ks*muac^2*mus^3-261*ks*mus^3*muac*kac+168*muac
> ^2*f*ks*mus^3+81*kac^2*mus^3*ks*f-90*kac*muac^4*ks*f-54*kac^2*muac^3*k
> s*f+5355*mus^2*muac^3*kac*f+1881*mus^2*muac^2*kac^2*f+909*ks*kac*muac^
> 3*mus+81*ks*kac^2*muac^2*mus+549*kac^2*mus^3*f*muac+1251*mus*muac^3*ka
> c^2*f+2607*f*muac^4*kac*mus+1761*f*muac^2*kac*mus^3+3180*f*muac^3*ks*m
> us^2+1656*f*muac^4*ks*mus-1863*ks*mus^2*muac^2*kac-729*ks*mus^2*muac*k
> ac^2+1248*muac^5*kac+756*muac^4*kac^2+504*ks*muac^5-896*muac^4*mus^2-2
> 12*f*muac^6+960*mus*muac^5-576*muac^3*mus^3+2691*f*muac^3*ks*mus*kac+5
> 12*muac^6+1404*kac^2*mus^2*ks*f*muac+4338*kac*mus^2*ks*f*muac^2+1269*k
> s*mus*muac^2*kac^2*f-81*muac^4*kac^2*f-204*f*muac^5*ks-123*f*muac^5*ka
> c+1540*f*muac^5*mus+1276*f*muac^3*mus^3+3796*f*muac^4*mus^2+744*ks*mua
> c^4*mus-756*kac^2*muac^2*mus^2+1215*ks*muac^4*kac-1680*muac^3*mus^2*ka
> c+1368*mus*muac^4*kac+324*mus*muac^3*kac^2+729*ks*muac^3*kac^2-1080*ks
> *muac^3*mus^2-324*mus^3*muac*kac^2-936*muac^2*mus^3*kac+261*muac*kac*m
> us^3*ks*f)/(2324*muac^3*mus^2*f+1476*muac^2*f*ks*mus*kac+2214*muac*kac
> *mus^2*ks*f+540*muac*ks*mus*kac^2*f-81*muac^3*kac^2*f-123*muac^4*kac*f
> +1359*muac^3*mus*f*kac+2739*muac^2*mus^2*f*kac+495*kac^2*muac^2*mus*f+
> 1028*muac^4*mus*f+801*mus^2*muac*kac^2*f+1248*muac^4*kac+756*muac^3*ka
> c^2-212*f*muac^5+512*muac^5+700*muac^2*f*mus^3+594*kac^2*mus^2*ks*f+11
> 52*muac^3*f*ks*mus+1932*muac^2*f*ks*mus^2+825*muac*f*kac*mus^3+225*kac
> ^2*mus^3*f-204*muac^4*f*ks-54*muac^2*kac^2*ks*f-90*muac^3*kac*ks*f+504
> *ks*muac^4+168*ks*muac^2*mus^2+1215*ks*muac^3*kac+2616*mus*muac^3*kac+
> 324*mus^2*muac*kac^2+261*ks*mus^2*muac*kac+810*ks*mus*muac*kac^2+81*ks
> *mus^2*kac^2+936*kac*muac^2*mus^2+576*muac^3*mus^2+1248*ks*muac^3*mus+
> 2124*ks*kac*muac^2*mus+1472*mus*muac^4+1080*mus*muac^2*kac^2+729*ks*mu
> ac^2*kac^2);



> eq111:=numer(simplify(subs(ks=1/3/(1-2*nus),mus=1/2/(1+nus),eq11)));

 > eq222:=numer(simplify(subs(ks=1/3/(1-2*nus),mus=1/2/(1+nus),eq2)));


> E1:=numer(simplify(subs(kac=Eac/3/(1-2*nuac),muac=Eac/2/(1+nuac),eq111
> )));subs(nus=1/4,E1);

 > E2:=numer(simplify(subs(kac=Eac/3/(1-2*nuac),
muac=Eac/2/(1+nuac),eq222)));

> Eac1:=solve(E1,Eac);

> nuac1:=solve(subs(Eac=Eac1[2],nus=0.2,E2),nuac);


> #plot(nuac1[3],f=0..1);
> #plot(subs(nuac=nuac1[3],subs(nus=0.2,Eac1[2])),f=0..1);
> solve({subs(f=1,nus=0.2,E1),subs(f=1,nus=0.2,E2)},{Eac,nuac});
```

```

  {Eac = 0, nuac = nuac},

        {nuac = nuac, Eac = -1.388888889 - 1.388888889 nuac},

        {nuac = 1., Eac = Eac}

> # determination of nuac, Eac as function of f for a certain nus
> # ----------------------------------------------------------------------
> E11:=subs(nus=0.2,E1):E22:=subs(nus=0.2,E2):
>
> a1:=solve({subs(f=0.1,E11),subs(f=0.1,E22),Eac>0,nuac>0,nuac<0.5},{Eac
> ,nuac});
> a2:=solve({subs(f=0.2,E11),subs(f=0.2,E22),Eac>0,nuac>0,nuac<0.5},{Eac
> ,nuac});
> a3:=solve({subs(f=0.3,E11),subs(f=0.3,E22),Eac>0,nuac>0,nuac<0.5},{Eac
> ,nuac});
> a4:=solve({subs(f=0.4,E11),subs(f=0.4,E22),Eac>0,nuac>0,nuac<0.5},{Eac
> ,nuac});
> a5:=solve({subs(f=0.5,E11),subs(f=0.5,E22),Eac>0,nuac>0,nuac<0.5},{Eac
> ,nuac});
> a6:=solve({subs(f=0.6,E11),subs(f=0.6,E22),Eac>0,nuac>0,nuac<0.5},{Eac
> ,nuac});
> a7:=solve({subs(f=0.7,E11),subs(f=0.7,E22),Eac>0,nuac>0,nuac<0.5},{Eac
> ,nuac});
> a8:=solve({subs(f=0.8,E11),subs(f=0.8,E22),Eac>0,nuac>0,nuac<0.5},{Eac
> ,nuac});
> a9:=solve({subs(f=0.9,E11),subs(f=0.9,E22),Eac>0,nuac>0,nuac<0.5},{Eac
> ,nuac});
> a10:=solve({subs(f=0.99,E11),subs(f=0.99,E22),Eac>0,nuac>0,nuac<0.5},{
> Eac,nuac});
>



> with(plots):
> q:=[[0,1],[0.1,rhs(a1[2])],[0.2,rhs(a2[2])],[0.3,rhs(a3[2])],[0.4,rhs(
> a4[1])],[0.5,rhs(a5[2])],[0.6,rhs(a6[2])],
> [0.7,rhs(a7[1])],[0.8,rhs(a8[1])],[0.9,rhs(a9[1])],[0.99,rhs(a10[1])]]
> :
> q1:=plot(q,view=[0..1,0..1]):
> display(q1);

> # Test if approximation nuac=nus is admissible
> Eac11:=subs(nuac=nus,Eac1[2]);


> q2:=plot(subs(nus=0.2,Eac11),f=0..1,title=`nus=0.20`,view=[0..1,0..1],
> color=green):
> display(q2);
>
> display(q1,q2);

>
> #plotsetup(ps,plotoutput=`test_Eac_020.ps`,plotoptions=`portrait,nobor
> der,color`);
> plotsetup(default);
>
```

A.3 expansion.mws

This MAPLE file concerns the approximation of the elastic constants k and μ in the vicinity of $f = 1$ and $f = 0$ by means of a first order expansion. This file relies on data from file eq_cyl_020.mws (Section A.2).

```
> # SCS for spherical/cylindrical inclusions (solid phase)
> # Approximation of k_ac, mu_ac in the vicinity of f=1
> # and f=0 for cylindrical inclusions
> # (first-order expansions)
> # ENPC, Mai 2005
> # *******************************************************
> restart:
> eq11 :=
> (4*ks*mus*muac*f-4*muac*ks*mus+12*ks*f*muac^2-12*muac^2*ks+24*ks*f*kac
> *muac-12*kac*muac*ks+9*ks*kac^2*f+4*kac*muac*mus+3*mus*kac^2*f+12*kac*
> muac^2-3*kac^2*f*muac+12*muac*kac^2)/(12*ks*muac*f+9*ks*f*kac+4*muac*
> mus+3*mus*f*kac+12*muac^2-3*f*kac*muac+12*kac*muac);


> eq2 :=
> (-81*ks*mus^3*kac^2-168*ks*muac^2*mus^3-261*ks*mus^3*muac*kac+168*muac
> ^2*f*ks*mus^3+81*kac^2*mus^3*ks*f-90*kac*muac^4*ks*f-54*kac^2*muac^3*k
> s*f+5355*mus^2*muac^3*kac*f+1881*mus^2*muac^2*kac^2*f+909*ks*kac*muac^
> 3*mus+81*ks*kac^2*muac^2*mus+549*kac^2*mus^3*f*muac+1251*mus*muac^3*ka
> c^2*f+2607*f*muac^4*kac*mus+1761*f*muac^2*kac*mus^3+3180*f*muac^3*ks*m
> us^2+1656*f*muac^4*ks*mus-1863*ks*mus^2*muac^2*kac-729*ks*mus^2*muac*k
> ac^2+1248*muac^5*kac+756*muac^4*kac^2+504*ks*muac^5-896*muac^4*mus^2-2
> 12*f*muac^6+960*mus*muac^5-576*muac^3*mus^3+2691*f*muac^3*ks*mus*kac+5
> 12*muac^6+1404*kac^2*mus^2*ks*f*muac+4338*kac*mus^2*ks*f*muac^2+1269*k
> s*mus*muac^2*kac^2*f-81*muac^4*kac^2*f-204*f*muac^5*ks-123*f*muac^5*ka
> c+1540*f*muac^5*mus+1276*f*muac^3*mus^3+3796*f*muac^4*mus^2+744*ks*mua
> c^4*mus-756*kac^2*muac^2*mus^2+1215*ks*muac^4*kac-1680*muac^3*mus^2*ka
> c+1368*mus*muac^4*kac+324*mus*muac^3*kac^2+729*ks*muac^3*kac^2-1080*ks
> *muac^3*mus^2-324*mus^3*muac*kac^2-936*muac^2*mus^3*kac+261*muac*kac*m
> us^3*ks*f)/(2324*muac^3*mus^2*f+1476*muac^2*f*ks*mus*kac+2214*muac*kac
> *mus^2*ks*f+540*muac*ks*mus*kac^2*f-81*muac^3*kac^2*f-123*muac^4*kac*f
> +1359*muac^3*mus*f*kac+2739*muac^2*mus^2*f*kac+495*kac^2*muac^2*mus*f+
> 1028*muac^4*mus*f+801*mus^2*muac*kac^2*f+1248*muac^4*kac+756*muac^3*ka
> c^2-212*f*muac^5+512*muac^5+700*muac^2*f*mus^3+594*kac^2*mus^2*ks*f+11
> 52*muac^3*f*ks*mus+1932*muac^2*f*ks*mus^2+825*muac*f*kac*mus^3+225*kac
> ^2*mus^3*f-204*muac^4*f*ks-54*muac^2*kac^2*ks*f-90*muac^3*kac*ks*f+504
> *ks*muac^4+168*ks*muac^2*mus^2+1215*ks*muac^3*kac+2616*mus*muac^3*kac+
> 324*mus^2*muac*kac^2+261*ks*mus^2*muac*kac+810*ks*mus*muac*kac^2+81*ks
> *mus^2*kac^2+936*kac*muac^2*mus^2+576*muac^3*mus^2+1248*ks*muac^3*mus+
> 2124*ks*kac*muac^2*mus+1472*mus*muac^4+1080*mus*muac^2*kac^2+729*ks*mu
> ac^2*kac^2);

> eq111:=numer(simplify(subs(ks=1/3/(1-2*nus),mus=1/2/(1+nus),eq11)));

> # limit developement in vicinity of f=1
> # -------------------------------------
> E1dv:=convert(series(subs(muac=m*(1-f),kac=k*(1-f),eq111),f=1,3),polyn
> om);E2dv:=(convert(series(subs(muac=m*(1-f),kac=k*(1-f),eq222),f=1,4),
> polynom));


> sol:=solve({E1dv,E2dv},{m,k});evalf(sol[3]);

> kk:=rhs(sol[3][2]);mm:=rhs(sol[3][1]);nu:=(3/2*kk/mm-1)/(1+3*kk/mm);


> toto:=solve(1575*_Z^2-142*_Z+3,_Z);mmm:=toto[2];kkk:=1/3-25/3*mmm;nunu
> :=simplify((3/2*kkk/mmm-1)/(1+3*kkk/mmm));nununu:=expand(3*(-19+3*sqrt
> (79))*(43+16*sqrt(79))/(16^2*79-43^2));evalf(nununu);


> # limit developement in vicinity of f=0
```

```
> # -------------------------------------
> E1dv:=simplify(convert(series(subs(muac=1/2/(1+nus)*(1-m*f),kac=1/3/(1
> -2*nus)*(1-k*f),eq111),f=0,2),polynom));E2dv:=simplify((convert(series
> (subs(muac=1/2/(1+nus)*(1-m*f),kac=1/3/(1-2*nus)*(1-k*f),eq222),f=0,2)
> ,polynom)));

> sol:=solve({E1dv,E2dv},{m,k});k0:=rhs(sol[1]);m0:=rhs(sol[2]);
>
> kac0:=1/3/(1-2*nus)*(1-k0*f):muac0:=1/2/(1+nus)*(1-m0*f):Eac0:=collect
> (simplify(convert(series(3*kac0*muac0/(kac0+muac0/3),f=0,2),polynom)),
> f);nuac0:=collect(simplify(convert(series(1/2*(kac0-2*muac0/3)/(kac0+m
> uac0/3),f=0,2),polynom)),f);

> factor(15*nus^2+12*nus-27);factor((15*nus^3-3*nus^2-15*nus+3));
```

A.4 SCS_cyl_thetamax.mws

This MAPLE file concerns the homogenization of a porous polycrystal with a self-consistent scheme. The solid phase is represented by axisymmetrically oriented needles (cylinders), the pores by spheres.

```
> # SCS for isotropic, cylindrical inclusions (solids) and spherical
> inclusions (empty pores)
> # Deviation of cylinders between 0 and theta_max
> # ENPC, Mai 2005
> #
> ************************************************************************
> *******************
> restart:with(tens3d):with(eshelby):Digits:=10:
> w1:=array(1..3,[cos(phi),sin(phi),0]):
> vectw1:=def_tenseur(w1,[cont],base_fond):
> w2:=array(1..3,[-sin(phi),cos(phi),0]):
> vectw2:=def_tenseur(w2,[cont],base_fond):
> e3:=array(1..3,[0,0,1]):
> vectw3:=def_tenseur(e3,[cont],base_fond):
> BW:=def_base(vectw1,vectw2,vectw3);

# Procedure for P
# --------------------
> P:=proc(wink,C1111,C1122,C1133,C3333,C2323) global compPter:
> theta:=wink:
> C:=rigi_orthrev(C1111,C1122,C1133,C3333,C2323):
> comp1:=array(1..3,[1,0,0]):
> vect1:=def_tenseur(comp1,[cont],base_fond):
>
> comp2:=array(1..3,[0,cos(theta),-sin(theta)]):
> vect2:=def_tenseur(comp2,[cont],base_fond):
>
> comp3:=array(1..3,[0,sin(theta),cos(theta)]):
> vect3:=def_tenseur(comp3,[cont],base_fond):
> B:=def_base(vect1,vect2,vect3):
> QQ:=(vect1 &t1 C) &t1 vect1:
> TT:=(vect2 &t1 C) &t1 vect2:
> RR:=(vect1 &t1 C) &t1 vect2:tRR:=(vect2 &t1 C) &t1 vect1:
> KZ:=((z^2) &** QQ)&++(z &** (RR &++ tRR))&++ TT:
>
>
> #Determination of comatrix
> compKZ:= composantes(KZ,[cont,cont],B):
> compCoKZ:= array(1..3,1..3):
> compCoKZ[1,1]:= compKZ[2,2]*compKZ[3,3]-(compKZ[2,3])^2:
> compCoKZ[1,2]:= -(compKZ[2,1]*compKZ[3,3]-compKZ[2,3]*compKZ[3,1]):
> compCoKZ[1,3]:= compKZ[2,1]*compKZ[3,2]-compKZ[2,2]*compKZ[3,1]:
> compCoKZ[2,1]:= compCoKZ[1,2]:
> compCoKZ[2,2]:= compKZ[1,1]*compKZ[3,3]-(compKZ[1,3])^2:
> compCoKZ[2,3]:= -(compKZ[1,1]*compKZ[3,2]-compKZ[1,2]*compKZ[3,1]):
> compCoKZ[3,1]:= compCoKZ[1,3]:
> compCoKZ[3,2]:= compCoKZ[2,3]:
> compCoKZ[3,3]:= compKZ[1,1]*compKZ[2,2]-(compKZ[1,2])^2:
> CoKZ:= def_tenseur(compCoKZ,[cont,cont],B):
>
> eq:= &det(KZ):
> EQ:= subs(z=sqrt(Z),eq):
>
> sol:=solve(EQ,Z):
> #Trouver les solutions avec la partie imaginaire strictement positive
> #-------------------------------------------------------------------
```

```
> sol1:=solve(z^2=sol[1],z):
> h1:= evalc(sol1[1]):h2:= evalc(sol1[2]):
> if evalf(Im(h1)) > evalf(Im(h2)) then sol1:=sol1[1] else sol1:=sol1[2]
> end if:
> sol2:=solve(z^2=sol[2],z):
> h1:= evalc(sol2[1]):h2:= evalc(sol2[2]):
> if evalf(Im(h1)) > evalf(Im(h2)) then sol2:=sol2[1] else sol2:=sol2[2]
> end if:
>
> sol3:=solve(z^2=sol[3],z):
> h1:= evalc(sol3[1]):h2:= evalc(sol3[2]):
> if evalf(Im(h1)) > evalf(Im(h2)) then sol3:=sol3[1] else sol3:=sol3[2]
> end if:
>
> #Trouver les poles multiples
> #---------------------------
> b:=array(1..2,1..4,[[I,sol1,sol2,sol3],[1,1,1,1]]):
> epsilon:= 0.01:
>
> # 1 avec 2,3 et 4
> for j from 2 to 4 do
>    i:=1:
>    if abs(b[1,i]-b[1,j]) < epsilon then
>    b[2,i]:=b[2,i]+1;
>    b[2,j]:=0;
>    end if:
>   #print(b[2,1]);
> end do:
>
> # 2 avec 3 et 4
> if b[2,2] <> 0 then
>    if abs(b[1,2]-b[1,3]) < epsilon then
>    b[2,2]:=b[2,2]+1;
>    b[2,3]:=0;
>    end if;
> end if:
>
> if b[2,2] <> 0 then
>    if abs(b[1,2]-b[1,4]) < epsilon then
>    b[2,3]:=b[2,3]+1;
>    b[2,4]:=0;
>    end if;
> end if:
>
> # 3 avec 4
> if b[2,3] <> 0 then
>    if abs(b[1,3]-b[1,4]) < epsilon then
>    b[2,3]:=b[2,3]+1;
>    b[2,4]:=0;
>    end if;
> end if:
>
> detK:=subs(Z=z^2,(EQ)):
> Q:=limit(detK/z^6,z=infinity)*(z^2+1)^b[2,1]*(z^2-sol1^2)^b[2,2]*(z^2-
> sol2^2)^b[2,3]*(z^2-sol3^2)^b[2,4]:
>
> xi:=(z&** vect1 )&++( vect2 ):
> QQ_:=(vect1 &t CoKZ) &t vect1:
> TT_:=(vect2 &t CoKZ) &t vect2:
> RR_:=(vect1 &t CoKZ) &t vect2:tRR_:=(vect2 &t CoKZ) &t vect1:
> M:=((z^2) &** QQ_)&++(z &** (RR_ &++ tRR_))&++ TT_:
> compM:=composantes(M,[cont,cont,cont,cont],B):
> compGR:=array(1..3,1..3,1..3,1..3):
> for i from 1 to 3 do
> for j from 1 to 3 do
> for k from 1 to 3 do
> for l from 1 to 3 do
> compGR[i,j,k,l]:=(compM[i,j,k,l]+compM[i,j,l,k]+compM[j,i,k,l]+compM[j
```

```
> ,i,l,k])/4:
> od:od:od:od:
> GR:=def_tenseur(compGR,[cont,cont,cont,cont],B):
> compPbis:=array(1..3,1..3,1..3,1..3):
> for i from 1 to 3 do
> for j from 1 to 3 do
> for k from 1 to 3 do
> for l from 1 to 3 do
> #Residue 1
>   if b[2,1] <> 0 then
>   n:=b[2,1]:
>   f1:= (compGR[i,j,k,l]/Q)*((z-b[1,1])^n):
>
> residue1:=coeff(convert(subs(z-b[1,1]=v,series(f1,z=b[1,1],n+1)),polyn
> om),v,n-1):
>   else residue1:=0:
>   end if:
> #Residue 2
>   if b[2,2] <> 0 then
>   n:=b[2,2]:
>   f2:= (compGR[i,j,k,l]/Q)*((z-b[1,2])^n):
>   residue2:=
> coeff(convert(subs(z-b[1,2]=v,series(f2,z=b[1,2],n+1)),polynom),v,n-1)
> :
>   else residue2:=0;
>   end if:
> #Residue 3
>   if b[2,3] <> 0 then
>   n:=b[2,3]:
>   f2:= (compGR[i,j,k,l]/Q)*((z-b[1,3])^n):
>   residue3:=
> coeff(convert(subs(z-b[1,3]=v,series(f2,z=b[1,3],n+1)),polynom),v,n-1)
> :
>   else residue3:=0;
>   end if:
> #Residue 4
>   if b[2,4] <> 0 then
>   n:=b[2,4]:
>   f4:= (compGR[i,j,k,l]/Q)*((z-b[1,4])^n):
>   residue4:=
> coeff(convert(subs(z-b[1,4]=v,series(f4,z=b[1,4],n+1)),polynom),v,n-1)
> :
>   else residue4:=0;
>   end if;
> #
> compPbis[i,j,k,l]:= ( 2*I*simplify(residue1 +  residue2 + residue3 +
> residue4)):
> od:od:od:od:
> Pbis:=def_tenseur(compPbis,[cont,cont,cont,cont],B):
> compPter:=array(1..3,1..3,1..3,1..3):
> compPter:=composantes(Pbis,[cont,cont,cont,cont],base_fond):
> return(compPter):
> end proc:
>
> # ------------------------------------------------------------------------------------

> f:=0.7:nus:=0.27:ks:=1/3/(1-2*nus):mus:=1/2/(1+nus):
> Cs:=rigi_iso(ks,mus):

> CMT:=((1-f)&** Cs)&t2 inv4(((1-f)&** Iso(1)) &++ (f&** inv4(Iso(1) &--
> esh_iso_sph(ks,mus))));

                      CMT := _tenseur_3d_ordre_4_

> Co:=CMT:
> # Increments for theta
> # --------------------
> theta_max:= 67.5*(Pi/180):
```

```
> incr:=30:                #Nombre des increments
> dtheta:=theta_max/incr;
> array_theta:=array(1..incr):for i from 0 to incr-1 do
>   array_theta[i+1]:= i*dtheta:
> end do:
> print(array_theta);
>
> # Start iteration for SCS
> # ------------------------
> for numit from 1 to 8 do
> print(numit);
>
>
> # Initialisation
> comptoto:= array(1..3,1..3,1..3,1..3):
>   for i from 1 to 3 do
>   for j from 1 to 3 do
>   for k from 1 to 3 do
>   for l from 1 to 3 do
>      comptoto[i,j,k,l]:=0:
>   end do:end do:end do:end do:
>
> # Calcul de sommes pour theta et d'integrals pour phi
> #
> for m from 1 to incr do
>   #print(m):print(array_theta[m]):
>
> P(array_theta[m],comp4(Co,1,1,1,1),comp4(Co,1,1,2,2),comp4(Co,1,1,3,3)
> ,comp4(Co,3,3,3,3),comp4(Co,2,3,2,3));
>   compPter:=map(Re,compPter):
>
>   PU:=def_tenseur(compPter,[cont,cont,cont,cont],base_fond);
>
>   A0:=inv4(Iso(1)&++(PU &t2 (Cs &-- Co))):
>
>
> compA0:=array(1..3,1..3,1..3,1..3):compA0:=composantes(A0,[cont,cont,c
> ont,cont],base_fond):
>   A:=def_tenseur(compA0,[cont,cont,cont,cont],BW);
>   compA:=array(1..3,1..3,1..3,1..3):
>   compA:=composantes(A,[cont,cont,cont,cont],base_fond):
>
>   for i from 1 to 3 do
>   for j from 1 to 3 do
>   for k from 1 to 3 do
>   for l from 1 to 3 do
>
> comptoto[i,j,k,l]:=comptoto[i,j,k,l]+evalf(Int(compA[i,j,k,l],phi=0..2
> *Pi)*sin(array_theta[m])):
>   end do:end do:end do:end do:
>
> end do:
>
> # Multiplication de la constante
> for i from 1 to 3 do
>   for j from 1 to 3 do
>   for k from 1 to 3 do
>   for l from 1 to 3 do
>
> comptoto[i,j,k,l]:=comptoto[i,j,k,l]*dtheta*(1-f)/(2*Pi*(1-cos(theta_m
> ax))):
> end do:end do:end do:end do:
>
> toto:=def_tenseur(comptoto,[cont,cont,cont,cont],base_fond):
> eshsph:=esh_orthrev_sph(comp4(Co,1,1,1,1),comp4(Co,1,1,2,2),comp4(Co,1
> ,1,3,3),comp4(Co,3,3,3,3),comp4(Co,2,3,2,3)):

> # SCS homogenization
> # ------------------
```

```
> locsph:=f &** inv4(Iso(1) &-- eshsph):
> Chom:=(Cs &t2 toto) &t2 inv4(locsph &++ toto):
> print(mat(Chom));
> Co:=Chom:
> end do:   # Next numit = iteration step




> # Determination of elastic constants
> # -------------------------------------------
> E_:=1/comp4(Shom1,1,1,1,1);nu_:=-comp4(Shom1,1,1,2,2)/comp4(Shom1,1,1,
> 1,1);Eaxe:=1/comp4(Shom1,3,3,3,3);nuaxe:=-comp4(Shom1,1,1,3,3)/comp4(S
> hom1,3,3,3,3);G_:=comp4(Chom1,2,3,2,3);
> Shom:=inv4(Chom);
> E_:=1/comp4(Shom,1,1,1,1);nu_:=-comp4(Shom,1,1,2,2)/comp4(Shom,1,1,1,1
> );Eaxe:=1/comp4(Shom,3,3,3,3);nuaxe:=-comp4(Shom,1,1,3,3)/comp4(Shom,3
> ,3,3,3);G_:=comp4(Chom,2,3,2,3);
> elastic:=[1/comp4(Shom,1,1,1,1),
> -comp4(Shom,1,1,2,2)/comp4(Shom,1,1,1,1), 1/comp4(Shom,3,3,3,3),
> -comp4(Shom,1,1,3,3)/comp4(Shom,3,3,3,3), comp4(Chom,2,3,2,3)];
```

Appendix B

Source codes for computation on elasticity of extracellular and extravascular bone material (Chapter 3)

All calculations were performed with MATLAB, Version 6.5.

B.1 trab.m

This MATLAB file contains experimental data of Ashman and Rho [1988] and McCarthy et al. [1990] as well as calculations. This file must be run before file ashman88.m (Section B.4) and mccarthy90_horse.m (Section B.7). This file was originally written for the investigations published in [Hellmich, 2005] and modified for the present work.

```
%-------------------------------
% experiments of Ashman and Rho (1988); cited Ashman:88
%-------------------------------
% material:
% human and bovine cancellous bone from femora
% (the fourth value is bovine cancellous bone)
% empty pores; wet (physiological saline solution)
%-------------------------------
% measurement of structural density (app. dens. of trab. bone)
rhostrashman88=[0.283 0.344 0.376 0.592];
%---------------------------------
% measurement of material density (mass dens. of solid bone matrix)
rhosolidashman88=[1.803 1.777 1.730 1.739];
%-------------------------------
% measurement of structural velocity (50 kHz) in longitudinal direction
vkHzashman88=[1.795 2.197 2.325 1.851];
%-------------------------------------
% measurement of material velocity (2.25 MHz) in longitudinal direction
vMHzashman88=[2.639 2.721 2.754 2.501];

%**********************************

```

```
% experiments of McCarthy et al. (1990)
% material:
% cortical bone from dorsal cortex of horse
% solid bone matrix wet; marrow removed
%--------------------------------
% measurement of porosity (porous space) from Fig. 4
pormccarthy90=[    5     6     6     7     7     7     8     9     9     9 ...
                   9    10    10    10    10    10   10.5   11    11    11 ...
                  12    12    12    13    14    14    18    18    22    25 ...
                  30    44];
%--------------------------------
% measurement of circumferential ultrasound velocity (from Fig. 4)
vt2mccarthy90= [3.550 3.575 3.625 3.675 3.400 3.400 3.550 3.325 3.400 3.425 3.550 ...
    3.400 3.500 3.525 3.525 3.600 3.450 3.400 3.425 3.500 3.350 3.400 3.425 3.500 ...
    3.525 3.550 3.425 3.450 3.500 3.150 3.200 2.950];
%--------------------------------
% measurement of apparent (structural) mass density (from Fig. 3)
rhostrmccarthy90= [  2.03  2.02  2.01  2.01  2.00  2.00  2.00  1.98  1.98  1.98  1.98 ...
                     1.97  1.97  1.96  1.96  1.95  1.95  1.95  1.95  1.95  1.95  1.93 ...
                     1.93  1.93  1.92  1.92  1.92  1.92  1.91  1.91  1.91  1.90  1.90 ...
                     1.82  1.76  1.65];
%--------------------------------
% measurement of longitudinal ultrasound velocity (from Fig. 3)
% 2.25 MHz frequency
vmccarthy90=  [ 4.300 4.200 4.100 4.400 4.200 4.200 4.300 4.100 4.150 4.150 4.300 4.025 ...
                4.200 4.025 4.200 3.950 4.025 4.100 4.100 4.150 4.150 4.025 4.100 4.250 ...
                4.000 4.025 4.200 4.200 4.125 4.175 4.350 3.950 4.000 4.000 3.850 3.650];
%--------------------------------
% measurement of transverse ultrasound velocity (from Fig. 3)
% 2.25 MHz frequency
vtmccarthy90= [ 3.600 3.550 3.450 3.650 3.550 3.400 3.575 3.425 3.350 3.500 3.600 3.500 3.350 ...
                3.500 3.600 3.525 3.400 3.350 3.425 3.450 3.550 3.350 3.300 3.475 3.350 3.400 ...
                3.350 3.400 3.350 3.475 3.450 3.125 3.400 3.300 3.200 2.950];


%***********************************
% C A L C U L A T I O N S
%***********************************
% calculations Ashman and Rho (1988)
%-------------------------------------
% calculation of the volume fraction of solid phase
%-------------------------------------
for i=1:length(rhostrashman88)
vfashman88(i)=rhostrashman88(i)/rhosolidashman88(i);
end
%-------------------------------------
% calculation of elastic stiffness constant of trab. bone
% (in the longitudinal direction)
%-------------------------------------
for i=1:length(rhostrashman88)
ckHzlongashman88(i)=rhostrashman88(i)*vkHzashman88(i)^2*1000;
end
%-------------------------------------
% calculation of elastic stiffness constant of solid phase
% (in the longitudinal direction)
%-------------------------------------
for i=1:length(rhostrashman88)
cMHzlongashman88(i)=rhosolidashman88(i)*vMHzashman88(i)^2*1000;
end

%***********************************
% calculations McCarthy et al. (1990)
%-------------------------------------
for i=1:length(pormccarthy90)
vfmccarthy90(i)=1-(pormccarthy90(i)/100);
end
```

```
for i=1:length(rhostrmccarthy90)
cMHzlongmccarthy90(i)=rhostrmccarthy90(i)*vmccarthy90(i)^2*1000;
end
for i=1:length(rhostrmccarthy90)
ctMHzlongmccarthy90(i)=rhostrmccarthy90(i)*vtmccarthy90(i)^2*1000;
end
%-----------------------------------
% assignment of porosity values to structural density
% values and longitudinal ultrasonic velocity values
% by comparison of the circumferential ultrasonic velocity
% (combination of Figures 3 and 4)
%-----------------------------------
for i=1:length(rhostrmccarthy90)
  for j=1:length(pormccarthy90)
    if vt2mccarthy90(j)==vtmccarthy90(i)
    corrpormccarthy90(i,j)=pormccarthy90(j);
    else
    corrpormccarthy90(i,j)=0;
    end
  end
% check for zero values  -- vary velocity by 0.025
  if sum(corrpormccarthy90(i,1:length(pormccarthy90)))==0
    for j=1:length(pormccarthy90)
% pay attention with equal non-zero values -- take tolerance
      if abs(vt2mccarthy90(j)-(vtmccarthy90(i)+0.025))<0.01
      corrpormccarthy90(i,j)=pormccarthy90(j);
      end
    end
  end
end
% sort the porosity values
%-----------------------------------
for i=1:length(rhostrmccarthy90)
corrsortmccarthy90(i,1:length(pormccarthy90))=sort(corrpormccarthy90(i,1:length(pormccarthy90)));
end
%-----------------------------------
% take the LARGEST porosity values
% assign one porosity value to each velocity
%-----------------------------------
for i=length(rhostrmccarthy90):-1:1
  count=0;
  for k=i:length(rhostrmccarthy90)
    if corrsortmccarthy90(i,1:length(pormccarthy90))==corrsortmccarthy90(k,1:length(pormccarthy90));
    count=count+1;
    end
  end
  count=count-1;
  por2mccarthy90(i)=0;
  for j=count:-1:0
    if corrsortmccarthy90(i,length(pormccarthy90)-j)>0
       if por2mccarthy90(i)==0
          por2mccarthy90(i)=corrsortmccarthy90(i,length(pormccarthy90)-j);
%--------------------------------------------------
% por2mccarthy90 are the ASSIGNED porosity values
%--------------------------------------------------
       end
    end
  end
end
% correct por2mccarthy such that the mean value accords with paper
%--------------------------------------------------
for i=1:length(rhostrmccarthy90)
  por22mccarthy90(i)=12.35/mean(por2mccarthy90)*por2mccarthy90(i);
end
for i=1:length(rhostrmccarthy90)
```

```
  vf2mccarthy90(i)=(1-por22mccarthy90(i)/100);
end
%-----------------------------------
% take the SMALLEST porosity values
% assign one porosity value to each velocity
%-----------------------------------
% get the number of porosities per velocity
for i=1:length(rhostrmccarthy90)
  numnonzero(i)=0;
  for j=1:length(pormccarthy90)
    if corrpormccarthy90(i,j)>0
      numnonzero(i)=numnonzero(i)+1;
    end
  end
end
for i=1:length(rhostrmccarthy90)
  count=0;
  for k=i:-1:1
    if corrsortmccarthy90(i,1:length(pormccarthy90))==corrsortmccarthy90(k,1:length(pormccarthy90));
    count=count+1;
    end
  end
  count=count-1;
  if numnonzero(i)<count+1
    por3mccarthy90(i)=corrsortmccarthy90(i,length(pormccarthy90));
  else
    por3mccarthy90(i)=corrsortmccarthy90(i,length(pormccarthy90)-numnonzero(i)+count+1);
  end
end

%---------------------------------------
% BMMB 2005:
% calculate the mass density of ultrastructure
% of the bone specimens of McCarthy et al. (1990)
%---------------------------------------
rhowaterpores=1.0;

for i=1:length(rhostrmccarthy90)
% extravascular bone matrix
% Eq.(17) with f_lac=2% and f_hav=3%
tildeflacmccarthy90=0.021;
tildefultramccarthy90=1-tildeflacmccarthy90;
% microstructure
% Eq.(19) and (17)
fhavmccarthy90(i)=(por22mccarthy90(i)/100-tildeflacmccarthy90)/(1-tildeflacmccarthy90);
flacmccarthy90(i)=tildeflacmccarthy90.*(1-fhavmccarthy90(i));
% mass density of extravascular bone material: Eq.(33)
rhoexhavEMPTYmccarthy90(i)=rhostrmccarthy90(i)/(1-fhavmccarthy90(i));
% mass density of ultrastructure: Eq.(34)
rhoultEMPTYHAVmccarthy90(i)=(rhoexhavEMPTYmccarthy90(i)-rhowaterpores.*tildeflacmccarthy90)/...
  (1-tildeflacmccarthy90);
end

%----------------------------------------
% BMMB 2005:
% calculate extra-Haversian stiffness of McCarthy(1990)
% Eq.(42) and (44)
%----------------------------------------
for i=1:length(rhostrmccarthy90)
  c_exhavEMPTY_ax_mccarthy90(i)=rhoexhavEMPTYmccarthy90(i)*vmccarthy90(i)^2*1000;
  c_exhavEMPTY_rad_mccarthy90(i)=rhoexhavEMPTYmccarthy90(i)*vtmccarthy90(i)^2*1000;
end
```

B.2 ultrasonic_BMMB2005.m

This MATLAB file contains experimental data of Lees et al. [1979, 1983, 1994] and calculations. This file must be run before file Lees_ultra_ax.m (Section B.5) and Lees_ultra_rad.m (Section B.6). This file was originally written for the investigations published in [Hellmich et al., 2004a] and modified for the present work.

```
% BMMB 2005
% Data of Lees 79, 83, 94
% ----------------------------------------

clear

%---------------------------------------------
% Calculate volume fractions
%---------------------------------------------
% microstructure
% --------------
fhav=0.03;
flac=0.02;
fmupor=fhav+flac;

% extravascular bone material
% ---------------------------
tildefultra=(1-fmupor)/(1-fhav);
tildeflac=1-tildefultra;

% real mass densities [g/ml]
rhowater=1.0;
rhocoll=1.41;
rhomin=3.00;
% constants for fibrillar morphology
b=1.47; % nm
D=64;   % nm
vcol=335.6; % nm^3

%*************************************************************************

% DATA according to Lees:94
% (1) BAPN-dosage: 0 0.05 0.1 0.2 0.4 0.6 1.0
rhomicroLees94=  [2.0500    2.0400    2.0400    2.0500    1.9800    1.9700    1.9600];
% Haversian canals measured from images in Lees:94 for all
% dosages except 0.6 (not used for validation)
fhavLees94=[0.10 0.09 0.03 0.06 0.06 fhav 0.22];
flacLees94=tildeflac*(1-fhavLees94);
fmuporLees94= fhavLees94+flacLees94;
% ultrastructural density
rhoultraLees94= (rhomicroLees94 - fmuporLees94)./(1-fmuporLees94);

% microstructural weight fractions
WFminmicroLees94=[0.6600    0.6600    0.6600    0.6500    0.6300    0.6200    0.6200];
WForgmicroLees94=[0.2000    0.2100    0.2100    0.2100    0.2100    0.1900    0.2100];
vradLees94= [3.3300    3.2700    3.2600    3.2400    3.1100    3.0700    3.0300];

% ultrastructural weight fraction
WFmupormicroLees94=1*fmupor./rhomicroLees94;
WFminultraLees94= WFminmicroLees94./(1-WFmupormicroLees94);
WForgultraLees94= WForgmicroLees94./(1-WFmupormicroLees94);

% diffraction spacing
dsLees94= -0.2000.*rhoultraLees94+1.658;   % linear relationship
```

```
% (2) Fluor-dosage:(1) (2) (4) 20 30 50 60 70 90 100
% 11 values are given for mass density and weight fractions
% but only 10 values are given for sonic velocities
rhomicroLees94_2=  [  2.00    2.03    2.040    2.05    2.02    1.97    1.86    1.73    1.65    1.75];
% Haversian canals measured from images in Lees:94 for
% dosages 4, 60, 90
fhavLees94_2= [fhav fhav 0.08 fhav fhav fhav 0.10 fhav 0.35 fhav];
flacLees94_2=tildeflac*(1-fhavLees94_2);
fmuporLees94_2= fhavLees94_2+flacLees94_2;

% ultrastructural density
rhoultraLees94_2= (rhomicroLees94_2 - fmuporLees94_2)./(1-fmuporLees94_2);

% microstructural weight fractions
WFminmicroLees94_2=[  0.70    0.70    0.710    0.71    0.70    0.67    0.65    0.62    0.56    0.62];
WForgmicroLees94_2=[  0.17    0.17    0.160    0.16    0.17    0.16    0.17    0.17    0.16    0.17];
vradLees94_2= [  3.20    3.22    3.220    3.26    3.22    2.93    2.74    2.72    2.57    2.78];

% ultrastructural weight fraction
WFmupormicroLees94_2=1*fmupor./rhomicroLees94_2;
WFminultraLees94_2= WFminmicroLees94_2./(1-WFmupormicroLees94_2);
WForgultraLees94_2= WForgmicroLees94_2./(1-WFmupormicroLees94_2);

% diffraction spacing
dsLees94_2= -0.2000.*rhoultraLees94_2+1.658;   % linear relationship


% calculate stiffness values and volume fractions
c1111Lees94=rhoultraLees94.*vradLees94.*vradLees94;
c1111Lees94_2=rhoultraLees94_2.*vradLees94_2.*vradLees94_2;
vfminLees94=rhoultraLees94.*WFminultraLees94/rhomin;
vfminLees94_2=rhoultraLees94_2.*WFminultraLees94_2/rhomin;
vfcollLees94=0.9*rhoultraLees94.*WForgultraLees94/rhocoll;
vfcollLees94_2=0.9*rhoultraLees94_2.*WForgultraLees94_2/rhocoll;

fHALees94=vfminLees94;fcolLees94=vfcollLees94;
vfibLees94=5*D.*dsLees94.*b;   % nm^3
ffibLees94=fcolLees94.*vfibLees94./vcol;
fefLees94=1-ffibLees94;
phiHAefLees94=(1-ffibLees94)./(1-fcolLees94);
brevefHALees94=fHALees94.*(1-phiHAefLees94)./ffibLees94;  % fibril
brevefwetcolLees94=1-brevefHALees94;
checkfHALees94=phiHAefLees94.*fHALees94./fefLees94;  % extrafibrillar space
circlefcolLees94=fcolLees94./brevefwetcolLees94;   % wet collagen

fHALees94_2=vfminLees94_2;fcolLees94_2=vfcollLees94_2;
vfibLees94_2=5*D.*dsLees94_2.*b;   % nm^3
ffibLees94_2=fcolLees94_2.*vfibLees94_2./vcol;
fefLees94_2=1-ffibLees94_2;
phiHAefLees94_2=(1-ffibLees94_2)./(1-fcolLees94_2);
brevefHALees94_2=fHALees94_2.*(1-phiHAefLees94_2)./ffibLees94_2;  % fibril
brevefwetcolLees94_2=1-brevefHALees94_2;
checkfHALees94_2=phiHAefLees94_2.*fHALees94_2./fefLees94_2;  % extrafibrillar space
circlefcolLees94_2=fcolLees94_2./brevefwetcolLees94_2;   % wet collagen

%*********************************************************************

% DATA according to Lees:79
% all bovine tibia

% *** AXIAL ***
% Table 1: Axial values
vaxLees79_2=   [3.92  3.92  3.81  3.86  3.90  3.88  3.88  3.92];
vaxdryLees79_2=[4.30  4.31  4.18  4.20  4.20  4.29  4.21  4.20];
```

```
% Table 2: Axial values
laxLees79_2=   [2.078 2.038 2.020 2.028 2.031 2.037 2.036 2.037];
laxdryLees79_2=[2.066 2.026 2.005 2.017 2.017 2.025 2.023 2.024];
%Table 3: Axial values
rhomicroLees79_2=   [2.06  2.05  2.02  2.02  2.00  2.05  2.10  2.08];

% Haversian canals:
fhavLees79_2=fhav*ones(1,length(rhomicroLees79_2));

% ultrastructural density
rhoultraLees79_2= (rhomicroLees79_2 - fmupor)/(1-fmupor);

% diffraction spacing
dsLees79_2= -0.2000.*rhoultraLees79_2+1.658;   % linear relationship

% microstructural weight fractions
WFh2omicroLees79_2= [0.123 0.126 0.140 0.140 0.129 0.127 0.118 0.120];
WForgmicroLees79_2= [0.219 0.219 0.239 0.232 0.227 0.230 0.211 0.216];
WFminmicroLees79_2= [0.658 0.656 0.621 0.627 0.644 0.643 0.671 0.664];

% ultrastructural weight fraction
WFmupormicroLees79_2=1*fmupor./rhomicroLees79_2;
WFminultraLees79_2= WFminmicroLees79_2./(1-WFmupormicroLees79_2);
WForgultraLees79_2= WForgmicroLees79_2./(1-WFmupormicroLees79_2);


% *** RADIAL ***
% Table 1: Radial values (labelled ‘nontangential,nonaxial’)
vradLees79=   [3.18  3.18  3.18  3.16  3.27  3.26];
vraddryLees79=[3.36  3.41  3.33  3.37  3.48  3.46];
% Table 2: Radial values (labelled ‘nontangential,nonaxial’)
lradLees79=   [2.083 2.080 2.081 2.021 2.013 2.022];
lraddryLees79=[2.013 2.003 1.997 1.952 1.948 1.957];
% Table 3: Radial values (labelled ‘nontangential,nonaxial’)
rhomicroLees79=    [2.02  1.99  1.95  2.01  2.04  2.05];

% Haversian canals
fhavLees79=fhav*ones(1,length(rhomicroLees79));

% ultrastructural density
rhoultraLees79= (rhomicroLees79 - fmupor)/(1-fmupor);

% diffraction spacing
dsLees79= -0.2000.*rhoultraLees79+1.658;   % linear relationship

% microstructural weight fractions
WFminmicroLees79=  [0.679 0.663 0.640 0.659 0.638 0.674];
WForgmicroLees79=  [0.219 0.219 0.228 0.218 0.242 0.210];
WFh2omicroLees79=  [0.123 0.126 0.131 0.123 0.121 0.116];

% ultrastructural weight fractions
WFmupormicroLees79=1*fmupor./rhomicroLees79;
WFminultraLees79= WFminmicroLees79./(1-WFmupormicroLees79);
WForgultraLees79= WForgmicroLees79./(1-WFmupormicroLees79);

% calculation of stiffness values and volume fractions
% RADIAL
c1111Lees79=rhoultraLees79.*vradLees79.*vradLees79;
vfminLees79=WFminultraLees79.*rhoultraLees79/rhomin;
vfcollLees79=WForgultraLees79.*rhoultraLees79*0.9/rhocoll;

fHALees79=vfminLees79;fcolLees79=vfcollLees79;
vfibLees79=5*D.*dsLees79.*b;   % nm^3
ffibLees79=fcolLees79.*vfibLees79./vcol;
fefLees79=1-ffibLees79;
```

```
phiHAefLees79=(1-ffibLees79)./(1-fcolLees79);
brevefHALees79=fHALees79.*(1-phiHAefLees79)./ffibLees79;  % fibril
brevefwetcolLees79=1-brevefHALees79;
checkfHALees79=phiHAefLees79.*fHALees79./fefLees79;  % extrafibrillar space
circlefcolLees79=fcolLees79./brevefwetcolLees79;   % wet collagen

% AXIAL
c3333Lees79_2=rhoultraLees79_2.*vaxLees79_2.*vaxLees79_2;
vfminLees79_2=WFminultraLees79_2.*rhoultraLees79_2/rhomin;
vfcollLees79_2=WForgultraLees79_2.*rhoultraLees79_2*0.9/rhocoll;
fHALees79_2=vfminLees79_2;fcolLees79_2=vfcollLees79_2;
vfibLees79_2=5*D.*dsLees79_2.*b;   % nm^3
ffibLees79_2=fcolLees79_2.*vfibLees79_2./vcol;
fefLees79_2=1-ffibLees79_2;
phiHAefLees79_2=(1-ffibLees79_2)./(1-fcolLees79_2);
brevefHALees79_2=fHALees79_2.*(1-phiHAefLees79_2)./ffibLees79_2;  % fibril
brevefwetcolLees79_2=1-brevefHALees79_2;
checkfHALees79_2=phiHAefLees79_2.*fHALees79_2./fefLees79_2;  % extrafibrillar space
circlefcolLees79_2=fcolLees79_2./brevefwetcolLees79_2;   % wet collagen

%*************************************************************************

% DATA according to Lees:83

% axial stiffness
% 1.bovine tibia 2.elephant radius 3.human femur 4.deer antler
% 5.deer antler 6.cod clythrum 7.cod clythrum
% velocities
vaxLees83=   [4.18 3.89 3.76 3.08 3.15 2.60 3.02];
vaxdryLees83=[4.47 4.22 3.97 3.72 3.93 3.91 3.67];

% microstructural density, wet bone
rhomicroLees83=   [2.06 1.93 1.96 1.74 1.73 1.61 1.57];

% Haversian canals
fhavLees83=fhav*ones(1,length(rhomicroLees83));

% ultrastructural density, wet bone
rhoultraLees83= (rhomicroLees83 - fmupor)/(1-fmupor);

% microstructrual density, dry bone
rhomicrodryLees83=[2.10 1.97 1.96 1.75 1.83 1.67 1.47];

% Haversian canals, dry bone
fhavdryLees83=fhav*ones(1,length(rhomicrodryLees83));

% ultrastructural density, dry bone
rhoultradryLees83= (rhomicrodryLees83)/(1-fmupor);


% diffraction spacing
dsLees83= -0.2000.*rhoultraLees83+1.658;   % linear relationship
dsdryLees83= 0.1923.*rhoultradryLees83+0.7465;   % linear relationship

% the (microstructural) weight fractions were taken from other publications of Lees et al.
% * bovine tibia from Lees79, see above with rho=2.06
% * elephant datum from Lees/rhoexp(6) see Lees:92/fig.3, see tests.m (bone_packing.d)
% * human femur datum from Lees/rhoexp(14)
% * deer data from Lees/rhoexp(2/3)
% there are no data for cod clythrum
WFminmicroLees83=[0.658 0.630 0.700 0.510 0.520 0 0];
WForgmicroLees83=[0.219 0.230 0.230 0.310 0.320 0 0];

% ultrastructural weight fraction
```

```
WFmupormicroLees83=1*fmupor./rhomicroLees83;
WFminultraLees83= WFminmicroLees83./(1-WFmupormicroLees83);
WForgultraLees83= WForgmicroLees83./(1-WFmupormicroLees83);

% calculate volume fractions and stiffness values
% wet bone
vfminLees83=rhoultraLees83.*WFminultraLees83/rhomin;
vfcollLees83=0.9*rhoultraLees83.*WForgultraLees83/rhocoll;
c3333Lees83=rhoultraLees83.*vaxLees83.*vaxLees83;

fHALees83=vfminLees83;fcolLees83=vfcollLees83;
vfibLees83=5*D.*dsLees83.*b;   % nm^3
ffibLees83=fcolLees83.*vfibLees83./vcol;
fefLees83=1-ffibLees83;
phiHAefLees83=(1-ffibLees83)./(1-fcolLees83);
brevefHALees83=fHALees83.*(1-phiHAefLees83)./ffibLees83;  % fibril
brevefwetcolLees83=1-brevefHALees83;
checkfHALees83=phiHAefLees83.*fHALees83./fefLees83;  % extrafibrillar space
circlefcolLees83=fcolLees83./brevefwetcolLees83;   % wet collagen

% dry bone
WFminmicrodryLees83=(WFminmicroLees83)./(WFminmicroLees83+WForgmicroLees83);
WForgmicrodryLees83=(WForgmicroLees83)./(WFminmicroLees83+WForgmicroLees83);

WFminultradryLees83=(WFminultraLees83)./(WFminultraLees83+WForgultraLees83);
WForgultradryLees83=(WForgultraLees83)./(WFminultraLees83+WForgultraLees83);
vfmindryLees83=rhoultradryLees83.*WFminultradryLees83/rhomin;
vfcolldryLees83=0.9*rhoultradryLees83.*WForgultradryLees83/rhocoll;
c3333dryLees83=rhoultradryLees83.*vaxdryLees83.*vaxdryLees83;

fHAdryLees83=vfmindryLees83;fcoldryLees83=vfcolldryLees83;
vfibdryLees83=5*D.*dsdryLees83.*b;   % nm^3
ffibdryLees83=fcoldryLees83.*vfibdryLees83./vcol;
fefdryLees83=1-ffibdryLees83;
phiHAefdryLees83=(1-ffibdryLees83)./(1-fcoldryLees83);
brevefHAdryLees83=fHAdryLees83.*(1-phiHAefdryLees83)./ffibdryLees83;  % fibril
brevefwetcoldryLees83=1-brevefHAdryLees83;
checkfHAdryLees83=phiHAefdryLees83.*fHAdryLees83./fefdryLees83;  % extrafibrillar space
circlefcoldryLees83=fcoldryLees83./brevefwetcoldryLees83;   % wet collagen


%-------------------------------------------------------------------

% DATA according to Lees:83
% radial stiffness
% 1.bovine tibia 2.dugong rib 3.elephant radius 4.human femur 5.deer antler
% 6.deer antler 7.cod clythrum 8.cod clythrum
% velocities
vradLees83_2=   [3.32 3.00 3.05 3.13 2.38 2.40 1.79 1.96];
vraddryLees83_2=[3.49 3.49 3.35 3.33 2.81 2.91 1.78 2.06];

% microstructrual density, wet bone
rhomicroLees83_2=    [2.07 2.02 1.94 1.93 1.78 1.74 1.26 1.41];

% Haversian canals
fhavLees83_2=fhav*ones(1,length(rhomicroLees83_2));

% ultrastructrual density, wet bone
rhoultraLees83_2= (rhomicroLees83_2 - fmupor)/(1-fmupor);

% microstructrual density, dry bone
rhomicrodryLees83_2= [2.09 2.03 1.97 1.92 1.76 1.82 1.09 1.31];

% Haversian canals, dry bone
```

```
fhavdryLees83_2=fhav*ones(1,length(rhomicrodryLees83_2));

% ultrastructrual density, dry bone
rhoultradryLees83_2= (rhomicrodryLees83_2)/(1-fmupor);

% diffraction spacing
dsLees83_2= -0.2000.*rhoultraLees83_2+1.658;   % linear relationship
dsdryLees83_2= 0.1923.*rhoultradryLees83_2+0.7465;   % linear relationship

% the (microstructural) weight fractions were taken from other publications of Lees et al.
% * bovine tibia from Lees79, see above with rho=2.06
% * dugong rib from Lees/rhoexp(16), see tests. (bone_packing.d)
% * elephant datum from Lees/rhoexp(6) see Lees:92/fig.3, see tests.m (bone_packing.d)
% * human femur datum from Lees/rhoexp(14)
% * deer data from Lees/rhoexp(2/3)
% there are no data for cod clythrum
WFminmicroLees83_2= [0.658 0.710 0.630 0.700 0.510 0.520 0 0];
WForgmicroLees83_2= [0.219 0.170 0.230 0.230 0.310 0.320 0 0];

% ultrastructural weight fraction
WFmupormicroLees83_2=1*fmupor./rhomicroLees83_2;
WFminultraLees83_2= WFminmicroLees83_2./(1-WFmupormicroLees83_2);
WForgultraLees83_2= WForgmicroLees83_2./(1-WFmupormicroLees83_2);

% calculate volume fractions and stiffness values
% wet bone
vfminLees83_2=rhoultraLees83_2.*WFminultraLees83_2/rhomin;
vfcollLees83_2=0.9*rhoultraLees83_2.*WForgultraLees83_2/rhocoll;
c1111Lees83_2=rhoultraLees83_2.*vradLees83_2.*vradLees83_2;

fHALees83_2=vfminLees83_2;fcolLees83_2=vfcollLees83_2;
vfibLees83_2=5*D.*dsLees83_2.*b;   % nm^3
ffibLees83_2=fcolLees83_2.*vfibLees83_2./vcol;
fefLees83_2=1-ffibLees83_2;
phiHAefLees83_2=(1-ffibLees83_2)./(1-fcolLees83_2);
brevefHALees83_2=fHALees83_2.*(1-phiHAefLees83_2)./ffibLees83_2;  % fibril
brevefwetcolLees83_2=1-brevefHALees83_2;
checkfHALees83_2=phiHAefLees83_2.*fHALees83_2./fefLees83_2;  % extrafibrillar space
circlefcolLees83_2=fcolLees83_2./brevefwetcolLees83_2;   % wet collagen

% dry bone
WFminmicrodryLees83_2=(WFminmicroLees83_2)./(WFminmicroLees83_2+WForgmicroLees83_2);
WForgmicrodryLees83_2=(WForgmicroLees83_2)./(WFminmicroLees83_2+WForgmicroLees83_2);

WFminultradryLees83_2=(WFminultraLees83_2)./(WFminultraLees83_2+WForgultraLees83_2);
WForgultradryLees83_2=(WForgultraLees83_2)./(WFminultraLees83_2+WForgultraLees83_2);
vfmindryLees83_2=rhoultradryLees83_2.*WFminultradryLees83_2/rhomin;
vfcolldryLees83_2=0.9*rhoultradryLees83_2.*WForgultradryLees83_2/rhocoll;
c1111dryLees83_2=rhoultradryLees83_2.*vraddryLees83_2.*vraddryLees83_2;

fHAdryLees83_2=vfmindryLees83_2;fcoldryLees83_2=vfcolldryLees83_2;
vfibdryLees83_2=5*D.*dsdryLees83_2.*b;   % nm^3
ffibdryLees83_2=fcoldryLees83_2.*vfibdryLees83_2./vcol;
fefdryLees83_2=1-ffibdryLees83_2;
phiHAefdryLees83_2=(1-ffibdryLees83_2)./(1-fcoldryLees83_2);
brevefHAdryLees83_2=fHAdryLees83_2.*(1-phiHAefdryLees83_2)./ffibdryLees83_2;  % fibril
brevefwetcoldryLees83_2=1-brevefHAdryLees83_2;
checkfHAdryLees83_2=phiHAefdryLees83_2.*fHAdryLees83_2./fefdryLees83_2;  % extrafibrillar space
circlefcoldryLees83_2=fcoldryLees83_2./brevefwetcoldryLees83_2;   % wet collagen
```

B.3 ashman84_human.m

This MATLAB file concerns prediction of stiffness and comparison to experiments of Ashman et al. [1984]. It calls file hom_wetcol_MT.m (Section B.8), hom_fib_SCS.m (Section B.9), hom_ef.m (Section B.10), hom_ultra_MT.m (Section B.11) and hom_exhav.m (Section B.12). This file was originally written for the investigations published in [Hellmich, 2005] and modified for the present work.

```
% BMMB 2005
% -----------------
% calculate the elastic stiffness of human cortical bone
% of Ashman et al. (1984)
% 2.25 MHz --> extravascular bone material
%-----------------------------------------------------
% 5-step-homogeniziation-model for ultrastructure
% wet collagen (MT), fibrils (SCS), extrafibrillar space (SCS),
% ultrastructure (MT), extravascular bone material (MT)
% Wien, August 2005
%
clc
%-----------------------------------------------
% stiffnesses of the elementary components
%-----------------------------------------
% collagen
%---------
ccol(1,1)=11.7;
ccol(2,2)=ccol(1,1);
ccol(3,3)=17.9;
ccol(1,2)=5.1;
ccol(2,1)=ccol(1,2);
ccol(1,3)=7.1;
ccol(3,1)=ccol(1,3);
ccol(3,2)=ccol(3,1);
ccol(2,3)=ccol(3,2);
ccol(4,4)=2*3.3;
ccol(5,5)=ccol(4,4);
ccol(6,6)=2*0.5*(ccol(1,1)-ccol(1,2));

% hydroxyapatite
%---------------
I=[1 0 0 0 0 0; 0 1 0 0 0 0; 0 0 1 0 0 0; 0 0 0 1 0 0; 0 0 0 0 1 0; 0 0 0 0 0 1];
K=[1/3 1/3 1/3 0 0 0; 1/3 1/3 1/3 0 0 0; 1/3 1/3 1/3 0 0 0; 0 0 0 0 0 0; 0 0 0 0 0 0; 0 0 0 0 0 0];
J=I-K;
kHA=82.6;
muHA=44.9;
cHA=2*muHA*J+3*kHA*K;

% ultrastructural water
%----------------------
kuw=2.3;
muuw=0.01;
cuw=3*kuw*K;
kmupores=0.01;
cmupores=3*kmupores*K;
cmupores=3*kuw*K;   %wet pores

%----------------------------------------------
% Calculate volume fractions
%----------------------------------------------
% General values from literature:
rhocoll=1.41; rhomin=3.00; rhowater=1.00;

```

```
% extravascular (extrahaversian) bone material
% ---------------------------------------------
tildeflac=0.021;          % Lees:79
% microstructure
fhav=0.03;                % Lees:79
flac=tildeflac*(1-fhav);  % Eq.(17)
fmupor=fhav+flac;         % Eq.(18)

% mass density of microstructure and ultrastructure; Eq.(20)
rhomicro=1.90;            % Fig. 9 of Ashman84
rhoult=(rhomicro-rhowater*fmupor)/(1-fmupor);  %water-filled Haversian canals+lacunae

% extrahaversian mass density; Eq.(33)
rhoexhav=(rhomicro)/(1-fhav);

% volume fractions ultrastructure barfHA, barfcol
% ----------------------------------------------
% Ultrastructural weight fractions from Lees 83 for wet human femur (axial)
rhomicroLees83=1.96; fmupor=0.05; %(axial)
WFmicro_minLees83=0.70;
WFmicro_orgLees83=0.23;
WFmupormicroLees83=1*fmupor./rhomicroLees83;                % Eq.(22)
WFultra_minLees83=WFmicro_minLees83/(1-WFmupormicroLees83); % Eq.(23)
WFultra_orgLees83=WFmicro_orgLees83/(1-WFmupormicroLees83); % Eq.(24)

WFultra_min=WFultra_minLees83;
WFultra_col=0.9*WFultra_orgLees83;

barfcol=rhoult/rhocoll*WFultra_col    % Eq.(25)
barfHA=rhoult/rhomin*WFultra_min      % Eq.(26)

% diffraction spacing, Eq.(36)
% ----------------------------
ds=-0.2000*rhoult+1.6580;

% volume fractions ultrastructure ffib, fef; Eq.(35)
% --------------------------------------------------
b=1.47; D=64;
vcol=335.6;
vfib=b*ds*5*D;
barffib=barfcol*vfib/vcol;
barfef=1-barffib;

% volume fractions extrafibrillar space; Eq.(37), (39)
% ----------------------------------------------------
phiHAef=(1-barffib)/(1-barfcol);
checkfHA=phiHAef*barfHA/barfef;
checkfuw=1-checkfHA;

% volume fractions fibril; Eq.(38)
% --------------------------------
brevefHA=barfHA*(1-phiHAef)/barffib;
brevefwetcol=1-brevefHA;

% volume fractions wet collagen; Eq.(40), (41)
% ---------------------------------------------
circlefcol=barfcol/brevefwetcol;
circlefuw=1-circlefcol;

%-----------------------------------------------
% Homogenization
%-----------------------------------------------

% Homogenization of wet collagen
% ------------------------------
```

```
hom_wetcol_MT;
cwetcol=Chom

% Homogenization of fibrils
% -------------------------
hom_fib_SCS;
cfib=Chom

% Homogenization of extrafibrillar matrix
% ---------------------------------------
hom_ef;

% Homogenization of ultrastructure
% --------------------------------
hom_ultra_MT;
Cultra=Chom

% Homogenization of extrahaversian matrix
% ---------------------------------------
hom_exhav;
Cexhav=Chom

% -------------------------------------------
% compare predictions and experiments
% -------------------------------------------

% experiments (Ashman 84) [GPa]:
% Ashman measured !microstructural! density with wet bone!
% -------------------------------------------------------
% Experimental stiffness tensor (orthotropic)
Cexp_ashman84=...
    [18.0 9.98 10.1 0 0 0;
     9.98 20.2 10.1 0 0 0;
     10.1 10.1 27.6 0 0 0;
     0 0 0 12.5 0 0;
     0 0 0 0 11.2 0;
     0 0 0 0 0 9.04];

% Experimental stiffness tensor (transverse isotropic)
c11_mean=(Cexp_ashman84(1,1)+Cexp_ashman84(2,2))/2;
c13_mean=(Cexp_ashman84(4,4)+Cexp_ashman84(5,5))/2;

Cexp_ashman84_mean=...
    [c11_mean 9.98 10.1 0 0 0;
     9.98 c11_mean 10.1 0 0 0;
     10.1 10.1 27.6 0 0 0;
     0 0 0 c13_mean 0 0;
     0 0 0 0 c13_mean 0;
     0 0 0 0 0 9.04];

% Corrected exp. stiffness tensor (extravascular mass density)
corr_stiff=rhoexhav/rhomicro      % Eq.(52)
C1111_ashman84=Cexp_ashman84_mean(1,1)*corr_stiff;
C3333_ashman84=Cexp_ashman84_mean(3,3)*corr_stiff;
C1133_ashman84=Cexp_ashman84_mean(1,3)*corr_stiff;
C1313_ashman84=Cexp_ashman84_mean(4,4)*corr_stiff;
C1212_ashman84=Cexp_ashman84_mean(6,6)*corr_stiff;


% predictions
% -----------
C1111_calc=Cexhav(1,1);
C3333_calc=Cexhav(3,3);
C1133_calc=Cexhav(1,3);
C1313_calc=Cexhav(4,4);
C1212_calc=Cexhav(6,6);
```

```

% calculate special errors
% ------------------------
err_ashman84_C3333=(C3333_calc-C3333_ashman84)/C3333_ashman84
err_ashman84_C1111=(C1111_calc-C1111_ashman84)/C1111_ashman84
err_ashman84_C1133=(C1133_calc-C1133_ashman84)/C1133_ashman84
err_ashman84_C1313=(C1313_calc-C1313_ashman84)/C1313_ashman84
err_ashman84_C1212=(C1212_calc-C1212_ashman84)/C1212_ashman84
```

B.4 ashman88.m

This MATLAB file concerns prediction of stiffness and comparison to experiments of Ashman and Rho [1988]. It must be run after file trab.m (Section B.1). It calls file hom_wetcol_MT.m (Section B.8), hom_fib_SCS.m (Section B.9), hom_ef.m (Section B.10), hom_ultra_MT.m (Section B.11) and hom_exhav.m (Section B.12). This file was originally written for the investigations published in [Hellmich, 2005] and modified for the present work.

```
% BMMB 2005
% calculate the elastic stiffness of cortical bone
% of horse bones of Ashman and Rho (1988)
% 2.25 MHz --> extravascular bone material
% RUN FIRST trab.m
%
%-----------------------------------------------------
% 5-step-homogeniziation-model for ultrastructure
% wet collagen (MT), fibrils (SCS), extrafibrillar space (SCS),
% ultrastructure (MT), extravascular bone material (MT)
% Wien, August
%
%----------------------------------------------
% stiffnesses of the elementary components
%-----------------------------------------
% collagen
%---------
ccol(1,1)=11.7;
ccol(2,2)=ccol(1,1);
ccol(3,3)=17.9;
ccol(1,2)=5.1;
ccol(2,1)=ccol(1,2);
ccol(1,3)=7.1;
ccol(3,1)=ccol(1,3);
ccol(3,2)=ccol(3,1);
ccol(2,3)=ccol(3,2);
ccol(4,4)=2*3.3;
ccol(5,5)=ccol(4,4);
ccol(6,6)=2*0.5*(ccol(1,1)-ccol(1,2));

% hydroxyapatite
%---------------
I=[1 0 0 0 0 0; 0 1 0 0 0 0; 0 0 1 0 0 0; 0 0 0 1 0 0; 0 0 0 0 1 0; 0 0 0 0 0 1];
K=[1/3 1/3 1/3 0 0 0; 1/3 1/3 1/3 0 0 0; 1/3 1/3 1/3 0 0 0; 0 0 0 0 0 0; 0 0 0 0 0 0; 0 0 0 0 0 0];
J=I-K;
kHA=82.6;
muHA=44.9;
cHA=2*muHA*J+3*kHA*K;

% ultrastructural water
%----------------------
kuw=2.3;
muuw=0.01;
cuw=3*kuw*K;
kmupores=2.3;
cmupores=3*kmupores*K;

%---------------------------------------------
% Calculate volume fractions
%---------------------------------------------
% General values from literature:
rhocoll=1.41;
rhowater=1.0;
rhomin=3.00;
```

```
% extravascular (extrahaversian) bone material
% ---------------------------------------------
tildeflac=0.021;
tildefultra=1-tildeflac;

% mass density of ultrastructure; Eq.(34)
% ---------------------------------------
rhoexvasashman88=rhosolidashman88;
rhoultashman88=(rhoexvasashman88-rhowater*tildeflac)./(1-tildeflac);

for j=1:length(rhosolidashman88)

% volume fractions ultrastructure barfHA, barfcol
% ----------------------------------------------
% Linear relationship rhoult-rhominapp
% correlation coefficients calculated in "stoi_curves_BONE.m" with fmupor=5%, Eq.(29), (31)
% ------------------------------------------------------------------
rhominapp_vec(j)=-2.2558+1.7757*rhoultashman88(j);    %5% micropores for Lees data
vfmin_vec(j)=rhominapp_vec(j)/rhomin;
WForg_vec(j)=rhocoll/rhoultashman88(j)*(vfmin_vec(j)*(rhomin-rhowater)-...
    rhoultashman88(j)+rhowater)/(rhowater-rhocoll);
vfcoll_vec(j)=0.9*WForg_vec(j)*rhoultashman88(j)/rhocoll;
barfHA=vfmin_vec(j);
barfHAashman88(j)=barfHA;
barfcol=vfcoll_vec(j);
barfcolashman88(j)=barfcol;

% diffraction spacing, Eq.(36)
% ----------------------------
ds=-0.2000*rhoultashman88(j)+1.6580;
dsashman88(j)=ds;

% volume fractions ultrastructure ffib, fef; Eq.(35)
% --------------------------------------------------
b=1.47; D=64;
vcol=335.6;
vfib=5*D*ds*b;   % nm^3
barffib=barfcol*vfib/vcol;
barffibashman88(j)=barffib;
barfef=1-barffib;

% volume fractions extrafibrillar space; Eq.(37), (39)
% ----------------------------------------------------
phiHAef=(1-barffib)/(1-barfcol);
checkfHA=phiHAef*barfHA/barfef;
checkfHAashman88(j)=checkfHA;
checkfuw=1-checkfHA;

% volume fractions fibril; Eq.(38)
% --------------------------------
brevefHA=barfHA*(1-phiHAef)/barffib;
brevefHAashman88(j)=brevefHA;

% volume fractions wet collagen; Eq.(40), (41)
% ---------------------------------------------
brevefwetcol=1-brevefHA;
circlefcol=barfcol/brevefwetcol;
circlefcolashman88(j)=circlefcol;
circlefuw=1-circlefcol;

%---------------------------------------------
% Homogenization
%---------------------------------------------
```

```
% Homogenization of wet collagen
% ------------------------------
hom_wetcol_MT;
cwetcol=Chom

% Homogenization of fibrils
% -------------------------
hom_fib_SCS;
cfib=Chom

% Homogenization of extrafibrillar matrix
% ---------------------------------------
hom_ef;

% Homogenization of ultrastructure
% --------------------------------
hom_ultra_MT;
Cultra=Chom

% Homogenization of extravascular matrix
% --------------------------------------
hom_exhav;
Cexhav=Chom

% Calculate elastic constants
% ---------------------------
Dest=inv(Cexhav);
Ehom=1/Dest(3,3);
Ethom=1/Dest(1,1);
nuhom=-Dest(1,3)*Ehom;
nuthom=-Dest(1,2)*Ethom;
calcEhomashman88(j)=1000*Ehom;
calcEthomashman88(j)=1000*Ethom;
calcC1111ashman88(j)=1000*Cexhav(1,1);
calcC3333ashman88(j)=1000*Cexhav(3,3);
calcC1313ashman88(j)=1000*0.5*Cexhav(5,5);
calcC1212ashman88(j)=1000*0.5*Cexhav(4,4);

end

%-------------------------------------------------------------
% compare prediction and experiments
%-------------------------------------------------------------
plot(cMHzlongashman88,calcC3333ashman88,'o')
axis([0 40000 0 40000])
hold on
plot([0 40000],[0 40000])
xlabel('C_l_o_n_g, measured')
ylabel('C_l_o_n_g, predicted')
grid on
pause
hold off

% compute correlation coefficient
% for comparison of c11, c12, c22 between
% experimental data and model results
%--------------------------------------------
realashman88=[cMHzlongashman88];
homashman88=[calcC3333ashman88];
for i=1:length(realashman88)
    helprealashman88(i)=realashman88(i)-mean(realashman88);
    helphomashman88(i)=homashman88(i)-mean(homashman88);
end
srealhomashman88=1/length(realashman88)*helprealashman88*helphomashman88';
srealashman88=sqrt(1/length(realashman88)*helprealashman88*helprealashman88');
```

```
shomashman88=sqrt(1/length(homashman88)*helphomashman88*helphomashman88');
corrcoeff=srealhomashman88/srealashman88/shomashman88;
rsqu_all=corrcoeff^2

% calculate relative prediction errors
%---------------------------------------
for i=1:length(realashman88)
err_ashman88(i)=(homashman88(i)-realashman88(i))/(realashman88(i));
end
rsqu_all=corrcoeff^2
meanerr_ashman88=mean(err_ashman88)
stderr_ashman88=std(err_ashman88)
plot(realashman88,err_ashman88,'o')
title('Ashman and Rho (1988), trabecular bone ultrastructure')
xlabel('measured stiffnesses')
ylabel('relative prediction error')
grid on


%*************************************************************************
%
% tables for article "BMMB 2005"
%table_ashman88=...
%    [rhosolidashman88' vMHzashman88' cMHzlongashman88'./1000   0.01*round(100*barfcolashman88')...
%     0.01*round(100*barfHAashman88') 0.01*round(100*dsashman88') 0.01*round(100*barffibashman88') ...
%     0.01*round(100*checkfHAashman88') 0.01*round(100*brevefHAashman88') ...
%     0.01*round(100*circlefcolashman88')]


% write matrix to file
%outfile=fopen('table.txt','w');
%fprintf(outfile,'Ashman88 (1)\r\n')
%fprintf(outfile,'human femur & wet & %3.2f & %3.2f & %3.1f & %3.2f & %3.2f & %3.2f & %3.2f
%         & %3.2f & %3.2f & %3.2f & %3.2f \\\\ \r\n',table_ashman88');
%fclose(outfile);

```

B.5 lees_ultra_ax.m

This file concerns prediction of stiffness and comparison to experiments of Lees et al. [1979, 1983]. It must be run after file ultrasonic_BMMB2005.m (Section B.2). It calls file hom_wetcol_MT.m (Section B.8), hom_fib_SCS.m (Section B.9), hom_ef.m (Section B.10) and hom_ultra_MT.m (Section B.11). This file was originally written for the investigations published in [Hellmich et al., 2004a] and modified for the present work.

```
% BMMB 2005
% calculate the elastic stiffness of cortical bone
% of Lees (79, 83)
% RUN first ultrasonic_BMMB2005
%-----------------------------------------------
% 4-step-homogeniziation-model for ultrastructure
% extrafibrillar space (SCS), wet HA (MT), fibrils (SCS),
% ultrastructure (MT)
% Wien, August 2005
%-------------------------------------------------------
% compare AXIAL stiffnesses
% of model and experiments
%-------------------------------------------------------

% constants for fibrillar morphology
b=1.47; % nm
D=64;   % nm
vcol=335.6; % nm^3

%---------------------------------------------
% stiffnesses of the elementary components
%-----------------------------------------
% collagen
%---------
ccol(1,1)=11.7;
ccol(2,2)=ccol(1,1);
ccol(3,3)=17.9;
ccol(1,2)=5.1;
ccol(2,1)=ccol(1,2);
ccol(1,3)=7.1;
ccol(3,1)=ccol(1,3);
ccol(3,2)=ccol(3,1);
ccol(2,3)=ccol(3,2);
ccol(4,4)=2*3.3;
ccol(5,5)=ccol(4,4);
ccol(6,6)=2*0.5*(ccol(1,1)-ccol(1,2));
% hydroxyapatite
%---------------
I=[1 0 0 0 0 0; 0 1 0 0 0 0; 0 0 1 0 0 0; 0 0 0 1 0 0; 0 0 0 0 1 0; 0 0 0 0 0 1];
K=[1/3 1/3 1/3 0 0 0; 1/3 1/3 1/3 0 0 0; 1/3 1/3 1/3 0 0 0; 0 0 0 0 0 0; 0 0 0 0 0 0; 0 0 0 0 0 0];
J=I-K;
kHA=82.6;
muHA=44.9;
cHA=2*muHA*J+3*kHA*K;
% ultrastructural water
%----------------------
kuw=2.3;
muuw=0.01;
cuw=3*kuw*K;


% Lees 79
% *******
```

```
clear c33hom vfmin vfcoll c33real tissuename errorc33

% define tissue types
%---------------
tissuename(1,:)=  ['cow-tibia             I   Lees et al. (79)'];
tissuename(2,:)=  ['cow-tibia            II   Lees et al. (79)'];
tissuename(3,:)=  ['cow-tibia           III   Lees et al. (79)'];
tissuename(4,:)=  ['cow-tibia            IV   Lees et al. (79)'];
tissuename(5,:)=  ['cow-tibia             V   Lees et al. (79)'];
tissuename(6,:)=  ['cow-tibia            VI   Lees et al. (79)'];
tissuename(7,:)=  ['cow-tibia           VII   Lees et al. (79)'];
tissuename(8,:)=  ['cow-tibia          VIII   Lees et al. (79)'];
vfmin=[vfminLees79_2];
vfcoll=vfcollLees79_2;
c33real=c3333Lees79_2;
ds=dsLees79_2;

%---------------------------------------------
% Calculate volume fractions
%---------------------------------------------
for j=1:length(vfmin)

% volume fractions ultrastructure barfHA, barfcol
% ----------------------------------------------
barfHA=vfmin(j);
barfcol=vfcoll(j);
vfib=5*D*ds(j)*b;

% volume fractions ultrastructure ffib, fef; Eq.(35)
% -------------------------------------------------
barffib=barfcol*vfib/vcol;
barfef=1-barffib;

% volume fractions extrafibrillar space; Eq.(37), (39)
% ----------------------------------------------------------------
phiHAef=(1-barffib)/(1-barfcol);
checkfHA=phiHAef*barfHA/barfef;
checkfuw=1-checkfHA;

% volume fractions fibril; Eq.(38)
% --------------------------------
brevefHA=barfHA*(1-phiHAef)/barffib;

% volume fractions wet collagen; Eq.(40), (41)
% ------------------------------------------------
brevefwetcol=1-brevefHA;
circlefcol=barfcol/brevefwetcol;
circlefuw=1-circlefcol;

%---------------------------------------------
% Homogenization
%---------------------------------------------

% Homogenization of wet collagen
% ------------------------------
hom_wetcol_MT;
cwetcol=Chom

% Homogenization of fibrils
% -------------------------
hom_fib_SCS;
cfib=Chom

% Homogenization of extrafibrillar matrix
% ---------------------------------------
hom_ef;
```

```

% Homogenization of ultrastructure
% -------------------------------
hom_ultra_MT;
Cultra=Chom

tissuename(j,:)
c33hom(j)=Cultra(3,3);

end

% determine error
%---------------
 for i=1:length(vfmin)
 errorc33(i)=(c33hom(i)-c33real(i))/c33real(i);
 end
 c3333homLees79=c33hom
 errorc3333Lees79=errorc33
 meanerrorc3333Lees79=mean(errorc33)
 stderrorc3333Lees79=std(errorc33)
 maxerrorc3333Lees79=max(errorc33)
 minerrorc3333Lees79=min(errorc33)
 plot(c3333Lees79_2,c3333homLees79,'o')
 hold on
 plot([0 50],[0 50])
 legend('Lees et al. (1979) -- cow tibia',2)
 grid on
 xlabel('C_{3333} experiment')
 ylabel('C_{3333} model')
 hold off
clear c33hom vfmin vfcoll c33real tissuename errorc33

% Lees 83 wet
% ***********
% define tissue types
%---------------
tissuename(1,:)= ['bovine tibia              Lees et al. (83)'];
tissuename(2,:)= ['elephant radius           Lees et al. (83)'];
tissuename(3,:)= ['human femur               Lees et al. (83)'];
tissuename(4,:)= ['deer antler I             Lees et al. (83)'];
tissuename(5,:)= ['deer antler II            Lees et al. (83)'];
vfmin=[vfminLees83(1) vfminLees83(2) vfminLees83(3) vfminLees83(4) vfminLees83(5)];
vfcoll=[vfcollLees83(1) vfcollLees83(2) vfcollLees83(3) vfcollLees83(4) vfcollLees83(5)];
diffsp=[dsLees83(1) dsLees83(2) dsLees83(3) dsLees83(4) dsLees83(5)];
c33real=[c3333Lees83(1) c3333Lees83(2) c3333Lees83(3) c3333Lees83(4) c3333Lees83(5)];

%---------------------------------------------
% Calculate volume fractions
%---------------------------------------------
for j=1:length(vfmin)

% volume fractions ultrastructure barfHA, barfcol
% ----------------------------------------------
ds=diffsp(j);
barfHA=vfmin(j);
barfcol=vfcoll(j);
vfib=5*D*ds*b;

% volume fractions ultrastructure ffib, fef; Eq.(35)
% -------------------------------------------------
barffib=barfcol*vfib/vcol;
barfef=1-barffib;

% volume fractions extrafibrillar space; Eq.(37), (39)
% ----------------------------------------------------------
phiHAef=(1-barffib)/(1-barfcol);
```

```
checkfHA=phiHAef*barfHA/barfef;
checkfuw=1-checkfHA;

% volume fractions fibril; Eq.(38)
% --------------------------------
brevefHA=barfHA*(1-phiHAef)/barffib;

% volume fractions wet collagen; Eq.(40), (41)
% ---------------------------------------------------
brevefwetcol=1-brevefHA;
circlefcol=barfcol/brevefwetcol;
circlefuw=1-circlefcol;

%---------------------------------------------
% Homogenization
%---------------------------------------------

% Homogenization of wet collagen
% ------------------------------
hom_wetcol_MT;
cwetcol=Chom

% Homogenization of fibrils
% -------------------------
hom_fib_SCS;
cfib=Chom

% Homogenization of extrafibrillar matrix
% ---------------------------------------
hom_ef;

% Homogenization of ultrastructure
% --------------------------------
hom_ultra_MT;
Cultra=Chom

tissuename(j,:)
c33hom(j)=Cultra(3,3);

end

% determine error
%---------------
for i=1:length(vfmin)
 errorc33(i)=(c33hom(i)-c33real(i))/c33real(i)
end

 c3333homLees83=c33hom
 errorc3333Lees83=errorc33
 meanerrorc3333Lees83=mean(errorc33)
 stderrorc3333Lees83=std(errorc33)
 maxerrorc3333Lees83=max(errorc33)
 minerrorc3333Lees83=min(errorc33)
 plot(c33real,c3333homLees83,'o')
 hold on
 plot([0 50],[0 50])
 legend('Lees et al. (1983) -- different mammalian bones',2)
 grid on
 xlabel('C_{3333} experiment')
 ylabel('C_{3333} model')
 hold off
%* pause
clear c33hom vfmin vfcoll c33real tissuename errorc33

% Lees83 dry
% **********
% no bulk modulus of air !!!!!!
```

```
kuw=0.01;
cuw=3*kuw*K;
% define tissue types
tissuename(1,:)= ['bovine tibia (DRY)        Lees et al. (83)'];
tissuename(2,:)= ['elephant radius (DRY)     Lees et al. (83)'];
tissuename(3,:)= ['human femur (DRY)         Lees et al. (83)'];
tissuename(4,:)= ['deer antler I (DRY)       Lees et al. (83)'];
tissuename(5,:)= ['deer antler II (DRY)      Lees et al. (83)'];
vfmin=[vfmindryLees83(1) vfmindryLees83(2) vfmindryLees83(3) vfmindryLees83(4) vfmindryLees83(5)];
vfminwet=[vfminLees83(1) vfminLees83(2) vfminLees83(3) vfminLees83(4) vfminLees83(5)];
vfcoll=[vfcolldryLees83(1) vfcolldryLees83(2) vfcolldryLees83(3) vfcolldryLees83(4) vfcolldryLees83(5)];
vfcollwet=[vfcollLees83(1) vfcollLees83(2) vfcollLees83(3) vfcollLees83(4) vfcollLees83(5)];
diffsp=[dsdryLees83(1) dsdryLees83(2) dsdryLees83(3) dsdryLees83(4) dsdryLees83(5)];
diffspwet=[dsLees83(1) dsLees83(2) dsLees83(3) dsLees83(4) dsLees83(5)];
c33real=[c3333dryLees83(1) c3333dryLees83(2) c3333dryLees83(3) c3333dryLees83(4) c3333dryLees83(5)];

%---------------------------------------------
% Calculate volume fractions
%---------------------------------------------
for j=1:length(vfmin)

% volume fractions ultrastructure barfHA, barfcol
% ---------------------------------------------
ds=diffsp(j);
dswet=diffspwet(j);
barfHA=vfmin(j);
barfHAwet=vfminwet(j);
barfcol=vfcoll(j);
barfcolwet=vfcollwet(j);
vfib=5*D*ds*b;
vfibwet=5*D*dswet*b;

% volume fractions ultrastructure ffib, fef; Eq.(35)
% ------------------------------------------------
barffib=barfcol*vfib/vcol;
barffibwet=barfcolwet*vfibwet/vcol;
barfef=1-barffib;

% volume fractions extrafibrillar space; Eq.(37), (39)
% ----------------------------------------------------------
phiHAef=(1-barffibwet)/(1-barfcolwet);
checkfHA=phiHAef*barfHA/barfef;
checkfuw=1-checkfHA;

% volume fractions fibril; Eq.(38)
% --------------------------------
brevefHA=barfHA*(1-phiHAef)/barffib;

% volume fractions wet collagen; Eq.(40), (41)
% ------------------------------------------------
brevefwetcol=1-brevefHA;
circlefcol=barfcol/brevefwetcol;
circlefuw=1-circlefcol;

%---------------------------------------------
% Homogenization
%---------------------------------------------

% Homogenization of wet collagen
% ------------------------------
hom_wetcol_MT;
cwetcol=Chom

% Homogenization of fibrils
% -------------------------
```

```
hom_fib_SCS;
cfib=Chom

% Homogenization of extrafibrillar matrix
% ----------------------------------------
hom_ef;

% Homogenization of ultrastructure
% --------------------------------
hom_ultra_MT;
Cultra=Chom

tissuename(j,:)
c33hom(j)=Cultra(3,3);

end

% determine error
%---------------
for i=1:length(vfmin)
errorc33(i)=(c33hom(i)-c33real(i))/c33real(i);
end
c3333dryhomLees83=c33hom
errorc3333dryLees83=errorc33
meanerrorc3333dryLees83=mean(errorc33)
stderrorc3333dryLees83=std(errorc33)
maxerrorc3333dryLees83=max(errorc33)
minerrorc3333dryLees83=min(errorc33)
plot(c33real,c3333dryhomLees83,'o')
hold on
plot([0 50],[0 50])
legend('Lees et al. (1983) -- different mammalian bones DRY',2)
grid on
xlabel('C_{3333} experiment')
ylabel('C_{3333} model')
hold off

%------------- plot all ---------------------
plot(c3333Lees79_2,c3333homLees79,'s','MarkerSize',11)
hold on
plot([c3333Lees83(1) c3333Lees83(2) c3333Lees83(3) c3333Lees83(4) ...
        c3333Lees83(5)],c3333homLees83,'o','MarkerSize',11)
plot([c3333dryLees83(1) c3333dryLees83(2) c3333dryLees83(3) c3333dryLees83(4) ...
        c3333dryLees83(5)],c3333dryhomLees83,'*','MarkerSize',11)
plot([0 50],[0 50],'LineWidth',2)
set(gca,'FontSize',17,'XTick',[0 10 20 30 40 50],'XTickLabel',{'0','10','20','30','40','50'},...
    'YTick',[0 10 20 30 40 50],'YTickLabel',{'0','10','20','30','40','50'});
legend('L79','L83 wet','L83 dry',0)
grid on
xlabel('axial stiffness C_{3333} [GPa] -  experiment')
ylabel('axial stiffness C_{3333} [GPa] -  model')
% print -deps comparison_ax_III.eps
print -deps lees_comp_ax.eps
hold off

% determine error for all wet tissues
%-----------------------------------
clear c33hom c33real
c33hom=[c3333homLees79 c3333homLees83 c3333dryhomLees83]
c33real=[c3333Lees79_2 c3333Lees83(1) c3333Lees83(2) c3333Lees83(3) c3333Lees83(4) c3333Lees83(5)...
    c3333dryLees83(1) c3333dryLees83(2) c3333dryLees83(3) c3333dryLees83(4) c3333dryLees83(5)];
for i=1:length(c33hom)
errorc33(i)=(c33hom(i)-c33real(i))/c33real(i);
end
errorc3333all=errorc33
```

```
meanerrorc3333all=mean(errorc33)
stderrorc3333all=std(errorc33)
maxerrorc3333all=max(errorc33)
minerrorc3333all=min(errorc33)
```

B.6 lees_ultra_rad.m

This file concerns prediction of stiffness and comparison to experiments of Lees et al. [1979, 1983, 1994]. It must be run after file ultrasonic_BMMB2005.m (Section B.2). It calls file hom_wetcol_MT.m (Section B.8), hom_fib_SCS.m (Section B.9), hom_ef.m (Section B.10) and hom_ultra_MT.m (Section B.11). This file was originally written for the investigations published in [Hellmich et al., 2004a] and modified for the present work.

```
% BMMB 2005
% calculate the elastic stiffness of cortical bone
% of Lees (79, 83, 94)
% RUN first ultrasonic_BMMB2005
%-----------------------------------------------
% 4-step-homogeniziation-model for ultrastructure
% extrafibrillar space (SCS), wet HA (MT), fibrils (SCS),
% ultrastructure (MT)
% Wien, August 2005
%-------------------------------------------------------
% compare RADIAL stiffnesses
% of model and experiments
%-------------------------------------------------------

% constants for fibrillar morphology
b=1.47; % nm
D=64;   % nm
vcol=335.6; % nm^3

clear c11hom vfmin vfcoll c11real tissuename errorc11
%---------------------------------------------
% stiffnesses of the elementary components
%-----------------------------------------
% collagen
%---------
ccol(1,1)=11.7;
ccol(2,2)=ccol(1,1);
ccol(3,3)=17.9;
ccol(1,2)=5.1;
ccol(2,1)=ccol(1,2);
ccol(1,3)=7.1;
ccol(3,1)=ccol(1,3);
ccol(3,2)=ccol(3,1);
ccol(2,3)=ccol(3,2);
ccol(4,4)=2*3.3;
ccol(5,5)=ccol(4,4);
ccol(6,6)=2*0.5*(ccol(1,1)-ccol(1,2));
% hydroxyapatite
%---------------
I=[1 0 0 0 0 0; 0 1 0 0 0 0; 0 0 1 0 0 0; 0 0 0 1 0 0; 0 0 0 0 1 0; 0 0 0 0 0 1];
K=[1/3 1/3 1/3 0 0 0; 1/3 1/3 1/3 0 0 0; 1/3 1/3 1/3 0 0 0; 0 0 0 0 0 0; 0 0 0 0 0 0; 0 0 0 0 0 0];
J=I-K;
kHA=82.6;
muHA=44.9;
cHA=2*muHA*J+3*kHA*K;
% ultrastructural water
%----------------------
kuw=2.3;
muuw=0.01;
cuw=3*kuw*K;


% Lees 79
```

```
% *******

% define tissue types
%---------------
tissuename(1,:)=  ['cow-tibia             I   Lees et al. (79)'];
tissuename(2,:)=  ['cow-tibia            II   Lees et al. (79)'];
tissuename(3,:)=  ['cow-tibia           III   Lees et al. (79)'];
tissuename(4,:)=  ['cow-tibia            IV   Lees et al. (79)'];
tissuename(5,:)=  ['cow-tibia             V   Lees et al. (79)'];
tissuename(6,:)=  ['cow-tibia            VI   Lees et al. (79)'];
vfmin=[vfminLees79];
vfcoll=vfcollLees79;
c11real=c1111Lees79;
ds=dsLees79;

%---------------------------------------------
% Calculate volume fractions
%---------------------------------------------
for j=1:length(vfmin)

% volume fractions ultrastructure barfHA, barfcol
% ----------------------------------------------
barfHA=vfmin(j);
barfcol=vfcoll(j);
vfib=5*D*ds(j)*b;

% volume fractions ultrastructure ffib, fef; Eq.(35)
% -------------------------------------------------
barffib=barfcol*vfib/vcol;
barfef=1-barffib;

% volume fractions extrafibrillar space; Eq.(37), (39)
% ----------------------------------------------------------
phiHAef=(1-barffib)/(1-barfcol);
checkfHA=phiHAef*barfHA/barfef;
checkfuw=1-checkfHA;

% volume fractions fibril; Eq.(38)
% --------------------------------
brevefHA=barfHA*(1-phiHAef)/barffib;

% volume fractions wet collagen + hom; Eq.(40), (41)
% --------------------------------------------------
brevefwetcol=1-brevefHA;
circlefcol=barfcol/brevefwetcol;
circlefuw=1-circlefcol;

%---------------------------------------------
% Homogenization
%---------------------------------------------

% Homogenization of wet collagen
% ------------------------------
hom_wetcol_MT;
cwetcol=Chom

% Homogenization of fibrils
% -------------------------
hom_fib_SCS;
cfib=Chom

% Homogenization of extrafibrillar matrix
% ---------------------------------------
hom_ef;

% Homogenization of ultrastructure
```

```
% -------------------------------
hom_ultra_MT;
Cultra=Chom

tissuename(j,:)
c11hom(j)=Cultra(1,1);

end

% determine error
%---------------
 for i=1:length(vfmin)
 errorc11(i)=(c11hom(i)-c11real(i))/c11real(i);
 end
 c1111homLees79=c11hom
 errorc1111Lees79=errorc11
 meanerrorc1111Lees79=mean(errorc11)
 stderrorc1111Lees79=std(errorc11)
 maxerrorc1111Lees79=max(errorc11)
 minerrorc1111Lees79=min(errorc11)
clear c11hom vfmin vfcoll c11real tissuename errorc11

% Lees 94 BAPN-rabbit
% *******************
% define tissue types
%---------------
tissuename(1,:)=  ['rabbit BAPN-treated   I   Lees et al. (94)'];
tissuename(2,:)=  ['rabbit BAPN-treated  II   Lees et al. (94)'];
tissuename(3,:)=  ['rabbit BAPN-treated III   Lees et al. (94)'];
tissuename(4,:)=  ['rabbit BAPN-treated  IV   Lees et al. (94)'];
tissuename(5,:)=  ['rabbit BAPN-treated   V   Lees et al. (94)'];
tissuename(6,:)=  ['rabbit BAPN-treated VII   Lees et al. (94)']; % 6th value missing
vfmin= [vfminLees94(1:5) vfminLees94(7)];
vfcoll=[vfcollLees94(1:5) vfcollLees94(7)];
diffsp=[dsLees94(1:5) dsLees94(7)];
c11real=[c1111Lees94(1:5) c1111Lees94(7)];

%---------------------------------------------
% Calculate volume fractions
%---------------------------------------------
for j=1:length(vfmin)

% volume fractions ultrastructure barfHA, barfcol
% ----------------------------------------------
ds=diffsp(j);
barfHA=vfmin(j);
barfcol=vfcoll(j);
vfib=5*D*ds*b;

% volume fractions ultrastructure ffib, fef; Eq.(35)
% -------------------------------------------------
barffib=barfcol*vfib/vcol;
barfef=1-barffib;

% volume fractions extrafibrillar space; Eq.(37), (39)
% ----------------------------------------------------------
phiHAef=(1-barffib)/(1-barfcol);
checkfHA=phiHAef*barfHA/barfef;
checkfuw=1-checkfHA;

% volume fractions fibril; Eq.(38)
% --------------------------------
brevefHA=barfHA*(1-phiHAef)/barffib;

% volume fractions wet collagen + hom; Eq.(40), (41)
% --------------------------------------------------
brevefwetcol=1-brevefHA;
```

```
circlefcol=barfcol/brevefwetcol;
circlefuw=1-circlefcol;

%---------------------------------------------
% Homogenization
%---------------------------------------------

% Homogenization of wet collagen
% ------------------------------
hom_wetcol_MT;
cwetcol=Chom

% Homogenization of fibrils
% -------------------------
hom_fib_SCS;
cfib=Chom

% Homogenization of extrafibrillar matrix
% ---------------------------------------
hom_ef;

% Homogenization of ultrastructure
% --------------------------------
hom_ultra_MT;
Cultra=Chom

tissuename(j,:)
c11hom(j)=Chom(1,1);

end

% determine error
%---------------
 for i=1:length(vfmin)
 errorc11(i)=(c11hom(i)-c11real(i))/c11real(i);
 end
 c1111homLees94=c11hom
 errorc1111Lees94=errorc11
 meanerrorc1111Lees94=mean(errorc11)
 stderrorc1111Lees94=std(errorc11)
 maxerrorc1111Lees94=max(errorc11)
 minerrorc1111Lees94=min(errorc11)
 clear c11hom vfmin vfcoll vfmincorr c11real kestvec2 muestvec2 tissuename errorc11


 % Lees 94 fluor-rabbit
% ********************

% define tissue types
%---------------
tissuename(1,:)= ['rabbit fluor-treated I    Lees et al. (94)'];
tissuename(2,:)= ['rabbit fluor-treated III  Lees et al. (94)'];
tissuename(3,:)= ['rabbit fluor-treated VII  Lees et al. (94)'];
tissuename(4,:)= ['rabbit fluor-treated IX   Lees et al. (94)'];
vfmin=[vfminLees94_2(1) vfminLees94_2(3) vfminLees94_2(7) vfminLees94_2(9)];
vfcoll=[vfcollLees94_2(1) vfcollLees94_2(3) vfcollLees94_2(7) vfcollLees94_2(9)];
diffsp=[dsLees94_2(1) dsLees94_2(3) dsLees94_2(7) dsLees94_2(9)];
c11real=[c1111Lees94_2(1) c1111Lees94_2(3) c1111Lees94_2(7) c1111Lees94_2(9)];

%---------------------------------------------
% Calculate volume fractions
%---------------------------------------------
for j=1:length(vfmin)

% volume fractions ultrastructure barfHA, barfcol
% ----------------------------------------------
ds=diffsp(j);
barfHA=vfmin(j);
```

```
barfcol=vfcoll(j);
vfib=5*D*ds*b;

% volume fractions ultrastructure ffib, fef; Eq.(35)
% ---------------------------------------------------
barffib=barfcol*vfib/vcol;
barfef=1-barffib;

% volume fractions extrafibrillar space; Eq.(37), (39)
% ----------------------------------------------------------
phiHAef=(1-barffib)/(1-barfcol);
checkfHA=phiHAef*barfHA/barfef;
checkfuw=1-checkfHA;

% volume fractions fibril; Eq.(38)
% --------------------------------
brevefHA=barfHA*(1-phiHAef)/barffib;

% volume fractions wet collagen + hom; Eq.(40), (41)
% ---------------------------------------------------
brevefwetcol=1-brevefHA;
circlefcol=barfcol/brevefwetcol;
circlefuw=1-circlefcol;

%---------------------------------------------
% Homogenization
%---------------------------------------------

% Homogenization of wet collagen
% ------------------------------
hom_wetcol_MT;
cwetcol=Chom

% Homogenization of fibrils
% -------------------------
hom_fib_SCS;
cfib=Chom

% Homogenization of extrafibrillar matrix
% ---------------------------------------
hom_ef;

% Homogenization of ultrastructure
% --------------------------------
hom_ultra_MT;
Cultra=Chom

tissuename(j,:)
c11hom(j)=Chom(1,1);

 end

 % determine error
 %---------------
  for i=1:length(vfmin)
  errorc11(i)=(c11hom(i)-c11real(i))/c11real(i);
  end
  c1111homLees94_2=c11hom
  errorc1111Lees94_2=errorc11
  meanerrorc1111Lees94_2=mean(errorc11)
  stderrorc1111Lees94_2=std(errorc11)
  maxerrorc1111Lees94_2=max(errorc11)
  minerrorc1111Lees94_2=min(errorc11)
clear c11hom vfmin vfcoll c11real tissuename errorc11


% Lees83 wet
```

```
% **********
% define tissue types
%---------------
tissuename(1,:)= ['bovine tibia              Lees et al. (83)'];
tissuename(2,:)= ['elephant radius           Lees et al. (83)'];
tissuename(3,:)= ['human femur               Lees et al. (83)'];
tissuename(4,:)= ['deer antler I             Lees et al. (83)'];
tissuename(5,:)= ['deer antler II            Lees et al. (83)'];
vfmin=[vfminLees83_2(1) vfminLees83_2(3) vfminLees83_2(4) vfminLees83_2(5) vfminLees83_2(6)];
vfcoll=[vfcollLees83_2(1) vfcollLees83_2(3) vfcollLees83_2(4) vfcollLees83_2(5) vfcollLees83_2(6)];
diffsp=[dsLees83_2(1) dsLees83_2(3) dsLees83_2(4) dsLees83_2(5) dsLees83_2(6)];
c11real=[c1111Lees83_2(1) c1111Lees83_2(3) c1111Lees83_2(4) c1111Lees83_2(5) c1111Lees83_2(6)];

%----------------------------------------------
% Calculate volume fractions
%----------------------------------------------
for j=1:length(vfmin)

% volume fractions ultrastructure barfHA, barfcol
% ----------------------------------------------
ds=diffsp(j);
barfHA=vfmin(j);
barfcol=vfcoll(j);
vfib=5*D*ds*b;

% volume fractions ultrastructure ffib, fef; Eq.(35)
% ---------------------------------------------------
barffib=barfcol*vfib/vcol;
barfef=1-barffib;

% volume fractions extrafibrillar space; Eq.(37), (39)
% ------------------------------------------------------------
phiHAef=(1-barffib)/(1-barfcol);
checkfHA=phiHAef*barfHA/barfef;
checkfuw=1-checkfHA;

% volume fractions fibril; Eq.(38)
% --------------------------------
brevefHA=barfHA*(1-phiHAef)/barffib;

% volume fractions wet collagen + hom; Eq.(40), (41)
% ---------------------------------------------------
brevefwetcol=1-brevefHA;
circlefcol=barfcol/brevefwetcol;
circlefuw=1-circlefcol;

%----------------------------------------------
% Homogenization
%----------------------------------------------

% Homogenization of wet collagen
% ------------------------------
hom_wetcol_MT;
cwetcol=Chom

% Homogenization of fibrils
% -------------------------
hom_fib_SCS;
cfib=Chom

% Homogenization of extrafibrillar matrix
% ---------------------------------------
hom_ef;

% Homogenization of ultrastructure
% --------------------------------
```

```
hom_ultra_MT;
Cultra=Chom

tissuename(j,:)
c11hom(j)=Chom(1,1);

end

% determine error
%---------------
 for i=1:length(vfmin)
 errorc11(i)=(c11hom(i)-c11real(i))/c11real(i);
 end
 c1111homLees83_2=c11hom
 errorc1111Lees83_2=errorc11
 meanerrorc1111Lees83_2=mean(errorc11)
 stderrorc1111Lees83_2=std(errorc11)
 maxerrorc1111Lees83_2=max(errorc11)
 minerrorc1111Lees83_2=min(errorc11)
clear c11hom vfmin vfcoll c11real tissuename errorc11


% Lees83 dry
% **********
% no bulk modulus of air !!!!!!
kuw=0.01;
cuw=3*kuw*K;
% define tissue types
tissuename(1,:)= ['bovine tibia (DRY)        Lees et al. (83)'];
tissuename(2,:)= ['elephant radius (DRY)     Lees et al. (83)'];
tissuename(3,:)= ['human tibia (DRY)         Lees et al. (83)'];
tissuename(4,:)= ['deer antler I (DRY)       Lees et al. (83)'];
tissuename(5,:)= ['deer antler II (DRY)      Lees et al. (83)'];
vfmin=[vfmindryLees83_2(1) vfmindryLees83_2(3) vfmindryLees83_2(4) vfmindryLees83_2(5)...
        vfmindryLees83_2(6)];
vfminwet=[vfminLees83_2(1) vfminLees83_2(3) vfminLees83_2(4) vfminLees83_2(5) vfminLees83_2(6)];
vfcoll=[vfcolldryLees83_2(1) vfcolldryLees83_2(3) vfcolldryLees83_2(4) vfcolldryLees83_2(5)...
        vfcolldryLees83_2(6)];
vfcollwet=[vfcollLees83_2(1) vfcollLees83_2(3) vfcollLees83_2(4) vfcollLees83_2(5) vfcollLees83_2(6)];
diffsp=[dsdryLees83_2(1) dsdryLees83_2(3) dsdryLees83_2(4) dsdryLees83_2(5) dsdryLees83_2(6)];
diffspwet=[dsLees83_2(1) dsLees83_2(3) dsLees83_2(4) dsLees83_2(5) dsLees83_2(6)];
c11real=[c1111dryLees83_2(1) c1111dryLees83_2(3) c1111dryLees83_2(4) c1111dryLees83_2(5)...
        c1111dryLees83_2(6)];


%---------------------------------------------
% Calculate volume fractions
%---------------------------------------------
for j=1:length(vfmin)

% volume fractions ultrastructure barfHA, barfcol
% ----------------------------------------------
ds=diffsp(j);
dswet=diffspwet(j);
barfHA=vfmin(j);
barfHAwet=vfminwet(j);
barfcol=vfcoll(j);
barfcolwet=vfcollwet(j);
vfib=5*D*ds*b;
vfibwet=5*D*dswet*b;

% volume fractions ultrastructure ffib, fef; Eq.(35)
% ------------------------------------------------
barffib=barfcol*vfib/vcol;
barffibwet=barfcolwet*vfibwet/vcol;
```

```
barfef=1-barffib;

% volume fractions extrafibrillar space; Eq.(37), (39)
% ----------------------------------------------------------
phiHAef=(1-barffibwet)/(1-barfcolwet);
checkfHA=phiHAef*barfHA/barfef;
checkfuw=1-checkfHA;

% volume fractions fibril; Eq.(38)
% --------------------------------
brevefHA=barfHA*(1-phiHAef)/barffib;

% volume fractions wet collagen + hom; Eq.(40), (41)
% ---------------------------------------------------
brevefwetcol=1-brevefHA;
circlefcol=barfcol/brevefwetcol;
circlefuw=1-circlefcol;

%---------------------------------------------
% Homogenization
%---------------------------------------------

% Homogenization of wet collagen
% ------------------------------
hom_wetcol_MT;
cwetcol=Chom

% Homogenization of fibrils
% -------------------------
hom_fib_SCS;
cfib=Chom

% Homogenization of extrafibrillar matrix
% ---------------------------------------
hom_ef;

% Homogenization of ultrastructure
% --------------------------------
hom_ultra_MT;
Cultra=Chom

tissuename(j,:)
c11hom(j)=Chom(1,1);

end

% determine error
%---------------
for i=1:length(vfmin)
errorc11(i)=(c11hom(i)-c11real(i))/c11real(i);
end
c1111dryhomLees83_2=c11hom
errorc1111dryLees83_2=errorc11
meanerrorc1111dryLees83_2=mean(errorc11)
stderrorc1111dryLees83_2=std(errorc11)
maxerrorc1111dryLees83_2=max(errorc11)
minerrorc1111dryLees83_2=min(errorc11)


%------------- plot all ---------------------
plot(c1111Lees79,c1111homLees79,'s','MarkerSize',11)
hold on
plot([c1111Lees83_2(1) c1111Lees83_2(3) c1111Lees83_2(4) c1111Lees83_2(5)...
        c1111Lees83_2(6)],c1111homLees83_2,'o','MarkerSize',11)
plot([c1111dryLees83_2(1) c1111dryLees83_2(3) c1111dryLees83_2(4) c1111dryLees83_2(5) ...
        c1111dryLees83_2(6)],c1111dryhomLees83_2,'*','MarkerSize',11)
```

```
plot([c1111Lees94(1:5) c1111Lees94(7)],c1111homLees94,'p','MarkerSize',11)
plot([c1111Lees94_2(1) c1111Lees94_2(3) c1111Lees94_2(7) c1111Lees94_2(9)],...
    c1111homLees94_2,'d','MarkerSize',11)
plot([0 50],[0 50],'LineWidth',2)
set(gca,'FontSize',17,'XTick',[0 10 20 30 40 50],'XTickLabel',{'0','10','20','30','40','50'},...
    'YTick',[0 10 20 30 40 50],'YTickLabel',{'0','10','20','30','40','50'});
legend('L79','L83 wet','L83 dry','L94 BAPN','L94 fluor',0)
grid on
xlabel('radial stiffness C_{1111} [GPa] -  experiment')
ylabel('radial stiffness C_{1111} [GPa] -  model')
% print -deps comparison_rad_III.eps
print -deps comparison_rad_III_rev.eps
hold off

% determine error for all tissues
%-----------------------------------
clear c11hom c11real
c11hom=[c1111homLees79 c1111homLees83_2 c1111dryhomLees83_2 c1111homLees94 c1111homLees94_2]
c11real=[c1111Lees79 c1111Lees83_2(1) c1111Lees83_2(3) c1111Lees83_2(4) c1111Lees83_2(5)...
        c1111Lees83_2(6) c1111dryLees83_2(1) c1111dryLees83_2(3) c1111dryLees83_2(4)...
        c1111dryLees83_2(5) c1111dryLees83_2(6) c1111Lees94(1:5) c1111Lees94(7)...
        c1111Lees94_2(1) c1111Lees94_2(3) c1111Lees94_2(7) c1111Lees94_2(9)];
for i=1:length(c11hom)
errorc11(i)=(c11hom(i)-c11real(i))/c11real(i);
end
errorc1111all=errorc11
meanerrorc1111all=mean(errorc11)
stderrorc1111all=std(errorc11)
maxerrorc1111all=max(errorc11)
minerrorc1111all=min(errorc11)
```

B.7 mccarthy90_horse.m

This file concerns prediction of stiffness and comparison to experiments of McCarthy et al. [1990]. It must be run after file trab.m (Section B.1). It calls file hom_wetcol_MT.m (Section B.8), hom_fib_SCS.m (Section B.9), hom_ef.m (Section B.10), hom_ultra_MT.m (Section B.11) and hom_exhav.m (Section B.12). This file was written for the investigations published in [Hellmich, 2005] and modified for the present work.

```
% BMMB 2005
% calculate the elastic stiffness of cortical bone
% of horse bones of McCarthy (1990)
% 2.25 MHz --> extravascular bone material
% RUN FIRST trab.m
%
%--------------------------------------------------
% 5-step-homogeniziation-model for ultrastructure
% wet collagen (MT), fibrils (SCS), extrafibrillar space (SCS),
% ultrastructure (MT), extravascular bone material (MT)
% Wien, August 2005
%
%----------------------------------------------
% stiffnesses of the elementary components
%-----------------------------------------
% collagen
%---------
ccol(1,1)=11.7;
ccol(2,2)=ccol(1,1);
ccol(3,3)=17.9;
ccol(1,2)=5.1;
ccol(2,1)=ccol(1,2);
ccol(1,3)=7.1;
ccol(3,1)=ccol(1,3);
ccol(3,2)=ccol(3,1);
ccol(2,3)=ccol(3,2);
ccol(4,4)=2*3.3;
ccol(5,5)=ccol(4,4);
ccol(6,6)=2*0.5*(ccol(1,1)-ccol(1,2));

% hydroxyapatite
%---------------
I=[1 0 0 0 0 0; 0 1 0 0 0 0; 0 0 1 0 0 0; 0 0 0 1 0 0; 0 0 0 0 1 0; 0 0 0 0 0 1];
K=[1/3 1/3 1/3 0 0 0; 1/3 1/3 1/3 0 0 0; 1/3 1/3 1/3 0 0 0; 0 0 0 0 0 0; 0 0 0 0 0 0; 0 0 0 0 0 0];
J=I-K;
kHA=82.6;
muHA=44.9;
cHA=2*muHA*J+3*kHA*K;

% ultrastructural water
%----------------------
kuw=2.3;
muuw=0.01;
cuw=3*kuw*K;
kmupores=2.3;
cmupores=3*kmupores*K;
%
%---------------------------------------------
% Calculate volume fractions
%---------------------------------------------
rhocoll=1.41;
rhowater=1.0;
rhomin=3.00;
```

```
for j=1:length(por22mccarthy90)-1    % last data point eliminated
j
% rhoexhavEMPTY, fhav, flac, tildefultra, tildeflac --> see trab.m
% ---------------------------------------------------------------

% volume fractions ultrastructure barfHA, barfcol
% ----------------------------------------------
% Linear relationship rhoult-rhominapp
% correlation coefficients calculated in "stoi_curves_BONE.m" with fmupor=5%, Eq.(29), (31)
% ---------------------------------------------------------------
rhominapp_vec(j)=-2.2558+1.7757*rhoultEMPTYHAVmccarthy90(j);
barfHAmccarthy90(j)=rhominapp_vec(j)/rhomin;

WForg_vec(j)=rhocoll/rhoultEMPTYHAVmccarthy90(j)*(barfHAmccarthy90(j)*(rhomin-rhowater)-...
    rhoultEMPTYHAVmccarthy90(j)+rhowater)/(rhowater-rhocoll);
barfcolmccarthy90(j)=0.9*WForg_vec(j)*rhoultEMPTYHAVmccarthy90(j)/rhocoll;

% diffraction spacing, Eq.(36)
% ----------------------------
dsmccarthy90(j)=-0.2000*rhoultEMPTYHAVmccarthy90(j)+1.658;

% volume fractions ultrastructure ffib, fef; Eq.(35)
% --------------------------------------------------
b=1.47; D=64;
vcol=335.6;
vfib=5.*D.*dsmccarthy90(j).*b;   % nm^3
barffibmccarthy90(j)=barfcolmccarthy90(j)*vfib/vcol;
barfefmccarthy90(j)=1-barffibmccarthy90(j);
barffib=barffibmccarthy90(j);
barfef=barfefmccarthy90(j);

% volume fractions extrafibrillar space; Eq.(37), (39)
% ----------------------------------------------------------
phiHAefmccarthy90(j)=(1-barffibmccarthy90(j))/(1-barfcolmccarthy90(j));
checkfHAmccarthy90(j)=phiHAefmccarthy90(j)*barfHAmccarthy90(j)/barfefmccarthy90(j);
checkfHA=checkfHAmccarthy90(j);
checkfuw=1-checkfHA;

% volume fractions fibril; Eq.(38)
% --------------------------------
brevefHAmccarthy90(j)=barfHAmccarthy90(j)*(1-phiHAefmccarthy90(j))/barffibmccarthy90(j);
brevefHA=brevefHAmccarthy90(j);

% volume fractions wet collagen; Eq.(40), (41)
% ---------------------------------------------
brevefwetcolmccarthy90(j)=1-brevefHAmccarthy90(j);
brevefwetcol=brevefwetcolmccarthy90(j);
circlefcolmccarthy90(j)=barfcolmccarthy90(j)/brevefwetcol;
circlefcol=circlefcolmccarthy90(j);
circlefuw=1-circlefcol;

%---------------------------------------------
% Homogenization
%---------------------------------------------

% Homogenization of wet collagen
% ------------------------------
hom_wetcol_MT;
cwetcol=Chom

% Homogenization of fibrils
% -------------------------
hom_fib_SCS;
cfib=Chom
```

```
% Homogenization of extrafibrillar matrix
% ---------------------------------------
hom_ef;

% Homogenization of ultrastructure
% --------------------------------
hom_ultra_MT;
Cultra=Chom

% Homogenization of extrahaversian matrix
% ---------------------------------------
tildefultra=tildefultramccarthy90;
tildeflac=1-tildefultra;
hom_exhav;
Cexhav=Chom

% Calculate elastic constants
% ---------------------------
Dest=inv(Cexhav);
Ehom=1/Dest(3,3);
Ethom=1/Dest(1,1);
nuhom=-Dest(1,3)*Ehom;
nuthom=-Dest(1,2)*Ethom;
calcEhommccarthy90(j)=1000*Ehom;
calcEthommccarthy90(j)=1000*Ethom;
calcC1111mccarthy90(j)=1000*Cexhav(1,1);
calcC3333mccarthy90(j)=1000*Cexhav(3,3);
calcC1313mccarthy90(j)=1000*0.5*Cexhav(5,5);
calcC1212mccarthy90(j)=1000*0.5*Cexhav(4,4);

end


%-------------------------------------------------------------
% compare prediction and experiments
%-------------------------------------------------------------
% skip last data point
% experimental stiffness, calculated in "trab.m"
c_exhavEMPTY_ax_mccarthy90=c_exhavEMPTY_ax_mccarthy90(1:35);
c_exhavEMPTY_rad_mccarthy90=c_exhavEMPTY_rad_mccarthy90(1:35);

% make figure for BMMB 2005
% comparison prediction-experiment
% --------------------------------
plot(c_exhavEMPTY_ax_mccarthy90./1000,calcC3333mccarthy90./1000,'o')
hold on
plot(c_exhavEMPTY_rad_mccarthy90./1000,calcC1111mccarthy90./1000,'s')
plot([0 60],[0 60])
axis([0 60 0 60])
set(gca,'FontSize',17,'XTick',[0 10 20 30 40 50 60],'XTickLabel',{'0','10','20','30','40','50','60'},...
   'YTick',[0 10 20 30 40 50 60],'YTickLabel',{'0','10','20','30','40','50','60'});
grid on
xlabel('experimental stiffness [GPa]')
ylabel('predicted stiffness [GPa]')
legend('longitudinal','transversal',2)
%print -deps mccarthy90_comp_axrad_CH.eps
pause
hold off

% compute correlation coefficient
% for comparison of c33, c11 between
% experimental data and model results
%--------------------------------------------
realmccarthy90=[c_exhavEMPTY_ax_mccarthy90 c_exhavEMPTY_rad_mccarthy90];
```

```
hommccarthy90=[calcC3333mccarthy90 calcC1111mccarthy90];
for i=1:length(realmccarthy90)
    helprealmccarthy90(i)=realmccarthy90(i)-mean(realmccarthy90);
    helphommccarthy90(i)=hommccarthy90(i)-mean(hommccarthy90);
end
srealhommccarthy90=1/length(realmccarthy90)*helprealmccarthy90*helphommccarthy90';
srealmccarthy90=sqrt(1/length(realmccarthy90)*helprealmccarthy90*helprealmccarthy90');
shommccarthy90=sqrt(1/length(hommccarthy90)*helphommccarthy90*helphommccarthy90');
corrcoeff=srealhommccarthy90/srealmccarthy90/shommccarthy90;
rsqu_all=corrcoeff^2

% calculate relative prediction errors
%-------------------------------------
for i=1:length(realmccarthy90)
  err_mccarthy90(i)=(hommccarthy90(i)-realmccarthy90(i))/(realmccarthy90(i));
end
rsqu_all=corrcoeff^2
meanerr_mccarthy90=mean(err_mccarthy90)
stderr_mccarthy90=std(err_mccarthy90)
plot(realmccarthy90,err_mccarthy90,'o')
title('McCarthy (1990), equine cortical bone')
xlabel('measured stiffnesses')
ylabel('relative prediction error')
grid on

% calculate special errors
%----------------------------------------
% axial
for i=1:length(calcC3333mccarthy90)
  err_mccarthy90C3333(i)=(calcC3333mccarthy90(i)-c_exhavEMPTY_ax_mccarthy90(i))/...
      c_exhavEMPTY_ax_mccarthy90(i);
end
meanerr_mccarthy90C3333=mean(err_mccarthy90C3333)
stderr_mccarthy90C3333=std(err_mccarthy90C3333)

% radial
for i=1:length(calcC1111mccarthy90)
  err_mccarthy90C1111(i)=(calcC1111mccarthy90(i)-c_exhavEMPTY_rad_mccarthy90(i))/...
      c_exhavEMPTY_rad_mccarthy90(i);
end
meanerr_mccarthy90C1111=mean(err_mccarthy90C1111)
stderr_mccarthy90C1111=std(err_mccarthy90C1111)
```

B.8 hom_wetcol_MT.m

This file concerns the homogenization of 'wet collagen'. It is called by file ashman84_human.m (Section B.3), ashman88 (Section B.4), lees_ultra_ax.m (Section B.5), lees_ultra_rad.m (Section B.6) and mccarthy90_horse.m (Section B.7). This file was originally written for the investigations published in [Hellmich et al., 2004a, Hellmich, 2005].

```
% Homogenization of wet collagen
% Mori-Tanaka-scheme, collagen matrix with cylindrical water inclusions
% Wien, March 2005
% needed variables: circlefuw, circlefcol

C0=ccol;

% evaluate P-tensor for cylindrical inclusions
% in transversely isotropic matrix
%-----------------------------------------
P1111=1/8*(5*C0(1,1)-3*C0(1,2))/C0(1,1)/(C0(1,1)-C0(1,2));
P1122=-1/8*(C0(1,1)+C0(1,2))/C0(1,1)/(C0(1,1)-C0(1,2));
P2222=1/8*(5*C0(1,1)-3*C0(1,2))/C0(1,1)/(C0(1,1)-C0(1,2));
P2323=1/8*1/(0.5*C0(4,4));    % 0.5*C0(4,4)=C0_2323
P1313=1/8*1/(0.5*C0(4,4));    % 0.5*C0(4,4)=C0_2323
P1212=1/8*(3*C0(1,1)-C0(1,2))/C0(1,1)/(C0(1,1)-C0(1,2));
Pcyl=zeros(6,6);
Pcyl(1,1)=P1111;
Pcyl(2,2)=P2222;
Pcyl(1,2)=P1122;
Pcyl(2,1)=Pcyl(1,2);
Pcyl(4,4)=2*P2323;
Pcyl(5,5)=2*P1313;
Pcyl(6,6)=2*P1212;
% evaluate [I+P:(c-C0)]^-1 for uw
%--------------------------
helpuw=inv(I+Pcyl*(cuw-ccol));                %cylindrical inclusions!!!
% evaluate homogenized stiffness
%------------------------------
Chom=(circlefcol*ccol+circlefuw*cuw*helpuw)*inv(circlefcol*I+circlefuw*helpuw);
```

B.9 hom_fib_SCS.m

This file concerns the homogenization of 'mineralized collagen fibril'. It is called by file ashman84_human.m (Section B.3), ashman88 (Section B.4), lees_ultra_ax.m (Section B.5), lees_ultra_rad.m (Section B.6) and mccarthy90_horse.m (Section B.7). This file was originally written for the investigations published in [Hellmich et al., 2004a, Hellmich, 2005].

```
% Homogenization of fibrils
% self-consistent-scheme, wetcol=cylindrical, transversely isotropic inclusions
%                         HA=isotropic, cylindrical inclusions
% Wien, March 2005
%cHA =...
   [137  42.5  54.9  0  0  0
    42.5  137  54.9  0  0  0
    54.9  54.9  172  0  0  0
         0  0  0  79.2  0  0
         0  0  0  0  79.2  0
         0  0  0  0  0  95];

i=0;
% start with cwetcol as the C0-matrix
%-----------------------------------
C0=cwetcol;
C0_old=0;
% iteration for calculation of self-consistent stiffness
%-------------------------------------------------------
while abs((norm(C0)-norm(C0_old))/norm(C0))>0.000001
i=i+1;

%-----------------------------------------------------------------------
% this program needs the following functions:
% fun_Psph_1111, fun_Psph_1122, fun_Psph_1133, fun_Psph_3333, fun_Psph_2323
% evaluate P-tensor for spherical inclusions
% in transversely isotropic matrix
%-----------------------------------------
 P1111=quad('fun_Psph_1111',-1,1,[],[],C0(1,1),C0(1,2),C0(1,3),C0(3,3),C0(4,4)/2);
 P1122=quad('fun_Psph_1122',-1,1,[],[],C0(1,1),C0(1,2),C0(1,3),C0(3,3),C0(4,4)/2);
 P1133=quad('fun_Psph_1133',-1,1,[],[],C0(1,1),C0(1,2),C0(1,3),C0(3,3),C0(4,4)/2);
 P3333=quad('fun_Psph_3333',-1,1,[],[],C0(1,1),C0(1,2),C0(1,3),C0(3,3),C0(4,4)/2);
 P2323=quad('fun_Psph_2323',-1,1,[],[],C0(1,1),C0(1,2),C0(1,3),C0(3,3),C0(4,4)/2);
Psph=zeros(6,6);
Psph(1,1)=P1111;
Psph(2,2)=Psph(1,1);
Psph(3,3)=P3333;
Psph(1,2)=P1122;
Psph(1,3)=P1133;
Psph(2,3)=Psph(1,3);
Psph(2,1)=Psph(1,2);
Psph(3,1)=Psph(1,3);
Psph(3,2)=Psph(2,3);
Psph(4,4)=2*P2323;
Psph(5,5)=Psph(4,4);
Psph(6,6)=2*0.5*(P1111-P1122);

% evaluate P-tensor for cylindrical inclusions
% in transversely isotropic matrix
%-----------------------------------------
P1111=1/8*(5*C0(1,1)-3*C0(1,2))/C0(1,1)/(C0(1,1)-C0(1,2));
P1122=-1/8*(C0(1,1)+C0(1,2))/C0(1,1)/(C0(1,1)-C0(1,2));
P2222=1/8*(5*C0(1,1)-3*C0(1,2))/C0(1,1)/(C0(1,1)-C0(1,2));
P2323=1/8*1/(0.5*C0(4,4));    % 0.5*C0(4,4)=C0_2323
```

```
P1313=1/8*1/(0.5*C0(4,4));    % 0.5*C0(4,4)=C0_2323
P1212=1/8*(3*C0(1,1)-C0(1,2))/C0(1,1)/(C0(1,1)-C0(1,2));
Pcyl=zeros(6,6);
Pcyl(1,1)=P1111;
Pcyl(2,2)=P2222;
Pcyl(1,2)=P1122;
Pcyl(2,1)=Pcyl(1,2);
Pcyl(4,4)=2*P2323;
Pcyl(5,5)=2*P1313;
Pcyl(6,6)=2*P1212;

% evaluate [I+P:(c-C0)]^-1 for wetcol
%----------------------------
helpwetcol=inv(I+Pcyl*(cwetcol-C0));

% evaluate [I+P:(c-C0)]^-1 for HA
%---------------------------
helpHA=inv(I+Psph*(cHA-C0));

% Homogenization
Chom=(brevefwetcol*cwetcol*helpwetcol+brevefHA*cHA*helpHA)*...
    inv(brevefwetcol*helpwetcol+brevefHA*helpHA);
C0_old=C0;
C0=Chom;
end
```

B.10 hom_ef.m

This file concerns the homogenization of 'extrafibrillar space'. It calls fun_kSCS.m (Section B.13) and fun_muSCS.m (Section B.14). It is called by file ashman84_human.m (Section B.3), ashman88 (Section B.4), lees_ultra_ax.m (Section B.5), lees_ultra_rad.m (Section B.6) and mccarthy90_horse.m (Section B.7). This file was originally written for the investigations published in [Hellmich et al., 2004a, Hellmich, 2005].

```
%-------------------------------------------------------------------------
% this program needs the following pre-defined variables:
% checkfHA, kHA, muHA, kuw, muuw
% this program needs the following functions:
% fun_kSCS, fun_muSCS
%-------------------------------------------------------------------------
i=0;
% start with uw as the C0-matrix
%-----------------------------------
k0=kuw;
mu0=muuw;
k0_old=0;
mu0_old=0;
% iteration for calculation of self-consistent stiffness
%-------------------------------------------------------
while abs((norm([k0 mu0])-norm([k0_old mu0_old]))/norm([k0 mu0]))>0.000001
i=i+1;
% evaluate update of khom, muhom
%-------------------------------
khom=fun_kSCS(checkfHA,kHA,muHA,kuw,muuw,k0,mu0);
muhom=fun_muSCS(checkfHA,kHA,muHA,kuw,muuw,k0,mu0);
k0_old=k0;
mu0_old=mu0;
k0=khom;
mu0=muhom;
end
cef=3*khom*K+2*muhom*J
```

B.11 hom_ultra_MT.m

This file concerns the homogenization of 'ultrastructure' or 'extracellular bone matrix'. It is called by file ashman84_human.m (Section B.3), ashman88 (Section B.4), lees_ultra_ax.m (Section B.5), lees_ultra_rad.m (Section B.6) and mccarthy90_horse.m (Section B.7). This file was originally written for the investigations published in [Hellmich et al., 2004a, Hellmich, 2005].

```
% Homogenization of ultrastructure
% Mori-Tanaka-scheme, ef=matrix, fib = inclusions
% Wien, March 2005


a=1;
% calculate Poisson's ratio of polycrystalline matrix
%---------------------------
nup=(3*khom-2*muhom)/(6*khom+2*muhom);
% construct Eshelby's tensor for cylindrical, compressible
% inclusions in compressible matrix
%---------------------------
Qesh=3/(8*pi*(1-nup));
Resh=(1-2*nup)/(8*pi*(1-nup));
% a=3.224 % help value
Ia=2*pi;
Iab=4*pi/(3*(2*a)^2);
Iaa=4*pi/(3*a^2)-Iab;
Sesh11=Qesh*a^2*Iaa+Resh*Ia;
Sesh22=Sesh11;
Sesh33=0;
Sesh12=Qesh*a^2*Iab-Resh*Ia;
Sesh21=Sesh12;
Sesh13=Qesh/3*Ia-Resh*Ia;
Sesh23=Sesh13;
Sesh31=0;
Sesh32=Sesh31;
Sesh44=1/4;
Sesh55=Sesh44;
Sesh66=Qesh/2*(2*a^2)*Iab+Resh*Ia;
Sesh=[Sesh11 Sesh12 Sesh13 0 0 0; Sesh21 Sesh22 Sesh23 0 0 0; ...
      Sesh31 Sesh32 Sesh33 0 0 0; 0 0 0 2*Sesh44 0 0;...
      0 0 0 0 2*Sesh55 0; 0 0 0 0 0 2*Sesh66];
Pcyl=Sesh*inv(cef);

% evaluate [I+P:(c-C0)]^-1 for fib
%--------------------------
helpfib=inv(I+Pcyl*(cfib-cef));                %cylindrical inclusions!!!

Chom=(barfef*cef+barffib*cfib*helpfib)*inv(barfef*I+barffib*helpfib);
```

B.12 hom_exhav.m

This file concerns the homogenization of 'extravascular bone material'. It is called by file ashman84_human.m (Section B.3), ashman88 (Section B.4) and mccarthy90_horse.m (Section B.7).

```
% homogenization of extra-Haversian matrix
%--------------------------------
% micropores=Haversian canals + lacunae

C0=Cultra;

%-------------------------------------------------------------------------
% this program needs the following functions:
% fun_Psph_1111, fun_Psph_1122, fun_Psph_1133, fun_Psph_3333, fun_Psph_2323
% evaluate P-tensor for spherical inclusions
% in transversely isotropic matrix
%-----------------------------------------
 P1111=quad('fun_Psph_1111',-1,1,[],[],C0(1,1),C0(1,2),C0(1,3),C0(3,3),C0(4,4)/2);
 P1122=quad('fun_Psph_1122',-1,1,[],[],C0(1,1),C0(1,2),C0(1,3),C0(3,3),C0(4,4)/2);
 P1133=quad('fun_Psph_1133',-1,1,[],[],C0(1,1),C0(1,2),C0(1,3),C0(3,3),C0(4,4)/2);
 P3333=quad('fun_Psph_3333',-1,1,[],[],C0(1,1),C0(1,2),C0(1,3),C0(3,3),C0(4,4)/2);
 P2323=quad('fun_Psph_2323',-1,1,[],[],C0(1,1),C0(1,2),C0(1,3),C0(3,3),C0(4,4)/2);
Psph=zeros(6,6);
Psph(1,1)=P1111;
Psph(2,2)=Psph(1,1);
Psph(3,3)=P3333;
Psph(1,2)=P1122;
Psph(1,3)=P1133;
Psph(2,3)=Psph(1,3);
Psph(2,1)=Psph(1,2);
Psph(3,1)=Psph(1,3);
Psph(3,2)=Psph(2,3);
Psph(4,4)=2*P2323;
Psph(5,5)=Psph(4,4);
Psph(6,6)=2*0.5*(P1111-P1122);
%-------------------------------------------------------------------------
% evaluate [I+P:(c-C0)]^-1 for lac
%---------------------------
helplac=inv(I+Psph*(cmupores-Cultra));                %spherical inclusions!!!

% Evaluate Cexhav
%------------------------------
%Cmicro=fmupores*cmupores*aa1+fultra*Cultra*aa2
Chom=((1-tildeflac)*Cultra+tildeflac*cmupores*helplac)*...
   inv((1-tildeflac)*I+tildeflac*helplac);
```

B.13 fun_kSCS.m

This file concerns the implicit solution of the self-consistent scheme for the 'extrafibrillar space': determination of elastic constant k^{SCS}. It is called by file hom_ef.m (Section B.10). This file was originally written for the investigations published in [Hellmich, 2005], see also [Hellmich and Ulm, 2002b].

```
function kest = kSCS(f1,k1,mu1,k2,mu2,k0,mu0)
kest=-(4*f1*k1*mu0+4*k2*mu0+3*k2*k1-4*k2*f1*mu0)/(-3*k2*f1-4*mu0-3*k1+3*f1*k1);
```

B.14 fun_muSCS.m

This file concerns the implicit solution of the self-consistent scheme for the 'extrafibrillar space': determination of elastic constant μ^{SCS}. It is called by file hom_ef.m (Section B.10). This file was originally written for the investigations published in [Hellmich, 2005], see also [Hellmich and Ulm, 2002b].

```
function muest=fun_muSCS(f1,k1,mu1,k2,mu2,k0,mu0)
muest=-(9*f1*mu1*mu0*k0+8*f1*mu1*mu0^2+9*mu2*mu0*k0+8*mu2*mu0^2+6*mu2*k0*mu1+...
       12*mu2*mu0*mu1-9*mu2*f1*mu0*k0-8*mu2*f1*mu0^2)/...
       (-6*f1*k0*mu2-12*f1*mu0*mu2-9*mu0*k0-8*mu0^2-6*k0*mu1-12*mu0*mu1+6*f1*k0*mu1+12*f1*mu0*mu1);
```

B.15 fun_Psph_1111.m

This file concerns the determination of the component P_{1111} of the Hill tensor $\mathbb{P}$ for spherical inclusions in a transversely isotropic matrix. It is called by file hom_fib_SCS.m (Section B.9) and hom_exhav.m (Section B.12). This file was originally written for the investigations published in [Hellmich et al., 2004a].

```
% P1111 for spherical inclusions
% in transversely isotropic matrix
%---------------------------------
function y=fun_Psph1111(x,C1111,C1122,C1133,C3333,C2323);
y=-1/16.*(-5.*C1111.*x.^4.*C3333-3.*C1122.*x.^2.*C3333-3.*C1122.*x.^4.*C2323+...
  3.*C1122.*x.^4.*C3333+5.*C1111.*x.^4.*C2323-10.*C1111.*C2323.*x.^2+...
  2.*x.^4.*C1133.^2+8.*C2323.*x.^4.*C3333-6.*C2323.^2.*x.^4+...
  4.*C2323.*x.^4.*C1133+6.*C1122.*C2323.*x.^2+5.*C1111.*C2323+...
  5.*C1111.*x.^2.*C3333-4.*C2323.*x.^2.*C1133+6.*C2323.^2.*x.^2-...
  2.*x.^2.*C1133.^2-3.*C1122.*C2323).*(-1+x.^2)./(-2*C1111.^2*x.^4*C3333+...
  2*C2323.^2*x.^6*C3333-4*C1111*C2323.^2*x.^4-3*C1111.^2*C2323*x.^2+...
  C1111.^2*x.^2*C3333+2*C1111*C2323.^2*x.^2-2*C2323*x.^4*C1133.^2-...
  C1111*C1133.^2*x.^6+2*C1111*C1133.^2*x.^4+4*C2323.^2*x.^6*C1133-...
  2*C1122*C1133.^2*x.^4+2*C2323*x.^6*C1133.^2+3*C1111.^2*x.^4*C2323+...
  C1122*C1133.^2*x.^6-C1111.^2*x.^6*C2323+2*C1111*x.^6*C2323.^2+...
  C1111.^2*x.^6*C3333-C1111*C1133.^2*x.^2-4*C2323.^2*x.^4*C1133+...
```

```
C1122*C1133.^2*x.^2+C1111.^2*C2323-C1122*C1111*C2323-C1122*x.^6*C1111*C3333+...
4*C1111*x.^4*C2323*C1133-2*C1111*x.^2*C2323*C1133-4*C1122*x.^4*C2323*C1133+...
2*C1122*x.^2*C2323*C1133+2*C1122*x.^6*C2323*C1133-2*C1111*x.^6*C2323*C1133-...
3*C1111*x.^6*C2323*C3333+2*C1122*C1111*x.^4*C3333-C1122*C2323*x.^4*C3333-...
3*C1122*C1111*x.^4*C2323-C1122*C1111*x.^2*C3333+3*C1122*C1111*C2323*x.^2+...
3*C1111*C2323*x.^4*C3333+C1122*x.^6*C1111*C2323+C1122*x.^6*C2323*C3333);
```

B.16 fun_Psph_1122.m

This file concerns the determination of the component P_{1122} of the Hill tensor $\mathbb{P}$ for spherical inclusions in a transversely isotropic matrix. It is called by file hom_fib_SCS.m (Section B.9) and hom_exhav.m (Section B.12). This file was originally written for the investigations published in [Hellmich et al., 2004a].

```
% P1122 for spherical inclusions
% in transversely isotropic matrix
%---------------------------------
function y=fun_Psph1122(x,C1111,C1122,C1133,C3333,C2323);
y=1./16.*(C1111.*C2323-2.*C1111.*C2323.*x.^2+C1111.*x.^2.*C3333+...
 C1122.*C2323-2.*C1122.*C2323.*x.^2+C1122.*x.^2.*C3333+C1111.*x.^4.*C2323-...
 C1111.*x.^4.*C3333+C1122.*x.^4.*C2323-C1122.*x.^4.*C3333-...
 2.*C2323.^2.*x.^2+2.*C2323.^2.*x.^4-4.*C2323.*x.^2.*C1133+...
 4.*C2323.*x.^4.*C1133-2.*x.^2.*C1133.^2+2.*x.^4.*C1133.^2).*(-1+x.^2)./...
 (-2.*C1111.^2.*x.^4.*C3333+2.*C2323.^2.*x.^6.*C3333-...
 4.*C1111.*C2323.^2.*x.^4-3.*C1111.^2.*C2323.*x.^2+C1111.^2.*x.^2.*C3333+...
 2.*C1111.*C2323.^2.*x.^2-2.*C2323.*x.^4.*C1133.^2-C1111.*C1133.^2.*x.^6+...
 2.*C1111.*C1133.^2.*x.^4+4.*C2323.^2.*x.^6.*C1133-2.*C1122.*C1133.^2.*x.^4+...
 2.*C2323.*x.^6.*C1133.^2+3.*C1111.^2.*x.^4.*C2323+C1122.*C1133.^2.*x.^6-...
 C1111.^2.*x.^6.*C2323+2.*C1111.*x.^6.*C2323.^2+C1111.^2.*x.^6.*C3333-...
 C1111.*C1133.^2.*x.^2-4.*C2323.^2.*x.^4.*C1133+C1122.*C1133.^2.*x.^2+...
 C1111.^2.*C2323-C1122.*C1111.*C2323-C1122.*x.^6.*C1111.*C3333+...
 4.*C1111.*x.^4.*C2323.*C1133-2.*C1111.*x.^2.*C2323.*C1133-...
 4.*C1122.*x.^4.*C2323.*C1133+2.*C1122.*x.^2.*C2323.*C1133+...
 2.*C1122.*x.^6.*C2323.*C1133-2.*C1111.*x.^6.*C2323.*C1133-...
 3.*C1111.*x.^6.*C2323.*C3333+2.*C1122.*C1111.*x.^4.*C3333-...
 C1122.*C2323.*x.^4.*C3333-3.*C1122.*C1111.*x.^4.*C2323-...
 C1122.*C1111.*x.^2.*C3333+3.*C1122.*C1111.*C2323.*x.^2+...
 3.*C1111.*C2323.*x.^4.*C3333+C1122.*x.^6.*C1111.*C2323+...
 C1122.*x.^6.*C2323.*C3333);
```

B.17 fun_Psph_1133.m

This file concerns the determination of the component P_{1133} of the Hill tensor $\mathbb{P}$ for spherical inclusions in a transversely isotropic matrix. It is called by file hom_fib_SCS.m (Section B.9) and hom_exhav.m (Section B.12). This file was originally written for the investigations published in [Hellmich et al., 2004a].

```
% P1133 for spherical inclusions
% in transversely isotropic matrix
%---------------------------------
function y=fun_Psph1133(x,C1111,C1122,C1133,C3333,C2323);
```

```
y=1./4.*(-1+x.^2).*x.^2.*(C2323+C1133)./...
  (2.*C2323.*x.^4.*C1133+C2323.*x.^4.*C3333+C1111.*x.^4.*C2323-...
  2.*C2323.*x.^2.*C1133-2.*C1111.*C2323.*x.^2+C1111.*C2323+...
  x.^4.*C1133.^2-C1111.*x.^4.*C3333-x.^2.*C1133.^2+C1111.*x.^2.*C3333);
```

B.18 fun_Psph_2323.m

This file concerns the determination of the component P_{2323} of the Hill tensor $\mathbb{P}$ for spherical inclusions in a transversely isotropic matrix. It is called by file hom_fib_SCS.m (Section B.9) and hom_exhav.m (Section B.12). This file was originally written for the investigations published in [Hellmich et al., 2004a].

```
% P2323 for spherical inclusions
% in transversely isotropic matrix
%---------------------------------
function y=fun_Psph2323(x,C1111,C1122,C1133,C3333,C2323);
y=1./16.*(4.*C1111.*C2323.*x.^2-8.*C2323.*x.^4.*C1133-...
  2.*x.^4.*C1133.^2-C1122.*x.^4.*C3333-8.*C1111.*x.^4.*C2323+...
  3.*C1111.*x.^4.*C3333+4.*C1111.*x.^4.*C1133-4.*C1122.*x.^4.*C1133+...
  2.*C1122.*x.^6.*C1133-2.*C1111.*x.^6.*C1133+C1122.*x.^6.*C1111-...
  3.*C1122.*x.^4.*C1111+3.*C1122.*C1111.*x.^2-2.*C1111.*x.^2.*C1133+...
  2.*C1122.*x.^2.*C1133+8.*x.^6.*C2323.*C1133-3.*x.^6.*C1111.*C3333+...
  4.*x.^6.*C2323.*C3333+4.*C1111.*x.^6.*C2323+C1122.*x.^6.*C3333+...
  3.*C1111.^2.*x.^4-C1111.^2.*x.^6+2.*C1133.^2.*x.^6-...
  3.*C1111.^2.*x.^2+C1111.^2-C1122.*C1111)./...
  (-2.*C1111.^2.*x.^4.*C3333+2.*C2323.^2.*x.^6.*C3333-...
  4.*C1111.*C2323.^2.*x.^4-3.*C1111.^2.*C2323.*x.^2+...
  C1111.^2.*x.^2.*C3333+2.*C1111.*C2323.^2.*x.^2-...
  2.*C2323.*x.^4.*C1133.^2-C1111.*C1133.^2.*x.^6+...
  2.*C1111.*C1133.^2.*x.^4+4.*C2323.^2.*x.^6.*C1133-...
  2.*C1122.*C1133.^2.*x.^4+2.*C2323.*x.^6.*C1133.^2+...
  3.*C1111.^2.*x.^4.*C2323+C1122.*C1133.^2.*x.^6-...
  C1111.^2.*x.^6.*C2323+2.*C1111.*x.^6.*C2323.^2+...
  C1111.^2.*x.^6.*C3333-C1111.*C1133.^2.*x.^2-...
  4.*C2323.^2.*x.^4.*C1133+C1122.*C1133.^2.*x.^2+...
  C1111.^2.*C2323-C1122.*C1111.*C2323-C1122.*x.^6.*C1111.*C3333+...
  4.*C1111.*x.^4.*C2323.*C1133-2.*C1111.*x.^2.*C2323.*C1133-...
  4.*C1122.*x.^4.*C2323.*C1133+2.*C1122.*x.^2.*C2323.*C1133+...
  2.*C1122.*x.^6.*C2323.*C1133-2.*C1111.*x.^6.*C2323.*C1133-...
  3.*C1111.*x.^6.*C2323.*C3333+2.*C1122.*C1111.*x.^4.*C3333-...
  C1122.*C2323.*x.^4.*C3333-3.*C1122.*C1111.*x.^4.*C2323-...
  C1122.*C1111.*x.^2.*C3333+3.*C1122.*C1111.*C2323.*x.^2+...
  3.*C1111.*C2323.*x.^4.*C3333+C1122.*x.^6.*C1111.*C2323+...
  C1122.*x.^6.*C2323.*C3333);
```

B.19 fun_Psph_3333.m

This file concerns the determination of the component P_{3333} of the Hill tensor $\mathbb{P}$ for spherical inclusions in a transversely isotropic matrix. It is called by file hom_fib_SCS.m (Section B.9) and hom_exhav.m (Section B.12). This file was originally written for the investigations published in [Hellmich et al., 2004a]. This file concerns the determination of the component P_{3333} of the Hill tensor $\mathbb{P}$ for spherical inclusions in a transversely isotropic matrix. It

is called by file hom_fib_SCS.m (Section B.9) and hom_exhav.m (Section B.12). This file was originally written for the investigations published in [Hellmich et al., 2004a].

```
% P3333 for spherical inclusions
% in transversely isotropic matrix
%---------------------------------
function y=fun_Psph3333(x,C1111,C1122,C1133,C3333,C2323);
y=1./2.*x.^2.*(x.^2.*C2323-C1111.*x.^2+C1111)./...
  (2.*C2323.*x.^4.*C1133+C2323.*x.^4.*C3333+C1111.*x.^4.*C2323-...
  2.*C2323.*x.^2.*C1133-2.*C1111.*C2323.*x.^2+C1111.*C2323+...
  x.^4.*C1133.^2-C1111.*x.^4.*C3333-x.^2.*C1133.^2+C1111.*x.^2.*C3333);
```

Bibliography

R.B. Ashman and J.Y. Rho. Elastic modulus of trabecular bone material. *Journal of Biomechanics*, 21(3):177 – 181, 1988.

R.B. Ashman, S.C. Cowin, W.C. van Buskirk, and J.C. Rice. A continuous wave technique for the measurement of the elastic properties of cortical bone. *Journal of Biomechanics*, 17(5):349 – 361, 1984.

M.A. Biot. Theory of elasticity and consolidation for a porous anisotropic solid. *Journal of Applied Physics*, 26:182 – 185, 1955.

L. Dormieux and D. Kondo. Approche micromécanique du couplage perméabilité-endommagement [Micromechanical approach to the coupling between permeability and damage]. *Comptes Rendus Mecanique*, 332(2): 135 – 140, 2004. In French.

L. Dormieux and F.-J. Ulm, editors. *CISM Courses and lectures, Volume 480. Applied Micromechanics of Porous Media.* Springer, Wien - New York, 2005.

T.P. Harrigan and R.W. Mann. Characterization of microstructural anisotropy in orthotropic materials using a second rank tensor. *Journal of Materials Science*, 19:761 – 767, 1984.

Ch. Hellmich. *Microelasticity of Bone*, pages 289 – 332. In , Dormieux and Ulm [2005], 2005.

Ch. Hellmich and F.-J. Ulm. Average hydroxyapatite concentration is uniform in extracollageneous ultrastructure of mineralized tissue. *Biomechanics and Modeling in Mechanobiology*, 2:21 – 36, 2003.

Ch. Hellmich and F.-J. Ulm. Are mineralized tissues open crystal foams reinforced by crosslinked collagen? – some energy arguments. *Journal of Biomechanics*, 35:1199 – 1212, 2002a.

Ch. Hellmich and F.-J. Ulm. A micromechanical model for the ultrastructural stiffness of mineralized tissues. *Journal of Engineering Mechanics (ASCE)*, 128(8):898 – 908, 2002b.

Ch. Hellmich and F.-J. Ulm. Drained and undrained poroelastic properties of healthy and pathological bone: a poro-micromechanical investigation. *Transport in Porous Media*, 58:243 – 268, 2005a.

Ch. Hellmich and F.-J. Ulm. Micro-porodynamics of bones: prediction of the 'Frenkel-Biot' slow compressional wave. *Journal of Engineering Mechanics (ASCE)*, 131(9):918 – 927, 2005b.

Ch. Hellmich, J.-F. Barthélémy, and L. Dormieux. Mineral-collagen interactions in elasticity of bone ultrastructure – a continuum micromechanics approach. *European Journal of Mechanics A-Solids*, 23:783 – 810, 2004a.

Ch. Hellmich, F.-J. Ulm, and L. Dormieux. Can the diverse elastic properties of trabecular and cortical bone be attributed to only a few tissue-independent phase properties and their interactions? – arguments from a multiscale approach. *Biomechanics and Modeling in Mechanobiology*, 2: 219 – 238, 2004b.

S. Lees, J.D. Heeley, and P.F. Cleary. A study of some properties of a sample of bovine cortical bone using ultrasound. *Calcified Tissue International*, 29:107 – 117, 1979.

S. Lees, J.M. Ahern, and M. Leonard. Parameters influencing the sonic velocity in compact calcified tissues of various species. *Journal of the Acoustical Society of America*, 74(1):28 – 33, 1983.

S. Lees, D. Hanson, E.A. Page, and H.A. Mook. Comparison of dosage-dependent effects of beta-aminopropionitrile, sodium fluoride, and hydrocortisone on selected physical properties of cortical bone. *Journal of Bone and Mineral Research*, 9(9):1377 – 1389, 1994.

R.N. McCarthy, L.B. Jeffcott, and R.N. McCartney. Ultrasound speed in equine cortical bone: effects of orientation, density, porosity and temperature. *Journal of Biomechanics*, 23(11):1139 – 1143, 1990.

A. Odgaard, E.B. Jensen, and H.J.G. Gundersen. Estimation of structural anisotropy based on volume orientation. A new concept. *Journal of Microscopy*, 157(2):149 – 162, 1990.

P. Suquet, editor. *Continuum micromechanics*. Springer, Wien – New York, 1997.

S. Torabia. Identification of a relationship between the chemical constituents of mineralized tissues: bridging computed tomography and micromechanical modeling, for noninvasive determination of elastic properties of bone. Master's thesis, Vienna University of Technology, 2004.

S. Torabia and Ch. Hellmich. In-vivo determination of elastic properties of bone, based on (p)QCT and micromechanical modeling. In P. Laugier and D. Hans, editors, *Proceedings of the 16th International Bone Densitometry Workshop, Annecy, France*, 2004.

W.J. Whitehouse. The quantitative morphology of anisotropic trabecular bone. *Journal of Microscopy*, 101:153 – 168, 1974.